# INFORMATION TO USERS

This manuscript has been reproduced from the microfilm master. UMI films the text directly from the original or copy submitted. Thus, some thesis and dissertation copies are in typewriter face, while others may be from any type of computer printer.

**The quality of this reproduction is dependent upon the quality of the copy submitted.** Broken or indistinct print, colored or poor quality illustrations and photographs, print bleedthrough, substandard margins, and improper alignment can adversely affect reproduction.

In the unlikely event that the author did not send UMI a complete manuscript and there are missing pages, these will be noted. Also, if unauthorized copyright material had to be removed, a note will indicate the deletion.

Oversize materials (e.g., maps, drawings, charts) are reproduced by sectioning the original, beginning at the upper left-hand corner and continuing from left to right in equal sections with small overlaps.

Photographs included in the original manuscript have been reproduced xerographically in this copy. Higher quality 6" x 9" black and white photographic prints are available for any photographs or illustrations appearing in this copy for an additional charge. Contact UMI directly to order.

Bell & Howell Information and Learning
300 North Zeeb Road, Ann Arbor, MI 48106-1346 USA
800-521-0600

**University of Alberta**

# An Input-Output Approach to Series DC Motor Speed Control

by

**Ke Xu**

A thesis submitted to the Faculty of Graduate Studies and Research in partial fulfillment of the requirements for the degree of **Master of Science**.

Department of Electrical and Computer Engineering

Edmonton, Alberta
Fall 1999

National Library of Canada
Acquisitions and Bibliographic Services
395 Wellington Street
Ottawa ON K1A 0N4
Canada

Bibliothèque nationale du Canada
Acquisitions et services bibliographiques
395, rue Wellington
Ottawa ON K1A 0N4
Canada

*Your file Votre reference*

*Our file Notre reference*

The author has granted a non-exclusive licence allowing the National Library of Canada to reproduce, loan, distribute or sell copies of this thesis in microform, paper or electronic formats.

L'auteur a accordé une licence non exclusive permettant à la Bibliothèque nationale du Canada de reproduire, prêter, distribuer ou vendre des copies de cette thèse sous la forme de microfiche/film, de reproduction sur papier ou sur format électronique.

The author retains ownership of the copyright in this thesis. Neither the thesis nor substantial extracts from it may be printed or otherwise reproduced without the author's permission.

L'auteur conserve la propriété du droit d'auteur qui protège cette thèse. Ni la thèse ni des extraits substantiels de celle-ci ne doivent être imprimés ou autrement reproduits sans son autorisation.

0-612-47120-9

Canada

**University of Alberta**

**Library Release Form**

**Name of Author**: Ke Xu

**Title of Thesis**: An Input-Output Approach to Series DC Motor Speed Control

**Degree**: Master of Science

**Year this Degree Granted**: 1999

Permission is hereby granted to the University of Alberta Library to reproduce single copies of this thesis and to lend or sell such copies for private, scholarly or scientific research purposes only.

The author reserves all other publication and other rights in association with the copyright in the thesis, and except as hereinbefore provided, neither the thesis nor any substantial portion thereof may be printed or otherwise reproduced in any material form whatever without the author's prior written permission.

Ke Xu
Apt. 1711, 8515, 112 Street
Edmonton, Alberta
Canada, T6G 1K7

**Date**: October 1, 1999

**University of Alberta**

**Faculty of Graduate Studies and Research**

The undersigned certify that they have read, and recommend to the Faculty of Graduate Studies and Research for acceptance, a thesis entitled **An Input-Output Approach to Series DC Motor Speed Control** submitted by Ke Xu in partial fulfillment of the requirements for the degree of **Master of Science**.

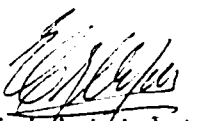

Dr. Horacio J. Marquez

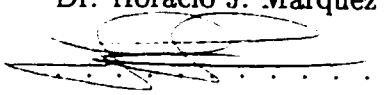

Dr. Fraser Forbes

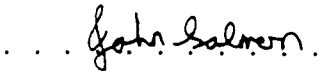

Dr. John Salmon

**Date:** Sep 30, 1999

# Abstract

One way to approach control design for complex plants is to obtain a linear approximation of the original nonlinear model at different operating conditions, followed by the application of linear control design techniques at each one of these points. The controllers so designed are then "scheduled" as the plant changes operating points. This practice, however, still lacks a systematic stability and performance analysis. This thesis investigates the virtues and shortcomings of the recently introduced input-output approach to systems described by multiple models by means of a case study. This theory is applied to the speed control of a series dc motor. Different experiments are designed and conducted to obtain a nonlinear model, which is linearized at various operating points. The mixed-sensitivity $H_\infty$ optimal control method is applied to design controllers for each local model. A gain scheduling algorithm is then implemented and the performance of the resulting controllers is evaluated.

# Acknowledgements

I would like to thank a great many people for making this thesis possible. My supervisor, Dr. Horacio J. Marquez, has been a great source of advice and inspiration throughout the period of my study. Dr. John Salmon was very helpful and supportive in modeling the nonlinear plant. Dr. Fraser Forbes has also given me useful comments and views on my work. My thanks go to all of them.

Writing a thesis is not only about academic discussion and debate. Without sufficient motivation and support from my dedicated parents Yongxin Xu, Maoli Yao, and my beloved husband Xinguang Chen, it would not be possible. For this, I am deeply grateful.

# Contents


**1 Introduction** 1

1.1 Introduction of Control System . . . . . 1

1.2 History and Development of Linear Control Systems . . . . . 2

1.3 Introduction of Nonlinear Control Systems . . . . . 5

1.3.1 Motivations for Nonlinear Control theory . . . . . 5

1.3.2 Behavior of Nonlinear Control Systems . . . . . 6

1.3.3 Difficulties for the Analysis of Nonlinear Control System . . . 6

1.3.4 Methods for Studying Nonlinear Control System . . . . . 7

1.4 Thesis Organization . . . . . 10

**2 Gain Scheduling** 12

2.1 Introduction of Gain Scheduling Method . . . . . 12

2.2 Development of Gain Scheduling Method . . . . . 13

2.3 An Input–Output Approach to Gain Scheduling Stability Analysis . . 14

2.3.1 Introduction . . . . . 14

2.3.2 Mathematical Preliminaries . . . . . 15

2.3.3 Stability Analysis . . . . . 18

**3 Motor** **22**

3.1 Introduction of Electrical Machinery . . . . . 22

3.2 DC Motor Speed Control . . . . . 23

3.3 Armature Voltage Controlled Series DC Motor . . . . . 25

3.4 Experiments for Constant Coefficients . . . . . 27

3.4.1 Measurements of Field and Armature Windings Resistance . . 27

3.4.2 Measurements of Field and Armature Windings Inductance . . 28

3.4.3 Measurements of Motor Constant . . . . . 29

3.4.4 Measurements of Motor Output or Load Torque . . . . . 32

3.4.5 Measurements of Total Motor Torque Loss . . . . . 34

3.4.6 Measurements of Rotor Inertia . . . . . 36

3.5 Analysis of Series DC Motor Characteristics . . . . . 37

3.5.1 Series DC Motor Power Flow and Efficiency . . . . . 37

3.5.2 Series DC Motor Speed, Current and Torque Characteristics . 38

3.5.3 Nonlinear Model from Experiments . . . . . 38

**4 Model Linearization** **44**

4.1 Linearization and Equilibrium Points . . . . . 44

4.2 First Local Linearized Model . . . . . 46

4.3 Second Local Linearized Model . . . . . 48

4.4 Other Local Linearized Models . . . . . 49

**5 Control System Design** **52**

5.1 $H_\infty$ Optimal Control System . . . . . 52

5.2 Continuous-Time $H_\infty$ Optimal Controller Design . . . . . 54

5.3 Characteristics of $H_\infty$ Optimal Controller . . . . . 60

**6 Simulation** **63**

6.1 Introduction of Simulation . . . . . 63

6.2 System Configuration . . . . . 63

6.2.1 2-D Look-Up Table and Its Supplement . . . . . 65

6.2.2 Reference Signals and Switches . . . . . 67

6.2.3 Logical Subsystems . . . . . 68

6.2.4 Local Linear $H_\infty$ Optimal Controllers . . . . . 70

6.2.5 Nonlinear Plant . . . . . 71

6.2.6 Simulation Termination . . . . . 71

6.3 Simulation Results . . . . . 72

**7 Discussion and Conclusions** **74**

7.1 Discussion . . . . . 74

7.2 Conclusions . . . . . 80

**Bibliography** **81**

**A Table** **86**

**B Figure** **114**

# List of Tables

6.1 2-D Look-Up Table . . . . . 65

A.1 Measured and Calculated Values of Field Resistance . . . . . 86

A.2 Measured and Calculated Values of Armature Resistance . . . . . 86

A.3 Measured and Calculated Values of Field Inductance Using $L = \frac{X}{\Omega}$ Method ($\Omega = 377$) . . . . . 87

A.4 Measured and Calculated Values of Armature Inductance Using $(2 \cdot \Omega \cdot L)^2 + R^2 = Z^2$ Method ($\Omega = 377$) . . . . . 87

A.5 Measured Values of $E_a - I_s$ Curve (first time testing–part I: before switched the connection between the two joints of the field winding) . 88

A.6 Measured Values of $E_a - I_s$ Curve (first time testing–part II: after switched the connection between the two joints of the field winding) . 88

A.7 Calculated Values of $E_a - I_s$ Curve (first time testing–part III) . . . . 89

A.8 Measured Values of $E_a - I_s$ Curve (second time testing–part I: before switched the connection between the two joints of the field winding) . 89

A.9 Measured Values of $E_a - I_s$ Curve (second time testing–part II: after switched the connection between the two joints of the field winding) . 90

A.10 Calculated Values of $E_a - I_s$ Curve (second time testing–part III) . . 90

A.11 Measured Values of $E_a - I_s$ Curve (third time testing–part I: before switched the connection between the two joints of the field winding) . 91

A.12 Measured Values of $E_a - I_s$ Curve (third time testing–part II: after switched the connection between the two joints of the field winding) . 91

A.13 Calculated Values of $E_a - I_s$ Curve (third time testing–part III) . . . 92

A.14 Measured and Calculated Values of $T_{load} - \omega$ Curve (dynamometer field flux strength 40%: first time testing) . . . . . 92

A.15 Measured and Calculated Values of $T_{load} - \omega$ Curve (dynamometer field flux strength 40%: second time testing) . . . . . 93

A.16 Measured and Calculated Values of $T_{load} - \omega$ Curve (dynamometer field flux strength 30%: first time testing) . . . . . 93

A.17 Measured and Calculated Values of $T_{load} - \omega$ Curve (dynamometer field flux strength 30%: second time testing) . . . . . 94

A.18 Measured and Calculated Values of $T_{load} - \omega$ Curve (dynamometer field flux strength 20%: first time testing) . . . . . 94

A.19 Measured and Calculated Values of $T_{load} - \omega$ Curve (dynamometer field flux strength 20%: second time testing) . . . . . 95

A.20 Measured and Calculated Values of $T_{load} - \omega$ Curve (dynamometer field flux strength 10%: first time testing) . . . . . 95

A.21 Measured and Calculated Values of $T_{load} - \omega$ Curve (dynamometer field flux strength 10%: second time testing) . . . . . 96

A.22 Measured and Calculated Values of $T_{loss} - \omega$ Curve (first time testing) 96

A.23 Measured and Calculated Values of $T_{loss} - \omega$ Curve (second time testing) 97

A.24 Measured and Calculated Values of Series DC Motor Characteristics (terminal voltage $V_t = 100$V: first time testing) . . . . . 97

A.25 Measured and Calculated Values of Series DC Motor Characteristics (terminal voltage $V_t = 100$V: second time testing) . . . . . 98

A.26 Measured and Calculated Values of Series DC Motor Characteristics (terminal voltage $V_t = 75$V: first time testing) . . . . . 98

A.27 Measured and Calculated Values of Series DC Motor Characteristics (terminal voltage $V_t = 75$V: second time testing) . . . . . 98

A.28 Measured and Calculated Values of Series DC Motor Characteristics (terminal voltage $V_t = 50$V: first time testing) . . . . . 99

A.29 Measured and Calculated Values of Series DC Motor Characteristics (terminal voltage $V_t = 50$V: second time testing) . . . . . 99

A.30 Measured and Calculated Values of Series DC Motor Characteristics (terminal voltage $V_t = 25$V: first time testing) . . . . . 100

A.31 Measured and Calculated Values of Series DC Motor Characteristics (terminal voltage $V_t = 25$V: second time testing) . . . . . 100

A.32 Measured and Calculated Values of $I_a$, $N_r$ and $\omega$ at Different $V_t$ (dynamometer field flux strength 40%: first time testing) . . . . . 101

A.33 Measured and Calculated Values of $I_a$, $N_r$ and $\omega$ at Different $V_t$ (dynamometer field flux strength 40%: second time testing) . . . . . 101

A.34 Simulated Values of $I_a$ and $\omega$ at Different $V_t$ (dynamometer field flux strength 40%: first time testing) . . . . . 102

A.35 Simulated Values of $I_a$ and $\omega$ at Different $V_t$ (dynamometer field flux strength 40%: second time testing) . . . . . 102

A.36 Equilibrium Points $(\mathbf{x_e}, u_e)$ of Nonlinear Model (part one) . . . . . 103

A.37 Equilibrium Points $(\mathbf{x_e}, u_e)$ of Nonlinear Model (part two) . . . . . 104

A.38 Steady State Values for $\Psi$ and $\mathbf{x}$ (first local linear model: $x_{1e} = 0.6655$, $x_{2e} = 0.0450$ and $u_{e1} = 7$) . . . . . 104

A.39 Steady State Values for $\Psi$ and $\mathbf{x}$ (second local linear model: $x_{1e} = 0.7548$, $x_{2e} = 0.3238$ and $u_{e2} = 8$) . . . . . 105

A.40 Values of Matrix $\mathbf{A}$ for Different Local Linear Models (part one) . . . 105

A.41 Values of Matrix $\mathbf{A}$ for Different Local Linear Models (part two) . . . 106

A.42 Steady State Values for $\Psi$ and $\mathbf{x}$ (third local linear model: $x_{1e} = 0.9283$, $x_{2e} = 0.9588$ and $u_{e3} = 10$) . . . . . 107

A.43 Steady State Values for $\Psi$ and $\mathbf{x}$ (fourth local linear model: $x_{1e} = 1.1757$, $x_{2e} = 2.0867$ and $u_{e4} = 13$) . . . . . 107

A.44 Steady State Values for $\Psi$ and $\mathbf{x}$ (fifth local linear model: $x_{1e} = 1.4807$, $x_{2e} = 3.8768$ and $u_{e5} = 17$) . . . . . 108

A.45 Steady State Values for $\Psi$ and $\mathbf{x}$ (sixth local linear model: $x_{1e} = 1.8229$, $x_{2e} = 6.5192$ and $u_{e6} = 22$) . . . . . 108

A.46 Steady State Values for $\Psi$ and $\mathbf{x}$ (seventh local linear model: $x_{1e} = 2.2840$, $x_{2e} = 11.6266$ and $u_{e7} = 30$) . . . . . 109

A.47 Steady State Values for $\Psi$ and $\mathbf{x}$ (eighth local linear model: $x_{1e} = 2.2840$, $x_{2e} = 11.6266$ and $u_{e8} = 40$) . . . . . 110

A.48 Steady State Values for $\Psi$ and $\mathbf{x}$ (ninth local linear model: $x_{1e} = 2.9311$, $x_{2e} = 29.6638$ and $u_{e9} = 49$) . . . . . 111

A.49 Steady State Values for $\Psi$ and $\mathbf{x}$ (tenth local linear model: $x_{1e} = 2.9424$, $x_{2e} = 40.7707$ and $u_{e10} = 56$) . . . . . 111

A.50 Steady State Values for $\Psi$ and $\mathbf{x}$ (eleventh local linear model: $x_{1e} = 2.8012$, $x_{2e} = 53.0047$ and $u_{e11} = 61$) . . . . . 112

A.51 Steady State Values for $\Psi$ and $\mathbf{x}$ (twelfth local linear model: $x_{1e} = 2.5003$, $x_{2e} = 72.1090$ and $u_{e12} = 66$) . . . . . 112

A.52 Steady State Values for $\Psi$ and $\mathbf{x}$ (thirteenth local linear model: $x_{1e} = 2.3269$, $x_{2e} = 88.9022$ and $u_{e13} = 71$) . . . . . 113

A.53 Steady State Values for $\Psi$ and $\mathbf{x}$ (fourteenth local linear model: $x_{1e} = 2.2778$, $x_{2e} = 110.6661$ and $u_{e14} = 81$) . . . . . 113

# List of Figures


2.1 Block Diagram of Gain Scheduling Method . . . . . 13

2.2 Local Model with Two Dimensional State Space . . . . . 19

2.3 Multiple Local Models with Two Dimensional State Space . . . . . 20

3.1 Circuit for Series DC Motor . . . . . 26

3.2 $E_a$ and $I_s$ Average Relationship ( No Load, No Belt and Speed = 1200 rpm ) . . . . . 31

3.3 Circuit for Shunt/Separately Excited DC Motor . . . . . 33

3.4 $T_{load}$ and $\omega$ Relationship ( Dynamometer Field Flux Strength: 40% ) 34

3.5 $T_{loss}$ and $\omega$ Average Relationship ( No Load and Keep Belt ) . . . . . 35

3.6 Power Flow of Series DC Motor . . . . . 37

3.7 $\omega$ and $T_e$ Relationships ( $V_t$ = 100v, 75v, 50v, 25v ) . . . . . 39

3.8 $\omega$ and $I_a$ Relationships ( $V_t$ = 100v, 75v, 50v, 25v ) . . . . . 39

3.9 $T_e$ and $I_a$ Relationships ( $V_t$ = 100v, 75v, 50v, 25v ) . . . . . 40

3.10 Block Diagram of Nonlinear Model for Series DC Motor . . . . . 42

4.1 Block Diagram of Local Linear Model . . . . . 47

4.2 Compare the Relationship of $I_a$ and $\omega$ between Nonlinear Model and Linearized Models . . . . . 50

5.1 Standard Continuous-Time Control System . . . . . 52

5.2 Control System . . . . . 53

5.3 Block Diagram of Closed-Loop System . . . . . 55

5.4 Block Diagram of Continuous-Time Feedback System . . . . . 57

5.5 The Bode Diagram of Closed-Loop Transfer Function $T$ for First Local Linear System . . . . . 57

5.6 The Closed-Loop Response of $\omega$ for First Local Linear System . . . . 58

5.7 The Response of the Input Signal to the Plant for First Local Linear System . . . . . 59

5.8 The Bode Diagram of the Sensitivity Function $S$ for First Local Linear System . . . . . 60

5.9 Multiple Local Linear Models in the State Space . . . . . 61

5.10 Multiple Local Linear Models . . . . . 62

6.1 Nonlinear Feedback System . . . . . 64

6.2 2-D Look-Up Table . . . . . 66

6.3 First Logical Subsystem . . . . . 69

6.4 Second Logical Subsystem . . . . . 69

6.5 First Local Linear $H_\infty$ Optimal Controller . . . . . 70

6.6 Simulation Result of the Motor Speed . . . . . 72

7.1 Slow and Non-Smooth Speed Acceleration with Small Intersections . 76

7.2 Fast and Smooth Speed Acceleration with Large Intersections . . . . 77

7.3 Exogenous Input Signals and Output Curve . . . . . 78

B.1 $E_a$ and $I_s$ Relationship of First Group Testing Data ( No Load, No Belt and Speed = 1200 rpm ) . . . . . 114

B.2 $E_a$ and $I_s$ Relationship of Second Group Testing Data ( No Load, No Belt and Speed = 1200 rpm ) . . . . . 115

B.3 $E_a$ and $I_s$ Relationship of Third Group Testing Data ( No Load, No Belt and Speed = 1200 rpm ) . . . . . 115

B.4 $T_{load}$ and $\omega$ Relationship ( Dynamometer Field Flux Strength: 30% ) 116

B.5 $T_{load}$ and $\omega$ Relationship ( Dynamometer Field Flux Strength: 20% ) 116

B.6 $T_{load}$ and $\omega$ Relationship ( Dynamometer Field Flux Strength: 10% ) 117

B.7 Compare the Average Relationship of $I_a$ and $V_t$ between Real Motor and Nonlinear Model . . . . . 117

B.8 Compare the Average Relationship of $\omega$ and $V_t$ between Real Motor and Nonlinear Model . . . . . 118

B.9 Absolute Error of $I_a$ between Real Motor and Nonlinear Model ( First Time Testing: Average=-0.0366A, | Average |=0.2454A ) . . . . . 118

B.10 Relative Error of $I_a$ between Real Motor and Nonlinear Model ( First Time Testing: Average=0.7929%, | Average |=10.1246% ) . . . . . 119

B.11 Absolute Error of $I_a$ between Real Motor and Nonlinear Model ( Second Time Testing: Average=0.0332A, | Average |=0.2029A ) . . . . . 119

B.12 Relative Error of $I_a$ between Real Motor and Nonlinear Model ( Second Time Testing: Average=3.4129%, | Average |=9.0767% ) . . . . . 120

B.13 Absolute Error of $\omega$ between Real Motor and Nonlinear Model ( First Time Testing: Average=-1.7520rad/sec, | Average |=3.2446rad/sec ) . 120

B.14 Relative Error of $\omega$ between Real Motor and Nonlinear Model ( First Time Testing: Average=-0.0421%, | Average |=5.3426% ) . . . . . 121

B.15 Absolute Error of $\omega$ between Real Motor and Nonlinear Model ( Second Time Testing: Average=-4.8686rad/sec, | Average |=6.6080rad/sec ) . 121

B.16 Relative Error of $\omega$ between Real Motor and Nonlinear Model ( Second Time Testing: Average=-2.6074%, | Average |=8.3561% ) . . . . . 122

B.17 Relative Error of $I_a$ between Nonlinear Model and Linearized Models 122

B.18 Relative Error of $\omega$ between Nonlinear Model and Linearized Models 123

# Chapter 1

# Introduction

## 1.1 Introduction of Control System

The art of automatic control systems has permeated into all of our lives: the toaster, the washing machine, the car, the aircraft and so on. It, together with other modern technologies, has totally changed our way of living.

During the development of modern technology, people not only have designed the machines, which release themselves from intolerable amount of monotonous work, but also constructed devices which automatically control or regulate the operation of machines and processes. Because of the development of these control systems, it has extended people's own physical capacities. For example: a coachman can handle a horse-drawn coach with his own experience and capacity. However, a complicated aircraft, on the other hand, cannot be flown without the help of various control systems, which can regulate the flight of the aircraft automatically or translate the pilot's manual commands to corresponding movements of the aircraft. Technological developments have made it possible for people to travel in the outer space and explore the unknown for this endless universe. All of these depend on using a large number of control systems.

## 1.2 History and Development of Linear Control Systems

As in the evolution of other engineering disciplines, control engineering began as an art, originated by those practicing engineers using their common sense and creativity. However, the early invention soon led to problems. People could not only rely on a collection of classical analytical and numerical methods and their intuition for most of the problems encountered in engineering. Furthermore, it was difficult for deeper analysis and better design without the assistance of theoretical guidance. At the same time, the growth of other scientific areas, especially in mathematics, motivated theoretical studies of automatic control systems. Since then, the development of control systems became an interaction between theory and practice. Control practice indicated the need for theoretical analysis. In turn, theoretical research enlarged the engineers' abilities for solving practical problems and designing better performance control systems [15].

A typical control problem is the following: Given a plant and a desirable reference signal, find a control input so that the output of the plant will be as close as possible to the desirable reference signal. The control signal is independent of the actual response of the plant. This is called the open-loop control systems. Of course, this type of control is not satisfactory if there are disturbances or changes in the system [9]. This disadvantage induces the key concept in control theory, which is that of feedback or closed-loop control system [15]. It means the control signal contains the actual response of the plant. Instead of using people for the purpose of checking the actual value for the plant with respect to the desirable or reference signal, the output of the plant is fed back to the control input. The difference between the reference signal and feedback signal acts to maintain the output at the desirable value. This improves the performance of the closed-loop control system.

James Watt's flyball governor for controlling speed, developed in 1788, can be considered the first widely used feedback control system [11]. J. C. Maxwell, in 1868, made an analytic study of the stability of the flyball governor [3]. He explained that flyball system could be described by an ordinary linear differential equation and the instability of the system came from the exponential functions in the solution

of the equation. Maxwell's famous work was followed later by two mathematicians: Routh and Hurwitz. In 1895, they independently discovered the remarkable criterion for analysis the stability of a system described by low or high-order ordinary linear differential equation [3].

Until 1940s, people devoted much attention to maintain the static value of the control system to the reference signal. But this emphasis changed during the second world war due to the need for designing advanced weapons. People eagerly wanted to capture the transient response characteristics of the control system. However, excluding relatively simplistic systems, methods based on trying to get the solution for ordinary linear differential equations is tedious. Use of Laplace transform to obtain the frequency response of the corresponding linear differential equation simplifies the analysis. Obviously, it was necessary to have the regulation for frequency response stability analysis. A significant stability criterion was discovered by H. Nyquist [3]. In fact, his criterion unlike that of Routh and Hurwitz, give a simple quantitative way for measuring how close to the edge of instability for a stable feedback control system. Moreover, Nyquist's criterion introduced concepts of gain margin and phase margin. These concepts turned out to be closely related, at least qualitatively, to the transient response of the feedback control system. These provide very useful tools for control engineers to design closed-loop systems with high quality transient performance as well as accurate static value. Nyquist's work was extended by Black and Bode, who furthered the development of control theory [5], [6]. Another important contribution to the theory was made by W. R. Evans in 1948, when he presented the root-locus method [12]. This method provides a simple, direct, graphical display of the roots' properties of the system. It is a major complementation to Nyquist criterion for control system analysis and design. By then, the well known classical control theory was established.

After the second world war, the rapid growth of feedback control system was also speeded up by use of computers [31],[21],[38], [39]. However, due to the increase of requirements for designing more complex control system in industry and society, the classical control theory turned out to have its limitations.

First, it is restricted to linear system, which satisfies the principle of superposition. However, in real life, physical systems are always inherently nonlinear. Actu-

ally, all control systems are nonlinear to a certain extent. Under certain conditions, nonlinear systems can be approximated by linear differential equations. This approximation however may lead to poor performance or even instability of the feedback loop. Thus, classical control theory may not be suitable to such complex nonlinear control problems.

Secondly, classical control theory is restricted to time-invariant systems. This means that the parameters of the system do not change with time, that is, the ordinary differential equation has constant coefficients. This is, however, not always the case. Therefore, time-variant systems have received a lot of attention since the 1950s.

Thirdly, classical control theory is constrained to single-loop feedback systems. In this class of systems, there is only one input terminal and only one output terminal [8]. Today, in many control problems we have to deal with multiple inputs as well as multiple outputs.

During the 1950s and the 1960s, the introduction of state-space expression overcame the drawbacks of the input-output description. It described not only the input-output relation, but also the internal behaviors of a system. Furthermore, by using the concepts of input, output and state vectors, it made the expression of multivariable system as easy as that of single-variable system. Simultaneously, a great deal of new concepts, design approaches and control theories were boomed, such as controllability, observability concepts, optimization techniques and so on [18], [23], [22], [42], [17]. All of these constituted the foundation of modern control theory and made people have more sophisticated understanding of the internal behaviors of the systems.

Since the 1970s, several important developments have been made in linear control theory, such as the geometric approach and the transfer-function matrices in fractional forms, called the matrix-fraction description. The geometric approach is well covered in [41]. And the transfer-function matrix in fractional form is included in [9].

## 1.3 Introduction of Nonlinear Control Systems

Interest in nonlinear systems started from 1950s. Kalman helped to emphasize Lyapunov's work, which was published in the late 19th century [28], [24]. However, no comprehensive theory of nonlinear control was available at that time. Phase plane analysis of second order nonlinear systems, describing function approximation approach and Lyapunov stability theorem dominated the scene in nonlinear systems analysis. Nonlinear control developed rapidly since 1970, motivated by increased demands in performance. Feedback linearization, sliding control, adaptive control [25], gain scheduling method and so on have occupied an increasingly important place in control theory.

### 1.3.1 Motivations for Nonlinear Control theory

The standard method dealing with nonlinear systems design is to replace the nonlinear model by a linearized version, which provides an acceptable description of plant dynamics in the vicinity of an equilibrium point. Therefore, the behavior of the nonlinear system can be investigated by the efficient tools available for linear systems. However, the assumption of small operating range is invalid in many cases. When the required operation range is large, the results derived from the linear models can be poor or even erroneous both quantitatively and qualitatively, because the linear theory fails to reveal the nonlinear characteristics.

Another assumption for linearizing the nonlinear system is that the actual performance of the nonlinear model does not differ considerably from that predicted using an approximate linear model. But some systems are highly nonlinear and a linear approximation may yield misleading results. These are called "hard nonlinearities" including saturation, dead-zones, and backlash, which are often found in control systems.

### 1.3.2 Behavior of Nonlinear Control Systems

The analysis of linear time-invariant systems is relatively easily accomplished using a variety of mathematical tools in both the time and complex frequency domain. However, nonlinear systems are more complex, since the superposition principle does not apply any more.

Nonlinear systems frequently have multiple equilibrium points [36]. Therefore, when a steady state is attained it may not be the same for all initial conditions. A further possibility is that a nonlinear system can display oscillations of fixed amplitude and fixed period, which is known as limit cycle. Unlike the linear second order system with no damping, where the oscillation amplitude depends on the initial conditions, in a nonlinear system the same limit cycle can result from many different initial conditions.

Another specific phenomenon in nonlinear systems is bifurcation. When the values of the parameters of nonlinear systems are changed, the stability of the equilibrium points and the number of the equilibrium points can change. The quantitative change of parameters causing the qualitative change of system properties is the topic of bifurcation theory [36].

Further characteristics of nonlinear systems include jump resonance, which means that a slight change in the input amplitude or frequency can cause the system to change states, and chaos, which indicates that the system output is extremely sensitive to initial conditions.

### 1.3.3 Difficulties for the Analysis of Nonlinear Control System

As mentioned above, nonlinear systems have much richer and more complex behaviors than linear systems. The development of nonlinear control faces real difficulties. It is impossible to encompass all these phenomena in a single method of analysis [40]. There are no universal mathematical methods for the solution of nonlinear differential equations which are the mathematical models of nonlinear systems, because the nonlinear differential equations cannot in general be solved analytically. Moreover,

the useful mathematical tools, such as Laplace and Fourier transforms are no longer suited for nonlinear systems. As a result, there are no general ways for analyzing nonlinear systems. There are many methods dealing with specific classes of nonlinear systems and therefore, best applicable to different problems. In recent years, more and more advanced techniques have been developed for nonlinear system analysis and design, which make this area fruitful.

### 1.3.4 Methods for Studying Nonlinear Control System

**Phase-plane Method.** The phase-plane method is a graphical approach which can be used to obtain the solutions for first and second order nonlinear differential equations. The result is a family of system motion trajectories on a two-dimensional plane, which is called the phase plane. The motion trajectories depend on system initial condition, and are helpful for examining the qualitative features of the system. This method allows us to have visual observation of the motion patterns of the system. It is useful for studying the transient behavior as well as the stability of first and second order systems. The fundamental disadvantage of the method is that its applications are essentially limited to first or second order systems [1].

**Describing Function Method.** Unlike the phase plane method, the describing function method is normally suitable for the study of higher order systems [2], [4]. The original and most widely used describing function is that for a single sinusoidal input. Its basic idea is to approximate the nonlinear components in nonlinear systems by an almost equivalent linear part. If a nonlinear element is excited with a sinusoidal function, then the output is periodic, but 1. We can thus represent the output by a Fourier series. In the describing function method, it is assumed that the fundamental frequency component of the output is the most significant part and the higher harmonics may be neglected [13].

**Lyapunov Method.** Stability as an essential characteristic of the motion of dynamic systems has long been under consideration. According to this theory, a stable equilibrium point $X_e$ is the one that satisfies the following property: if the initial condition is near $X_e$, then the resulting trajectory remains in the neighborhood of $X_e$ for future time. Lyapunov theory was initiated in 1892 by A. M. Lyapunov. His

work, however, received little attention outside Russia until late 1950s. An accurate introduction to Lyapunov's work was provided by LaSalle and Lefschetz [27]. Since then, research in the application of Lyapunov theory to nonlinear system analysis and design rapidly developed.

**Differential Geometric Method.** During the past two decades or so, there has been a great deal of interest in the study of the differential geometric theory of nonlinear control systems,such as [20], [19] and [30]. The method attempts to deal with the basic questions in the state space formulation of nonlinear control systems, including the problems of controllability and observability, (minimal) realization theory and more importantly, feedback linearization [7].

Feedback linearization involves techniques for transforming original complex nonlinear models into equivalent simpler models. Feedback linearization can be used as a good nonlinear control design method or model-simplifying technique. First, it transforms the nonlinear dynamics into a linear form by using state feedback, with input-state linearization corresponding to complete linearization and input-output linearization to partial linearization. By choosing different state representation, we get a simpler fully or partially linear form. Then we can use the well-known and powerful linear design approaches to complete the design target. The "linearization" concept used here is totally different from the conventional linearization idea. Because feedback linearization is achieved by exact transformation and feedback. Unlike Jacobian linearization, there is no linear approximation of the dynamics. Feedback linearization method can be used for both stabilization and tracking problems, with single-input or multiple-inputs. It has been successfully applied to a number of practical nonlinear control problems, such as helicopter control, industrial robots control and aircraft control.

The important shortcomings for feedback linearization method are apparent. It does not apply to all kinds of nonlinear control systems. Some specific conditions must be satisfied. Since full state has to be measured, it also causes difficulties in finding observers for nonlinear control systems. And due to the fact that the sensitivity to modeling errors may be particularly severe, there is no guarantee for the robustness when parameter uncertainties or unmodeled dynamics occur [36]. Of course, great efforts have been made to overcome these drawbacks.

**Robust Control.** In general, it is impossible to get a precise model for a physical system. Those model imprecision may come from the actual uncertainties about the plant, such as some unknown parameters, or from the simplified model of real dynamics, such as neglected nonlinearities or time-delays. These model inaccuracies can have severe effects on linear or nonlinear control systems. Robust control theory deals with the effects of model uncertainties in control design. Robust controller design is based on the consideration of both the nominal and some characterization of the model uncertainties.

**Gain Scheduling Method.** The basic idea of gain scheduling is conceptually simple. In many situations, it is well known how the dynamics of a process will change when the operating conditions change. So the first step is to select a number of operating points. Then, linearize the nonlinear plant at each operating point so as to get the linear time-invariant model. Thus linear design methods can be applied to these models. We have a set of linear feedback systems. Each of them satisfies all of the performance requirements when it is operated near the corresponding operating point. The next step is where the term "gain scheduling" comes from. It devises a scheme to change the parameters of the linear controllers by monitoring the operating conditions of the process. Usually, the parameters of the controllers are changed as a function of scheduling variables, which have close relationships with operating conditions.

The main advantage of gain scheduling method is that the powerful linear design methods can be applied to the linearized models at each operating point. This method based on the measurements of different operating conditions is often a good way to compensate for the variations in process or the known nonlinearities of process due to its real-time computation and fast response.

On the other hand, the main problem in gain scheduling is that it has only limited theoretical guarantees of stability in nonlinear operation. And how to find suitable scheduling variable is also a problem. There are only some loose practical rules of thumb, such as "the scheduling variables should change slowly" and "the scheduling variable should capture the plant's nonlinearities". Of course, as the complexity of the system increases, these simple rules are not sufficient. We need to search for the theoretical guidelines for the development of gain scheduling method.

An elementary introduction to this method is provided in [37]. An analytical framework for the design of gain scheduled controllers for nonlinear systems is proposed by W. J. Rugh [32]. J. S. Shamma and M. Athans [33], [34] study the conditions which guarantee stability, robustness and performance properties of the global gain scheduled designs and the limitations of current gain scheduling practice together with some reformulations. However, due to the very restrictive assumptions in their papers, the analysis approach is impossible to use in practice. There is a big gap between theory and applications in the stability analysis of gain scheduling method. All of these motivate our interest in providing a different theory that can deal with the stability analysis of system described by multiple models in a systematic manner, assuming only local information available.

## 1.4 Thesis Organization

The rest of this thesis is organized as follows: Chapter 2 introduces the input-output approach to systems described by multiple local models, which is proposed in reference [29]. This reference gives us a rather simple, yet complete characterization of stability analysis for the gain scheduling method. The main objective of this thesis is to investigate the virtues and shortcomings of the input-output approach by means of a case study: the speed control of the armature voltage controlled series dc motor. In chapter 3, by conducting a series of experiments, the nonlinear model of the series dc motor is obtained. It is built in a computer and to be used throughout the rest of the thesis. In chapter 4, according to the input-output approach, the complex nonlinear model is linearized at different operating points, and a number of local linear models are obtained. In chapter 5, the powerful mixed-sensitivity $H_\infty$ optimal control method is applied to the local linear models, and closed-loop local systems are acquired. For the purpose of verifying the theory, in chapter 6, all of the $H_\infty$ optimal controllers are connected with the nonlinear model in the computer and performance of the nonlinear feedback system is simulated. Finally, in chapter 7, the problems encountered are discussed. We also elaborate on ideas which might improve the performance of the nonlinear systems for which the input-output approach is applicable, and the relationship with other methods. All of these comprise the principal part of

this thesis.

# Chapter 2

# Gain Scheduling

## 2.1 Introduction of Gain Scheduling Method

Physical systems are inherently nonlinear. Thus, good mathematical models of physical systems contain at least some form of nonlinearity. Despite this fact, for a variety of reasons, control system design is often based on a simplified linearized version of the original nonlinear model. These approximations, however, deteriorate rapidly under large excursions about normal operating conditions. In many cases, the nonlinear control system works in a rather large operation range. This occurs frequently especially when dealing with large industrial facilities, such as in process control and flight control. In these situations, control design based on a linear approximation can result in very poor performance.

One way to improve controller performance, while still employing linear techniques is to linearize the original (nonlinear) plant at a number of different operating points, and then design linear controllers for each one of the resulting linearized models of the plant. These controllers can then be switched as the plant changes operating conditions.

This technique, in its many forms, is known as gain scheduling. Many successful applications of gain scheduling have been reported, particularly when the process is such that there exists a variable (usually known as the scheduling variable) which correlates well with the changes in process dynamics. This can be represented graph-

ically in figure 2.1. However, gain scheduling remains largely an *ad hoc* technique where stability and performance are typically evaluated by simulation.

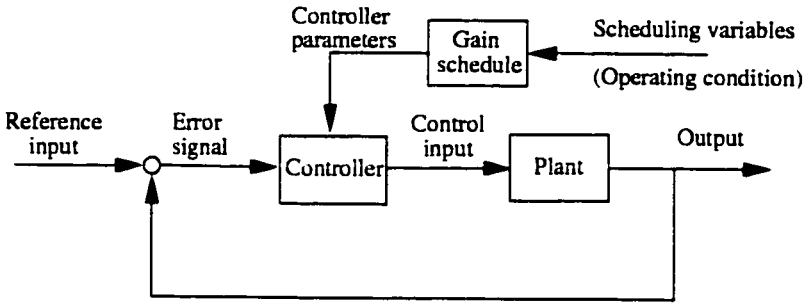


Figure 2.1: Block Diagram of Gain Scheduling Method

## 2.2 Development of Gain Scheduling Method

The concept of gain scheduling originated with the development of flight control systems. In this application, the speed and the dynamic pressure are measured by sensors and used as scheduling variables in order to adjust the flight controllers to different operating conditions. The idea of relating the controller parameters to operating condition is old. However, since the controller parameters must be determined for many operating points, and the performance must be checked by extensive simulations, there is a big computational burden involved in the gain scheduling design. This method has thus only been used in high-performance aircraft control and other special cases. In recent years, the development of high-speed hardware and computer-controlled systems makes it possible to easily implement the gain scheduling method. The controller parameters can be changed very quickly in response to the changing conditions. So gain scheduling has become a widely used design methodology in many practical applications. Some results have been reported over the last 10 years, which try to put gain scheduling in a proper theoretical framework. K. J. Åström and B. Wittenmark give an elementary introduction to gain scheduling, along with some applications [37]. W. J. Rugh [32] describes the analytical framework for the design of gain-scheduled controller for nonlinear systems. He gives some hints on how to deal with difficulties in the design procedure. J. S. Shamma and M. Athans [33],

[34] prove that the gain scheduling approach "can" work, provided the verification of the theorems, which guarantee stability, robustness and performance properties of the global gain scheduled designs. However, their results have little practical value in application, since these theorems require hard-to-obtain information in real dynamical systems. So the gain scheduling control approach is still in the absence of a sound systematic stability theory.

In this thesis, the input-output approach recently proposed by H. J. Marquez [29] will be applied to the speed control of the series dc motor. In the remainder of this chapter the main features of the results from reference [29] are summarized.

## 2.3 An Input–Output Approach to Gain Scheduling Stability Analysis

### 2.3.1 Introduction

As mentioned before, in control systems, when dealing with complex nonlinear systems, it is a standard practice to use the gain scheduling design approach. We assume that the universal global model of the physical system in question is obtained from physical principles and experimental data, but it is too complex to be of any practical use. Local models, which are derived from the nonlinear model by linearization at different operating points, on the other hand, are readily available for use in control system design. The stability theory proposed in reference [29] is designed to deal with this class of complex systems, which have multiple models of the same physical device, assuming only local information.

Unlike most references who search for the *global stability,* the approach in reference [29] is novel in that it concentrates on local stability and provides a mechanism that ensures "safe" transitions between different operating points. Specific questions studied in [29] are: How can these local models remain stable? More importantly, how can we keep the local stability when the system switches from one local model to another? What class of stability would this be? Lyapunov? Input-output?

Roughly speaking, there are two conceptually different approaches to stability

theory, namely (i) Lyapunov, and (ii) input-output methods. The former studies the stability of an equilibrium state of the free or unforced system, while the latter regards systems as mappings between inputs and outputs, and assumes that the system is initially at rest (*i.e.*, all initial conditions are nil). Moreover, the Lyapunov theory is essentially a local theory and due to the lack of external excitations, it is impossible to deal with systems which work on different operating conditions and need various input control signals. On the contrary, the input-output theory is essentially a global theory. It is applicable for a very general space of input functions. As a result of null initial conditions, this theory can hardly deal with multiple models system whose initial conditions of each model may be non-zero. Therefore, none of the classical stability theories can solve the stability problem involved in gain scheduling method.

Reference [29] provides a definite answer to this stability problem based on the new introduced concept of *stable motion*. It can be regarded as a generalization of stability along a trajectory associated with the Lyapunov theory. Thus, this work not only keeps the essence of the classical stability theory, but also has its own spirit. It has two fundamental aspects. First only *local models* are used for the design and analysis. All of these local models are only valid for a well defined class of input functions. The selection of the space of the input functions will have profound implications in the whole theory. The space of the input functions will be chosen to be meaningful from a systems point of view, and at the same time permits generalization of the fundamental results of the classical input-output theory. Secondly, systems will be defined as a mapping from *input* to *state*, rather than from *input* to *output*. This understanding of systems will overcome the drawback of the classical input-output theory, which could not incorporate the initial conditions into the systems stability analysis. This big improvement makes it possible for us to use input-output approach to analyze the long lasting gain scheduling stability problem.

### 2.3.2 Mathematical Preliminaries

In the sequel, $\mathbf{R}$ represents the field of real numbers, $\mathbf{R}^n$ the set of n-tuples of real numbers, and $\mathbf{R}^+$ the set of non-negative real numbers. $\Omega$ will represent a subset of $\mathbf{R}^+$, which has the form $\Omega = [t_1, t_2]$, or $\Omega = [t_1, \infty)$. $\mathcal{Z}$ is the linear space of measurable

functions $z$: $\Omega \to \mathbf{R}^q$. Now, we will define a space of input functions which captures the properties of small signal and has general characteristics of input signals from practical point of view. We will denote by $\mathcal{X}$, the binormed linear subspace $\mathcal{X}$ of $\mathcal{Z}$ defined as follows:

$$\mathcal{X} = \{u \in \mathcal{Z} : \| \cdot \|_\infty < \infty, \ and \ \ \| \cdot \|_2 < \infty\}$$

where $\| \cdot \|_\infty$ and $\| \cdot \|_2$ are the usual $\mathcal{L}_\infty$ and $\mathcal{L}_2$ norms.

In other words, $\mathcal{X}$ is the space of measurable functions, which have finite energy and are essentially bounded. We will use $\mathcal{X}([t_0, t_1])$ to indicate that $\mathcal{X}$ is defined at the time $t \in [t_0, t_1]$. Typically, the input function $u$ is assumed to be vector-valued, *i.e.*, $u : \Omega \to \mathbf{R}^q$. However, the dimension of $u$ is no need to be explicit in our notation. So we will use $u \in \mathcal{L}_p$ instead of $u \in \mathcal{L}_p^q$. The extension of the space $\mathcal{X}$, denoted by $\mathcal{X}_e$, is defined as the space of all input functions $u$ whose truncation $u_T$ belongs to $\mathcal{X}$, where

$$u_T(t) = \begin{cases} u(t) & \text{if } t \leq T \\ 0 & \text{if } t > T \end{cases}$$

We will also need the subset $\mathcal{X}_Q$ of $\mathcal{X}$, defined as follows:

$$\mathcal{X}_Q = \{u \in \mathcal{X} : \| u \|_\infty < Q\}$$

In general, $x \in \mathbf{R}^n$ represents the state of the system. Thus $x(t)$ represents a motion in the state space. It can be seen as a function $\mathbf{R} \to \mathbf{R}^n$ as well. Similarly, the set of bounded motions, denoted by $\mathcal{X}_\alpha$, is defined as follows:

$$\mathcal{X}_\alpha = \{x \in \mathcal{X}([0, \infty)) : \| x(t) \|_\infty < \alpha\}$$

In our applications, the local models to be considered are linear time-invariant.

**Definition 2.3.1** *For a given physical system, a local linear time-invariant model about $(x_e, u_e)$, denoted $H[x_e, u_e]$, has the following form:*

$$\begin{aligned} \dot{x}(t) &= Ax + Bu \quad t, t_0 \in \mathbf{R}^+, t \geq t_0, (u - u_e) \in \mathcal{X}_Q, |x_0 - x_e| \leq \alpha \\ y(t) &= Cx \in \mathcal{X}_e \end{aligned}$$

where $t_0$ and $x_0$ represent the time instant and initial state at which the input $u$ was applied. $(x_e, u_e)$ is an equilibrium point. The mappings from input to state and also from state to output are well defined provided that two assumptions are satisfied. (i) the initial $x_0$ at $t_0$ is within an $\alpha$-neighborhood of $x_e$, with the neighborhood defined according to the Euclidean norm in $\mathbf{R}^n$, and (ii) the input function $u$ is in a $Q$-neighborhood of $u_e$, with neighborhood defined in the sense of the binormed linear space $\mathcal{X}$.

As mentioned above, the main limitation of the classical input-output theory is that it cannot deal with the effect of non-zero initial conditions. However, by considering the system as a mapping from input to state, and then from state to output in the definition of a local linear time-invariant model, we not only keep the input-output formulation, but also easily incorporate the effect of non-zero initial conditions into the state equation. This makes the stability theory proposed in reference [29] overcome the drawback of the classical input-output theory. Furthermore, the definition 2.3.1 tries to emphasize that the local linear time-invariant model $H[x_e, u_e]$ is used to estimate the behavior of a more complex nonlinear system, about the equilibrium point $(x_e, u_e)$. It is also clear that when the size of the input function increases (*i.e.*, for large excursions from the equilibrium point), the error in the predictions obtained by this model will tend to increase as well. Thus the local linear time-invariant models are only valid, namely within the tolerance limit, for the well defined small space of input functions. This means a model should be considered along with some form of uncertainty description, as well as the space of the input functions for which the model is assumed to be valid.

In general, a local linear time-invariant model can be seen as a mapping from $\mathcal{X}_Q \rightarrow \mathcal{X}_e$. We can say that $H[x_e, u_e]$ is locally stable whenever $x(t)$ is a bounded subset of $\mathcal{X}_e$. More precisely,

**Definition 2.3.2** *$H[x_e, u_e]$ is said to be locally stable if*

$$u - u_e \in \mathcal{X}_Q, \ |x_0 - x_e| \leq \alpha \Rightarrow (x - x_e) \in \mathcal{X}_\alpha$$

In other words, a locally stable system is one where small signal inputs produce motions which have finite energy, and are also bounded within a defined amplitude.

### 2.3.3 Stability Analysis

In order to pursue the precise solution to the stability problem in gain scheduling method, we now introduce the concept of stable motion from $x_0$ to $x_f$.

**Definition 2.3.3** *A system is said to experience a stable motion from an initial state $x_0$ at $t = 0$ to a final state $x_f$ at $t = t_f$ if the following conditions are satisfied:*

1. *There are $m$ locally stable local models $H[x_{ei}, u_{ei}]$, $i = 1, 2, \ldots, m$, with $x_0 \in \mathcal{A}_1$, and $x_f \in \mathcal{A}_m$.*
2. *For each $t = t^*$ we have:*
   (a) *$x(t^*) \in \mathcal{A}_k$ for some $k = 1, 2, \ldots, m$.*
   (b) *$\exists \epsilon > 0 : \ (u(t) - u_{ek}(t)) \in \mathcal{X}([t^*, t])_{Qk}, \ t^* \leq t \leq t^* + \epsilon$.*

where $\mathcal{A}_k = \{x \in \mathbf{R}^n : \ |x - x_{ek}| \leq \alpha_k\}$, $k = 1, 2, \ldots, m$. This definition can be regarded as a generalization of the concept of stability along a trajectory in the sense of Lyapunov. There are several key elements in this concept. First, all of local models considered must be locally stable, in the sense of definition 2.3.2. Secondly, the condition 1 indicates that the initial state $x_0$ is in the domain of the first local model and the final state $x_f$ is in the image of the last model. Thirdly, the condition $2(a)$ implies that for each $t$, $x(t)$ must be in the domain of at least one of the local models. Furthermore, the condition $2(b)$ implies that the instantaneous value of the input function $u(t)$ must be in the domain of the same local model. Therefore, at any time, the instantaneous evolution of the state is captured by one of the local models.

The following is the most important stability theorem.

**Theorem 2.3.1** *Consider a physical system and m local models, $H[x_{ei}, u_{ei}]$, $i = 1, 2, \ldots, m$. If condition 1–2 below are satisfied, then it is possible to steer the system from an initial state $x_0 \in \mathbf{R}^n$ to a final state $x_f \in \mathbf{R}^n$ at $t = t_f$ following a stable motion.*

1. $x_0 \in \mathcal{A}_1$, $x_f \in \mathcal{A}_m$.
2. $\mathcal{A}_i \cap \mathcal{A}_{i+1} \neq \emptyset$, $i = 1, 2, \ldots, m-1$.

This theorem, together with the important concept of *stable motion* provides a precise solution to the stability problem in gain scheduling. Every local model can be seen as a mapping from an initial state $x_{0i}$, which near the equilibrium point $(x_{ei}, u_{ei})$, to a neighborhood $\mathcal{A}_i$ of $(x_{ei}, u_{ei})$ in the state space. An instance with two dimensional state space is shown in figure 2.2.

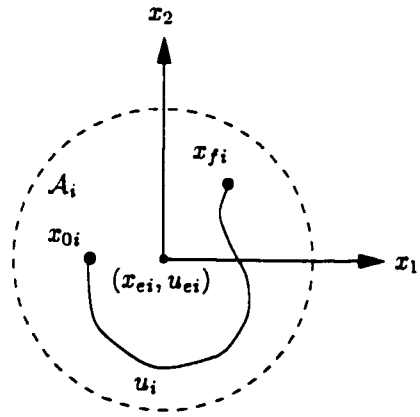


Figure 2.2: Local Model with Two Dimensional State Space

In practice, people are typically interested in making a physical system free to move around a region of state space, denoted by $\mathcal{M}$. If $m$ local models are available, according to the theorem 2.3.1, the following conditions will guarantee that the stable motions can occur between any two points in $\mathcal{M}$.

- $\mathcal{M} \in \bigcup_{i=1}^{m} \mathcal{A}_i$.

- Given any two points $x_0$, $x_f \in \mathcal{M}$, the $\mathcal{A}_i$ are such that

  1. $x_0 \in \mathcal{A}_i = \mathcal{A}_1$, (*i.e.*, $x_0$ belongs to some $\mathcal{A}_i$, denoted by $\mathcal{A}_1$).
  2. $x_f \in \mathcal{A}_k$, $1 \leq k \leq m$.
  3. $\mathcal{A}_i \cap \mathcal{A}_{i+1} \neq \emptyset$, $i = 1, 2, \ldots, k-1$.

This idea can be shown in figure 2.3 with two dimensional state space.

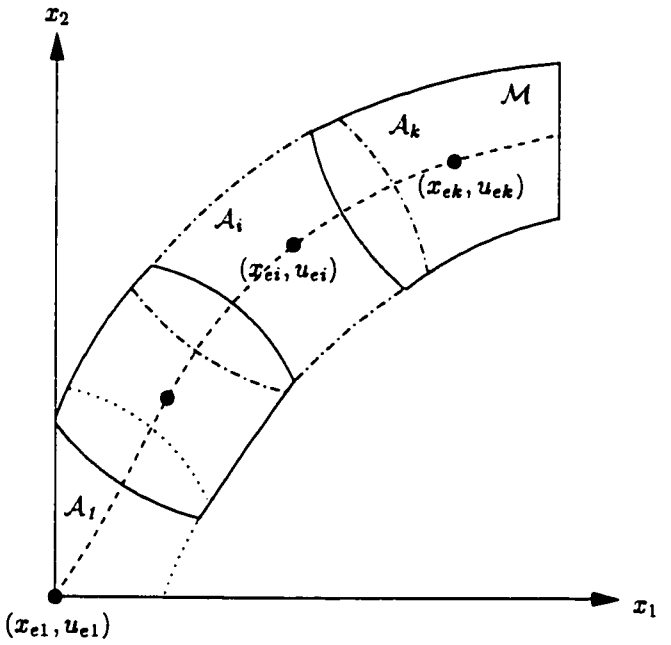


Figure 2.3: Multiple Local Models with Two Dimensional State Space

The theorem is a re-formulation of the classical input-output theory. It can be seen as a local version, which preserve the essential stability results from the classical theory. By using small signal analysis, it demonstrates that a model can be regarded as accurate with well defined model uncertainties, only if explicitly defining the class of input signals. This is because no model can remain accurate for arbitrarily large signals. This important idea which was overlooked by robust control theory is now presented in reference [29]. In this paper, local stability is defined with respect to the size of the input functions, thus it can be directly verified by user and enforced by designer. The paper also points out the key concept of stable motion between

two states and uses it in the study of stability of systems described by multiple local models. The application of this simple, yet complete characterization of the stability problem to gain scheduled control system will be discussed in following chapters.

# Chapter 3

# Motor

## 3.1 Introduction of Electrical Machinery

In general, an electrical machine can be defined as an apparatus that can be used either to convert electrical energy into mechanical energy or to convert mechanical energy into electrical energy. The former is called a motor; the latter is called a generator. The energy conversion in both of them is associated with the action of the magnetic field.

The use of electrical machines has been quickly and widely developed during this century. It makes our lives much more convenient than ever. There are three main classes of rotating electrical machines: (i) polyphase synchronous machines, (ii) polyphase induction (*i.e.*, asynchronous) machines, and (iii) direct-current (*i.e.*, dc) machines. Moreover, there are other rotating machines which operate basically on the same principles, such as rotating rectifier, permanent magnet machines and so on. A synchronous machine is an ac machine, which can work as a generator or as a motor. Typically, such machines are used as motors in constant speed drives in industrial applications. On the other hand, almost all three-phase power is generated by three-phase synchronous generators [26]. Even though the induction machines can be used as generators, their performance characteristics, especially in comparison to synchronous generators are not satisfactory for most applications. Thus, induction generators are occasionally used. However, because of their relatively low cost, simple

construction, minimal maintenance requirements, and good operating characteristics which satisfy a wide variety of loads, the induction motors are the most commonly used type of motors. Direct-current (*i.e.*, dc) machines are versatile. However, the use of dc machines as dc generators to produce bulk power has rapidly disappeared due to the economic advantages involved in the use of alternating-current generation, transmission, and distribution. Today, the need for dc power is often met by the use of solid-state-controlled rectifiers. Nevertheless, by means of various combinations of series and separately excited (shunt) field windings, dc motors can be designed to display a wide variety of volt-ampere or speed-torque characteristics for both dynamic and steady-state operation. They provide constant mechanical power output or constant torque, adjustable motor speed over wide ranges, precise speed or position control, efficient operation over a wide speed range, rapid acceleration and deceleration, and responsiveness to feedback signals. Because of these advantages, dc motors are still extensively used in many industrial applications: from fractional horsepower motors used in small mechanical systems to hundreds of watts and kilowatts servo systems and so on [14].

## 3.2 DC Motor Speed Control

The speed of dc motors can be controlled easily over a wide range above and below the rated speed. Speed control methods for dc motors are simpler and less expensive than those used for ac motors. The motor speed equation is known as follows [16]:

$$\omega = \frac{V_t - I_a \cdot R_a}{K_a \cdot \Phi_f}$$

where the speed of a dc motor depends on the applied terminal voltage $V_t$, the armature current $I_a$, the armature resistance $R_a$, and the field flux per pole $\Phi_f$. The parameter $K_a$ is the armature constant, which depends on the armature winding and cannot be changed to control the motor speed. By observing the speed equation, we can conclude that there are three most common speed control methods:

1. Field control method.
2. Armature resistance control method.

3. Armature voltage control method.

The Field control method is the simplest and cheapest method of all three and is most applicable to shunt motors. In this method, the armature resistance $R_a$ and the terminal voltage $V_t$ are kept constant. The armature current $I_a$ is fixed at the nameplate value in shunt motor. The speed is controlled by adjustment of the field current and hence the flux. Within the speed range, the back e.m.f. $E_a$ and the motor output $E_a \cdot I_a$ remain constant in shunt motor. Thus this speed control method is also called a constant power drive. Torque, however, varies directly with flux and hence has its highest allowable value at the lowest speed. Therefore, field control method is best suited for drives requiring increased torque at low speed.

The Armature resistance control method consists of obtaining reduced speed by the insertion of external series resistance in the armature circuit. In this method, the armature terminal voltage $V_t$, the field current $I_f$ thus the field flux $\Phi_f$ and the armature current $I_a$ are maintained constant at their rated values. The armature resistance control method can be used in series, shunt, and compound motors. It is simple to perform and requires a small initial investment. It offers a constant torque drive due to the constant armature current $I_a$ in the speed range. However, the considerable power loss in the external resistance and the overall low efficiency are the main disadvantages, especially when the speed is greatly reduced [35].

The Armature voltage control method is the most flexible method of speed control and avoids the disadvantages of power loss and low efficiency in armature resistance control method. The armature resistance $R_a$ and the field current $I_f$ are kept constant in this method, and the speed is controlled by varying the armature terminal voltage $V_t$. It can be applied to series, shunt, and compound motors. The speed is easily controlled from zero to maximum safe speed in either forward or backward directions. Therefore, this method has been widely used in practical industrial applications. The following sections in this chapter focus on armature voltage controlled series dc motor's parameter testing and model simulation.

## 3.3 Armature Voltage Controlled Series DC Motor

A series dc motor is a dc motor whose field winding is connected in series with the armature winding and therefore, its field current is the armature current. In the experiments, a small fractional horsepower portable dc machine set is used and the various dc and ac power supplies are obtained from the lab bench. The machine set consists of a dc motor which is connected mechanically to an electrodynamometer. The dynamometer is used to apply a load to the dc motor. It has a field on the stator, similar to that of a dc machine. The stator has a variable voltage supply which is obtained using a diode rectifier and a variac. The rotor consists of conductors similar to that of the cage induction machine. When these conductors rotate, they pass through the dc field of the stator and experience an induced voltage. The resultant current flowing through the rotor conductors dissipates power in the form of $I^2R$ Cu losses. This power is drawn from the dc motor and represents the load. Therefore, the dc motor load can be controlled via the dynamometer supply variac. The circuit is shown as figure 3.1:

The equations relating the variables of the series dc motor in figure 3.1 are:

$$V_t = E_a + I_a \cdot (R_a + R_s) + (L_a + L_s) \cdot \frac{dI_a}{dt} \tag{3.1}$$

$$J \cdot \frac{d\omega}{dt} = T_e - T_{load} - T_{loss} \tag{3.2}$$

In the above equations, $J$ is the rotor inertia and $T_e$ is the airgap torque. $T_{load}$ represents the output or load torque. $T_{loss}$ is the total torque loss by friction and windage and so on.

Consider the back e.m.f. voltage $E_a$ and the airgap torque $T_e$,

$$E_a = K_a \cdot \Phi_f \cdot \omega = K \cdot I_s \cdot \omega = K \cdot I_a \cdot \omega \tag{3.3}$$

$$T_e = \frac{E_a \cdot I_a}{\omega} = \frac{K \cdot I_a \cdot \omega \cdot I_a}{\omega} = K \cdot I_a^2 \tag{3.4}$$

Substituting the equations (3.3), (3.4) into (3.1) and (3.2), we get

$$V_t = K \cdot I_a \cdot \omega + I_a \cdot (R_a + R_s) + (L_a + L_s) \cdot \frac{dI_a}{dt} \tag{3.5}$$

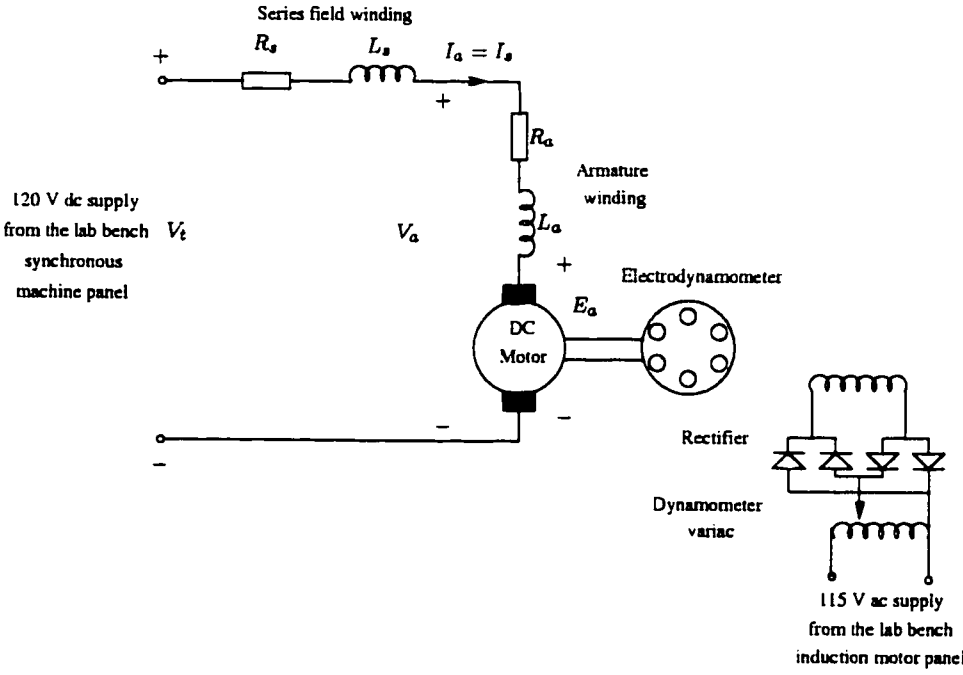


Figure 3.1: Circuit for Series DC Motor

$$J\frac{d\omega}{dt} = K \cdot I_a^2 - T_{load} - T_{loss} \tag{3.6}$$

Now, we want to obtain the state space model of the series dc motor from the circuit equations. When we use armature voltage control method, the armature terminal voltage $V_t$ is considered as control input, and of course the speed $\omega$ is the interested output. The armature current $I_a$ and speed $\omega$ can be seen as states. Substituting the following equations (3.7) into (3.10) to (3.5) and (3.6):

$$u = V_t \tag{3.7}$$

$$x_1 = I_a \tag{3.8}$$

$$x_2 = \omega \tag{3.9}$$

$$y = \omega \tag{3.10}$$

We get the state space model:

$$\dot{x_1} = -\frac{R_a + R_s}{L_a + L_s} \cdot x_1 - \frac{K}{L_a + L_s} \cdot x_1 \cdot x_2 + \frac{1}{L_a + L_s} \cdot u \tag{3.11}$$

$$\dot{x}_2 = \frac{K}{J} \cdot x_1^2 - \frac{T_{load} + T_{loss}}{J} \tag{3.12}$$

$$y = x_2 \tag{3.13}$$

where $K$, $J$, $R_a$, $R_s$, $L_a$, $L_s$,$T_{load}$ and $T_{loss}$ are constant coefficients.

By observing the above state space model, we can easily find that the armature voltage controlled series dc motor is a nonlinear system. In general, the speed of the series dc motor can start from zero to the maximum allowable speed in either forward or backward directions. Due to its nonlinearities and wide speed control range, this model can be regarded as a good control object to apply the gain scheduling method, so as to verify the control theory proposed by H. J. Marquez. Before starting the control system design, it is necessary to get the nonlinear model of the armature voltage controlled series dc motor. Therefore, we need to do a series of experiments in order to obtain all the constant coefficients in the state space model.

## 3.4 Experiments for Constant Coefficients

### 3.4.1 Measurements of Field and Armature Windings Resistance

First, the field and armature resistance are measured directly across each winding using a Fluke 25 meter. This gave the resistance when the motor was cool, namely before the motor was ran. However, these measured values would become inaccurate after the motor begins to run, because the current went through the windings generating heat and thus increasing the values of the field and armature resistance. So the values of them after the motor ran for 10 minutes need to be measured as well. This time, the resistance values are obtained by Ohm's law. In another words, tested the corresponding values of voltage and current, then used $R = \frac{V}{I}$ to get $R_a$ and $R_s$. When conducting these tests, attention should be made on the current going through the field and armature windings to make sure that it was within the maximum value. Otherwise, the excessive current would damage the field and armature windings of the dc motor. These experiments were conducted several times so as to acquire the average values for $R_a$ and $R_s$. In this way, the errors can be eliminated as

much as possible and more accurate nonlinear model for the series dc motor can be acquired. Tables A.1 and table A.2 are the measured and calculated values for field and armature resistance $R_s$ and $R_a$.

Average field resistance:

$$R_s = 1.9\Omega \tag{3.14}$$

Average armature resistance:

$$R_a = 8.6\Omega \tag{3.15}$$

### 3.4.2 Measurements of Field and Armature Windings Inductance

Since the armature and field current $I_a$ and $I_s$ vary when we adjust the speed of the series dc motor. The effect of field inductance $L_s$ and armature inductance $L_a$ in the circuit cannot simply be ignored. Therefore, it is necessary to measure the value of the inductance. Two methods have been used to measure the inductance in order to reduce the errors.

First, 115V ac supply from the lab bench induction motor panel was connected with the bridge rectifier circuit, which consisted of diodes. The output of the bridge rectifier was taken as the power supply to the armature winding. By adjusting the trigger circuit, various values of rectified dc voltage were obtained. It still included ac components. Then Fluke 39 meter together and another Fluke camp-on meter were used to measure the voltage and current of the armature winding at 0 Hz and 120 Hz frequencies. The formulas to calculate the inductance are as follows:

$$\frac{V_0}{I_0} = R_a \tag{3.16}$$

$$\frac{V_{120}}{I_{120}} = Z_{120} \tag{3.17}$$

$$(2 \cdot \Omega \cdot L_a)^2 + R_a^2 = Z_{120}^2 \tag{3.18}$$

where $\Omega = \pi \cdot 120 = 377$. Substituting the equations (3.16) and (3.17) into (3.18), I obtained the value of armature inductance $L_a$.

The second method was to introduce the ac power supply from the lab bench induction motor panel to the field winding. Regulated the induction motor panel variac so as to get a range of ac voltages. A Fluke 39 meter was used to measure the voltage, the current, and the angle out of phase with respect to each other at 60 Hz. Then the following formulas are used to calculate the field inductance:

$$\frac{V_{60}}{I_{60}} \cdot \cos\theta = R_s \tag{3.19}$$

$$\frac{V_{60}}{I_{60}} \cdot \sin\theta = X_s \tag{3.20}$$

$$\frac{X_s}{\Omega} = \frac{X_s}{377} = L_s \tag{3.21}$$

Now, the values of field and armature inductance $L_s$, $L_a$ have been acquired by two different methods. Both of experiments need to be repeated several times. The average values are used as the results. Tables A.3 and A.4 show the measured and calculated values.

Average field inductance:

$$L_s = 55mH \tag{3.22}$$

Average armature inductance:

$$L_a = 65mH \tag{3.23}$$

### 3.4.3 Measurements of Motor Constant

Observing the back e.m.f. voltage $E_a$ equation:

$$E_a = K_a \cdot \Phi_f \cdot \omega = K \cdot I_s \cdot \omega \tag{3.24}$$

We know that in order to get the value of motor constant $K$, we need to fix the speed of the motor $\omega$, namely the motor revolution $N_r$, then find the relationship between $I_s$ and $E_a$. This was achieved by a carefully designed experiment to acquire the $E_a - I_s$ curve.

In the experiment, the 0-24V dc supply from the lab bench synchronous machine panel was connected with the series field winding. This voltage is represented by $V_f$.

The 115V ac supply from the lab bench induction motor panel was introduced to the bridge rectifier circuit, which consisted of four diodes and the output of the bridge rectifier $V_a$ was connected with the dc motor armature winding. By controlling the synchronous machine panel variac, a variable voltage $V_f$ was obtained to make the series field current $I_s$ vary from 3.5A to 0A. Due to the changes in $I_s$, thus the field flux, the motor revolution $N_r$ would change correspondingly. In order to keep the motor revolution $N_r$ at the rated value 1200rpm, the trigger circuit had to be adjusted to change the output voltage of the bridge rectifier $V_a$ simultaneously. Hence the current which went through the dc motor armature winding $I_a$ would vary at the same time. Then using the following equation:

$$E_a = V_a - I_a \cdot R_a \tag{3.25}$$

The values of back e.m.f. $E_a$ corresponding to various field current $I_s$ was found. At this point, we make the following observations: First, there was no load in this experiment. The motor belt was even took off so as to reduce the influence from friction and so on. Second, the connection between the two joints of the field winding was switched, and the above procedure was repeated. Then, the average values of $I_s$ and corresponding $E_a$ were used as the data points for further analysis. Third, the motor revolution $N_r$ was measured by a frequency counter, which was connected to the connector on the dc machine apparatus. Since it was very difficult to fix the dc motor revolution $N_r$ at exact 1200rpm, I transfered the $E_a$ at, for example, 1210rpm to the $E'_a$ at 1200rpm by the following formula:

$$E'_a = E_a \cdot \frac{1200}{1210} \tag{3.26}$$

These experiments were repeated several times. Tables A.5 to A.13 are the measured and calculated values.

By using the averaged data of $\bar{I}_s$ and $\bar{E}_a$, we get groups of points. Then in MATLAB, the first-degree, second-degree, and even higher degree curves are fitted to the groups of data by the least-squares method, so as to get the best fitting curves. The plots for different groups of the measured and calculated values and the averaged curves are shown in figures B.1, B.2, B.3 and 3.2.

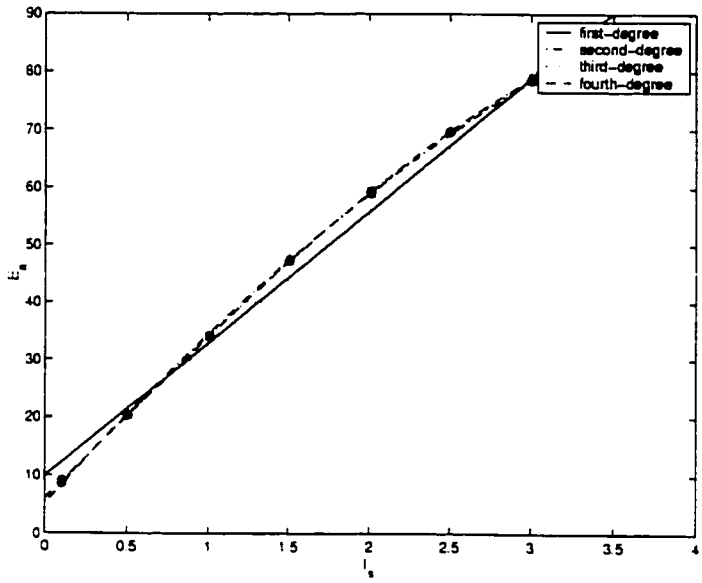


Figure 3.2: $E_a$ and $I_s$ Average Relationship ( No Load, No Belt and Speed = 1200 rpm )

According to figures B.1, B.2, B.3 and 3.2, which corresponding to the relationships of $E_a$ and $I_s$, I find that $E_a$ and $I_s$ are not related with a simple linear equation. Even though the first-degree line can be fitted to the data points, the sum of the squares of the errors is much higher than that of higher degree curves. Therefore, second-degree, third-degree, and even higher degree curves are fitted to the points. It turns out that there is no big difference in the sum of the squares of the errors between second-degree and higher degree curves. Thus, in order to reduce the errors between real world nonlinear system and the nonlinear model, as well as make the mathematical description concise, the second-degree curve is used to represent the relationship between $E_a$ and $I_s$:

$$\begin{aligned} E_a &= \frac{-2.4889 \cdot I_s^2 + 31.8393 \cdot I_s + 5.1727}{\omega_{1200}} \cdot \omega \\ &= \frac{-2.4889 \cdot I_s^2 + 31.8393 \cdot I_s + 5.1727}{125.6637} \cdot \omega \end{aligned} \tag{3.27}$$

### 3.4.4 Measurements of Motor Output or Load Torque

In order to obtain the relationship between the dc motor speed $\omega$ and the dc motor output or load torque $T_{load}$, the load part of the dc machine set, namely the electrodynamometer need to be studied. As mentioned earlier, the dynamometer is mechanically connected with the dc motor and works as the load. Its field winding on the stator has a variable voltage supply, obtained by the diode rectifier and the variac. When the percentage meter on the dynamometer is changed, actually, the variac is changed. Thus different field voltages are applied, in other word, various strengths of the field flux are applied. When the rotor is rotated by the dc motor, it passes through the field of the stator and experiences an induced voltage, which is related to the strength of the field flux and the speed of the dc motor $\omega$. The induced current flowing through the rotor conductors dissipates power in the form of $I^2R$ Cu losses. This power represents the load. The load torque can be read directly from the torque meter, which is attached to the dynamometer. By fixing the percentage meter at various graduation, namely, fixing the field flux and changing the dc motor speed $\omega$, the motor load torque $T_{load}$ can be represented as a function of dc motor speed $\omega$. Moreover, no matter what kind of connection between the field circuit and the armature circuit of the dc motor, for example, shunt/separately excited field winding or series field winding, there is no influence on the relationship between motor load torque $T_{load}$ and dc motor speed $\omega$.

The following experiments were conducted several times. 115V ac supply from the lab bench induction motor panel was introduced to the dynamometer variac. The percentage meter on the dynamometer was fixed at 40%, 30%, 20% and 10% separately. The dc source from the field supply on the lab bench dc machine panel was introduced to the shunt field winding of the dc motor. By adjusting the shunt field rheostat, the shunt field current was kept constant at approximate 0.4A, and 0-120V dc supply from the lab bench synchronous machine panel was connected with the dc motor armature winding. At first, the synchronous machine panel variac was set to zero, then applied power. The variac was adjusted gradually so as to obtain the dc motor revolution $N_r$ at approximate 100rpm, 200rpm,..., and 1200rpm. At the same time, the motor load torque $T_{load}$, the motor revolution $N_r$ and so on were written down. The circuit is shown as figure 3.3.

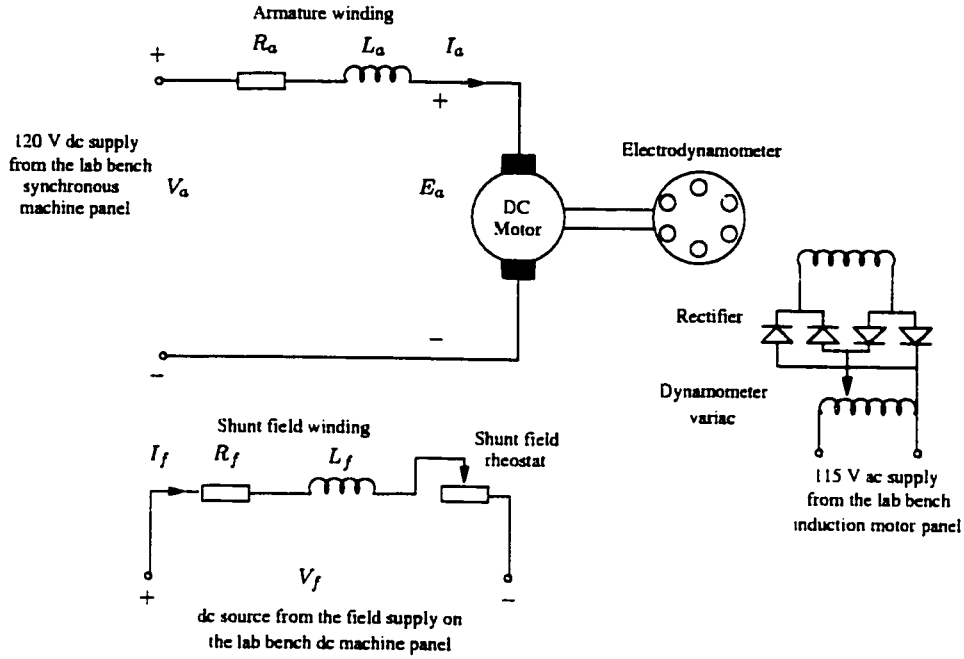


Figure 3.3: Circuit for Shunt/Separately Excited DC Motor

Tables A.14 to A.21 list the measured and calculated values. The formula of transferring the dc motor revolution $N_r$ to its speed $\omega$ is as follows:

$$\omega = N_r \cdot \frac{\pi}{30} \tag{3.28}$$

In MATLAB, the third-degree and higher degree curves are fitted to the measured and calculated values of different dynamometer field flux strengths by the least-squares method. The plots are shown in figures 3.4, B.4, B.5 and B.6.

From the motor load torque $T_{load}$ and motor speed $\omega$ plots shown in figures 3.4, B.4, B.5 and B.6, we can see that they had relatively complex relationships. The third-degree, fourth-degree and fifth-degree polynomials are fitted to the measured and calculated values, in order to make the sum of the squares of the errors smaller. Anyone of the dynamometer field flux strengths can be used in the further experiments. We select the 40% field flux strength. According to figure 3.4, the fourth-degree polynomial curve is more suitable to the measured and calculated values than others. Although the fifth-degree curve fits well, it also increases the

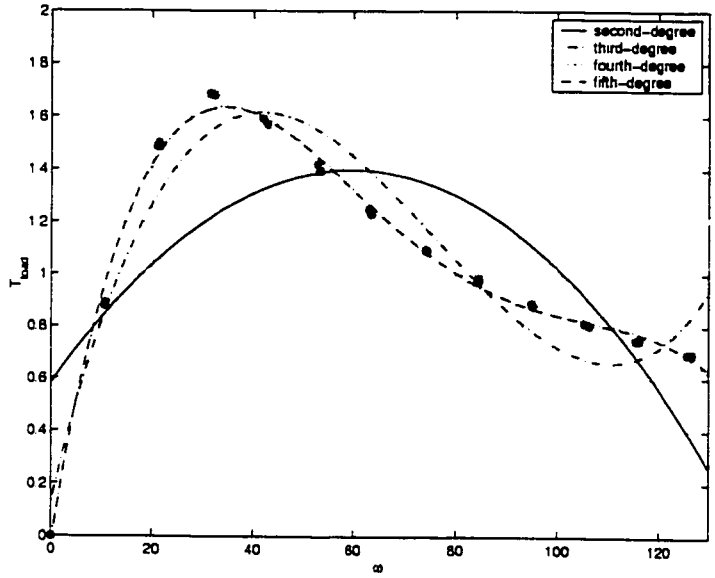


Figure 3.4: $T_{load}$ and $\omega$ Relationship ( Dynamometer Field Flux Strength: 40% )

complexity for application. Thus the fourth-degree curve is used as our $T_{load}$ and $\omega$ function. From the program written in MATLAB, we get:

$$T_{load} = -7.3401 \cdot 10^{-8} \cdot \omega^4 + 2.4414 \cdot 10^5 \cdot \omega^3 - 0.0028 \cdot \omega^2 + 0.1190 \cdot \omega - 0.0215 \quad (3.29)$$

### 3.4.5 Measurements of Total Motor Torque Loss

We know that except for the field winding loss, armature copper loss, and brush contact loss, there are torque loss due to friction and windage as well. For the purpose of measuring the total motor torque loss $T_{loss}$ as a function of the motor speed $\omega$, the following experiment were conducted in the circumstances of no load. Since the total motor torque loss $T_{loss}$ does not relate to the connection between the field circuit and the armature circuit, either shunt/separately excited field winding or series field winding can be used.

In the experiment, we chose the shunt/separately excited field winding. Its circuit is shown in figure 3.3. By adjusting the dc source from the field supply on the lab bench dc machine panel, the field current $I_f$ was kept at approximate 0.4A. The synchronous machine panel variac, namely the armature voltage $V_a$ was changed, so

as to make the motor revolution $N_r$ at approximate 1200rpm, 1100rpm,..., 100rpm. At the same time, the armature voltage $V_a$ and armature current $I_a$ were written down. Then the following calculation formulas are used to obtain the total motor torque loss $T_{loss}$ at the corresponding motor speed $\omega$.

$$E_a = V_a - I_a \cdot R_a \tag{3.30}$$

$$P_{loss} = E_a \cdot I_a \tag{3.31}$$

$$\omega = N_r \cdot \frac{\pi}{30} \tag{3.32}$$

$$T_{loss} = \frac{P_{loss}}{\omega} \tag{3.33}$$

The measured and calculated values are listed in the tables A.22 and A.23.

In MATLAB, the first-degree, second-degree, and third-degree polynomial curves are fitted to the above measured and calculated values by the least-squares method. Figure 3.5 shows the curves.

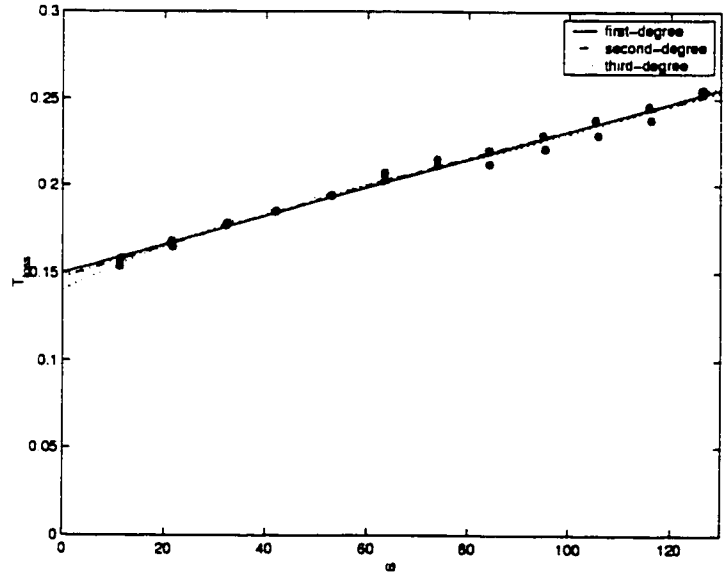


Figure 3.5: $T_{loss}$ and $\omega$ Average Relationship ( No Load and Keep Belt )

It is obvious that there is no much difference between the first-degree curve and higher degree curves. In order to keep the mathematical description of the nonlinear system concise, the first-degree curve is chosen to represent the relationship between

the total motor torque loss $T_{loss}$ and the motor speed $\omega$. Thus, the following equation is obtained:

$$T_{loss} = 0.0008 \cdot \omega + 0.1499 \tag{3.34}$$

### 3.4.6 Measurements of Rotor Inertia

In order to measure the rotor inertia $J$, at first, we want to get the decreasing curve of motor revolution $N_r$ with respect to the time $t$ after the power to the field circuit and the armature circuit is turned off. However, the equipment is a small fractional horsepower portable dc machine set. Its rotor inertia $J$ is quite small and it only takes the motor a few seconds to stop after turn off the power. Thus it is impossible to precisely write down the motor revolution $N_r$ at different time before the motor stops. It is easier to estimate how long it will take for the motor to stop after cutting off the power. Hence, another method is used to measure the rotor inertia $J$.

Under the circumstances of no load, the motor was run at the rated speed, namely 1200rpm. Then the power supplies to both the field circuit and the armature circuit were turned off. A stopwatch was used to see how long it would take for the motor to stop, for example, $t_0$ seconds. From the total motor torque loss measurements, we have already known the function of $T_{loss}$ and the motor speed $\omega$, which is shown in equation (3.34). After cutting off the power supplies to the motor circuits, the friction and windage make the motor stop. Therefore, the following equation is obtained:

$$T_{loss} = J \cdot \frac{d\omega}{dt} \tag{3.35}$$

Substituting (3.34) into (3.35), we get:

$$J \cdot \frac{d\omega}{dt} = 0.0008 \cdot \omega + 0.1499 \tag{3.36}$$

It is easy to see that the motor speed $\omega$ is a function of time $t$ and an unknown constant $J$. Solve the above differential equation (3.36) analytically by using MAPLE and get the function $\omega(t, J)$. As measured early, it takes $t_0$ seconds for the motor to stop after cut off the power. Thus substituting $t_0$ into the function $\omega(t, J)$, we get:

$$\omega(t_0, J) = 0 \tag{3.37}$$

Solve the equation (3.37) again using MAPLE, the constant rotor inertia $J$ is obtained:

$$J = 0.0062Kg \cdot m^2 \tag{3.38}$$

## 3.5 Analysis of Series DC Motor Characteristics

### 3.5.1 Series DC Motor Power Flow and Efficiency

Consider the circuit diagram of the series dc motor shown in 3.1, the power flow diagram of the motor is shown in figure 3.6.

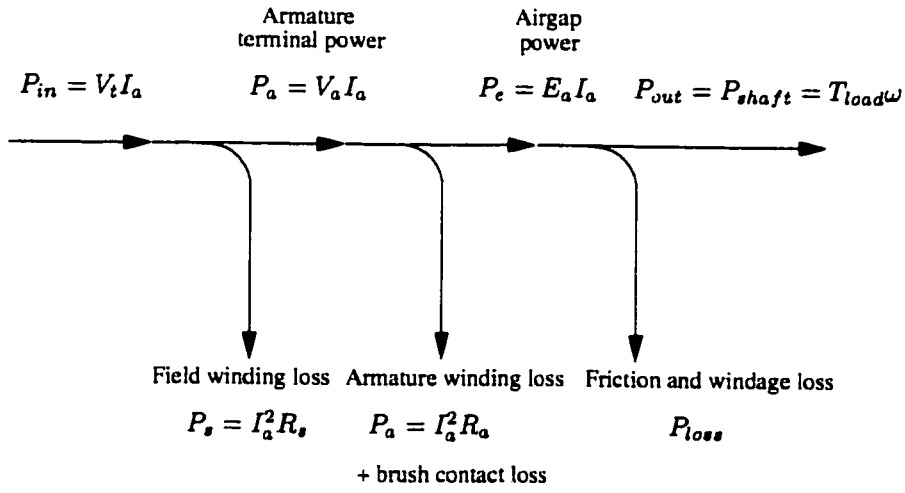


Figure 3.6: Power Flow of Series DC Motor

The efficiency of the series dc motor can be determined from:

$$Efficiency = \frac{P_{out}}{P_{in}} \tag{3.39}$$

Thus, the percentage efficiency can be expressed as:

$$\eta = \frac{P_{out}}{P_{in}} \cdot 100\% \tag{3.40}$$

### 3.5.2 Series DC Motor Speed, Current and Torque Characteristics

In order to study the series dc motor characteristics of the speed $\omega$ or the revolution $N_r$, the armature current $I_a$ and the airgap torque $T_e$, the following experiments were conducted. The 115V ac supply from the lab bench induction motor panel was applied to the dynamometer, which worked as the load to the series dc motor. The dynamometer variac was set to the lowest point. Then connected the series dc motor as shown in the 3.1. The synchronous machine panel variac was changed so as to maintain the terminal voltage $V_t$ at 100V. The dynamometer variac was used to vary the machine load, thus different armature currents $I_a$ were obtained. At the same time, the terminal voltage had to be kept constant at 100V. The armature current $I_a$, the motor revolution $N_r$ and the motor load torque $T_{load}$ were recorded. Then the terminal voltage $V_t$ was maintained at 75V, 50V, and 25V separately, and the similar experiments were repeated several times. By using the following formulas, the back e.m.f. $E_a$ and the airgap torque $T_e$ are determined:

$$E_a = V_t - I_a \cdot (R_a + R_s) \tag{3.41}$$

$$T_e = \frac{E_a \cdot I_a}{N_r \cdot \frac{\pi}{30}} \tag{3.42}$$

The measured and calculated values are shown in tables A.24 to A.31.

According to the measured and calculated values, we draw the plots of $\omega - T_e$, $\omega - I_a$, and $T_e - I_a$ using MATLAB. In each plot, different degrees of polynomial curves are fitted to the measured and calculated values, when the terminal voltage $V_t$ is equal to 100V, 75V, 50V, and 25V separately. The plots are shown in figures 3.7, 3.8 and 3.9.

These plots give us clear idea about how the motor speed $\omega$, the airgap torque $T_e$, and the armature current $I_a$ relate to each other in series dc motor.

### 3.5.3 Nonlinear Model from Experiments

According to the above experiment results, I substitute the measured and calculated data and estimated functions in equations (3.14), (3.15), (3.22), (3.23), (3.27), (3.29),

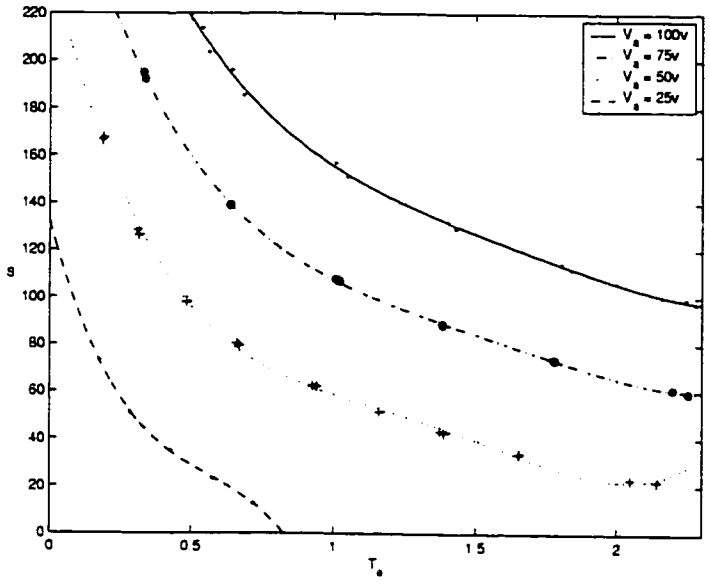


Figure 3.7: $\omega$ and $T_e$ Relationships ( $V_t$ = 100v, 75v, 50v, 25v )

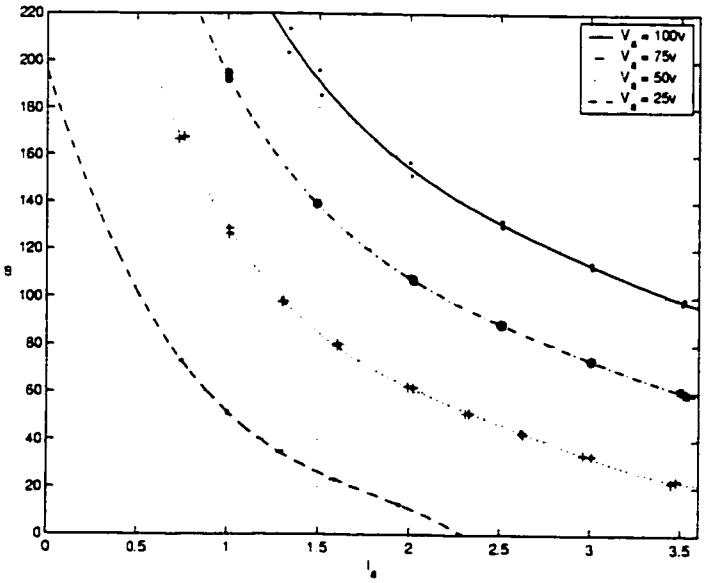


Figure 3.8: $\omega$ and $I_a$ Relationships ( $V_t$ = 100v, 75v, 50v, 25v )

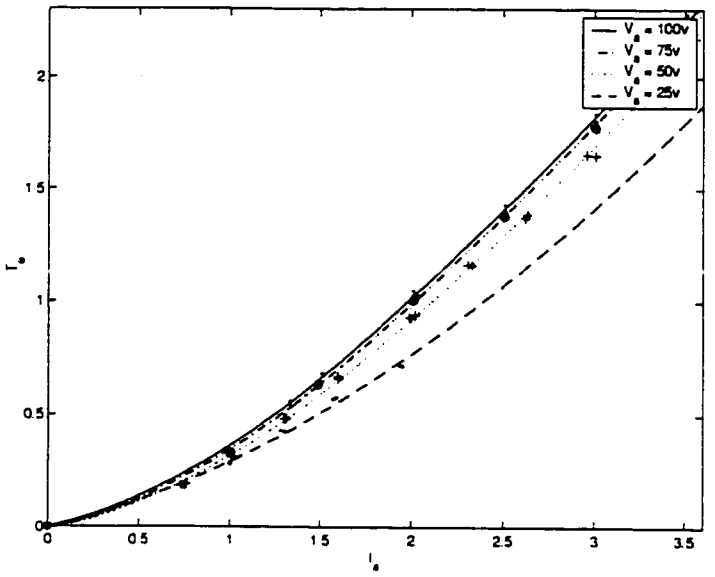


Figure 3.9: $T_e$ and $I_a$ Relationships ( $V_t$ = 100v, 75v, 50v, 25v )

(3.34) and (3.38) into the state space model (3.11) and (3.12). Therefore, we have the mathematical nonlinear state space model:

$$\begin{aligned}
\dot{x}_1 &= -\frac{R_a + R_s}{L_a + L_s} \cdot x_1 - \frac{K(I_a)}{L_a + L_s} \cdot x_2 + \frac{1}{L_a + L_s} \cdot u \\
&= -\frac{10.5}{0.12} \cdot x_1 - \frac{-2.4889 \cdot x_1^2 + 31.8393 \cdot x_1 + 5.1727}{0.12 \cdot 125.6637} \cdot x_2 + \frac{1}{0.12} \cdot u \\
&= -87.5 \cdot x_1 + 0.16505031 \cdot x_1^2 \cdot x_2 - 2.1114092 \cdot x_1 \cdot x_2 \\
&\quad -0.343025 \cdot x_2 + 8.33 \cdot u \qquad (3.43) \\
\dot{x}_2 &= \frac{K(I_a)}{J} \cdot x_1 - \frac{T_{load} + T_{loss}}{J} \\
&= \frac{-2.4889 \cdot x_1^2 + 31.8393 \cdot x_1 + 5.1727}{0.0062 \cdot 125.6637} \cdot x_1 \\
&\quad -\frac{1}{0.0062}(-7.3401 \cdot 10^{-8} \cdot x_2^4 + 2.4414 \cdot 10^{-5} \cdot x_2^3 - 0.0028 \cdot x_2^2 \\
&\quad +0.1190 \cdot x_2 - 0.0215 + 0.0008 \cdot x_2 + 0.1499) \\
&= -3.194522081 \cdot x_1^3 + 40.86598372 \cdot x_1^2 + 6.639199794 \cdot x_1 \\
&\quad +1.1838871 \cdot 10^{-5} \cdot x_2^4 - 3.937742 \cdot 10^{-3} \cdot x_2^3 + 0.451613 \cdot x_2^2 \\
&\quad -19.32258 \cdot x_2 - 20.71 \qquad (3.44)
\end{aligned}$$

Using SIMULINK toolbox in MATLAB, we build the block diagram of the nonlinear model for the series dc motor, which is our plant. The diagram is shown in figure 3.10.

In order to confirm the correctness of the nonlinear model, some experiments were performed. At first, the series dc motor was connected as in figure 3.1. 0-120V dc supply from the lab bench synchronous machine panel was introduced as the control input voltage. The 115V ac supply from the lab bench induction motor panel was given to the dynamometer, which worked as the load. The percentage meter on the dynamometer was fixed at 40%, *i.e.*, 40% strength of the field flux was applied. Then by tuning the control input voltage $V_t$ at various values, the corresponding armature current $I_a$ and motor revolution $N_r$, namely motor speed $\omega$ were obtained. These measured values were recorded. The above experiments were repeated. The measured and calculated values are shown in the tables A.32 and A.33.

In the simulation, I introduced the same control input voltage $V_t$ as the different values which were given to the real series dc motor in the former experiment, to the nonlinear model. By using the nonlinear model, which was built in MATLAB, I simulated the real series dc motor performance in a computer and wrote down the simulation results of the armature current $I_a$ and the motor speed $\omega$ in the following tables A.34 and A.35.

According to the measured data from the real series dc motor and the simulated data from the nonlinear model, different degrees of polynomials are fitted to the points by the least-squares method. The plots of $I_a - V_c$ and $\omega - V_c$ averaged relationships are shown separately in figure B.7 and figure B.8.

Comparing the averaged relationships of $I_a - V_c$ and $\omega - V_c$ between measured data and simulated data, we can find that there is no big difference between them. For the purpose of having quantitative estimation of their difference, the bar graphs of absolute errors and relative errors for $I_a - V_c$ and $\omega - V_c$ curves are shown in figure B.9 to figure B.16.

From the calculation, we know that there is less than 10% relative errors in the armature current $I_a$ and the motor speed $\omega$ between the real series dc motor and the nonlinear model. It is within the accuracy of our requirements. Therefore,

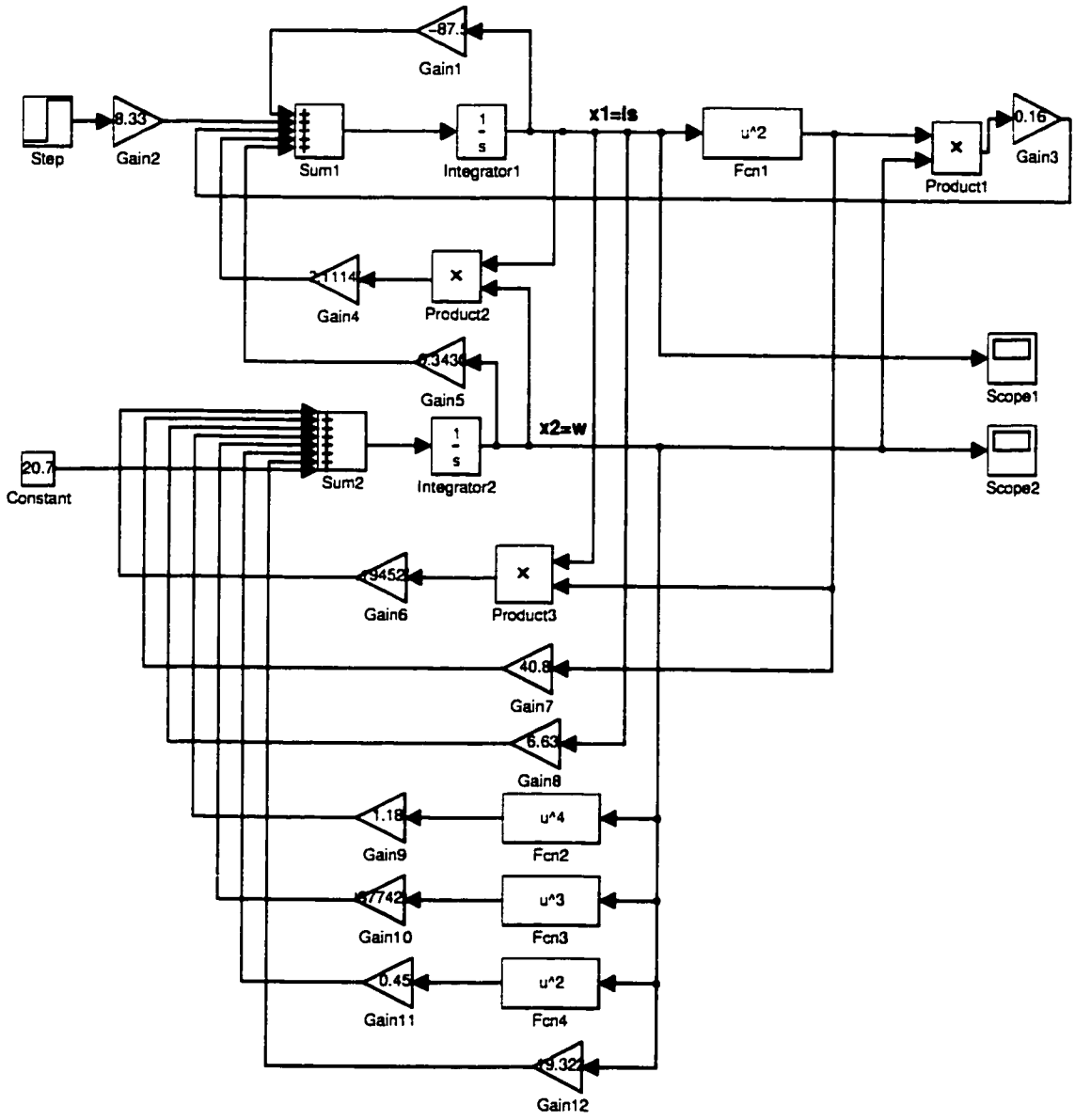


Figure 3.10: Block Diagram of Nonlinear Model for Series DC Motor

the nonlinear model will represent the real series dc motor in future control system design.

# Chapter 4

# Model Linearization

## 4.1 Linearization and Equilibrium Points

In chapter 3, we obtained the mathematical nonlinear state space model, described by equations (3.43) and (3.44). It is quite difficult to directly design a nonlinear controller for this nonlinear plant. According to the control theory explained in chapter 2, instead of dealing with the complicated nonlinear model, we linearize it at different operating points, so as to get a number of linearized models. Then the powerful linear control design techniques can be applied to each linear model with respect to various design requirements.

Consider a non-autonomous nonlinear system with the control input $\mathbf{u}$ and assume that $\mathbf{f}(\mathbf{x}, \mathbf{u})$ is continuously differentiable:

$$\dot{\mathbf{x}} = \mathbf{f}(\mathbf{x}, \mathbf{u}) \tag{4.1}$$

Using Taylor expansion at the equilibrium point $(\mathbf{x_e}, \mathbf{u_e})$, such that $\mathbf{f}(\mathbf{x_e}, \mathbf{u_e}) = \mathbf{0}$, then

$$\begin{aligned} \dot{\mathbf{x}} &= \mathbf{f}(\mathbf{x_e}, \mathbf{u_e}) + \left(\frac{\partial \mathbf{f}}{\partial \mathbf{x}}\right)_{\mathbf{x_e}, \mathbf{u_e}} \cdot (\mathbf{x} - \mathbf{x_e}) + \left(\frac{\partial \mathbf{f}}{\partial \mathbf{u}}\right)_{\mathbf{x_e}, \mathbf{u_e}} \cdot (\mathbf{u} - \mathbf{u_e}) + \mathbf{f}_{h.o.t.}(\mathbf{x}, \mathbf{u}) \\ &= \left(\frac{\partial \mathbf{f}}{\partial \mathbf{x}}\right)_{\mathbf{x_e}, \mathbf{u_e}} \cdot (\mathbf{x} - \mathbf{x_e}) + \left(\frac{\partial \mathbf{f}}{\partial \mathbf{u}}\right)_{\mathbf{x_e}, \mathbf{u_e}} \cdot (\mathbf{u} - \mathbf{u_e}) + \mathbf{f}_{h.o.t.}(\mathbf{x}, \mathbf{u}) \end{aligned} \tag{4.2}$$

where $\mathbf{f}_{h.o.t.}$ stands for higher-order terms in $\mathbf{x}$ and $\mathbf{u}$. Let $\mathbf{A}$ denotes the Jacobian

matrix of $\mathbf{f}$ with respect to $\mathbf{x}$ at the equilibrium point $(\mathbf{x_e}, \mathbf{u_e})$, and $\mathbf{B}$ denotes the Jacobian matrix of $\mathbf{f}$ with respect to $\mathbf{u}$ at the same equilibrium point $(\mathbf{x_e}, \mathbf{u_e})$:

$$\mathbf{A} = \left(\frac{\partial \mathbf{f}}{\partial \mathbf{x}}\right)_{\mathbf{x_e},\mathbf{u_e}} \tag{4.3}$$

$$\mathbf{B} = \left(\frac{\partial \mathbf{f}}{\partial \mathbf{u}}\right)_{\mathbf{x_e},\mathbf{u_e}} \tag{4.4}$$

If the dimension of the state vector $\mathbf{x}$ is $n$, and the dimension of the input vector $\mathbf{u}$ is $m$, then $\mathbf{A}$ is an $n \times n$ matrix of elements $\frac{\partial f_i}{\partial x_j}$, $i = 1, \ldots, n$, $j = 1, \ldots, n$, and $\mathbf{B}$ is an $n \times m$ matrix of elements $\frac{\partial f_i}{\partial u_j}$, $i = 1, \ldots, n$, $j = 1, \ldots, m$. Substituting the equations (4.3) and (4.4) into (4.2), and omitting the higher-order terms in $\mathbf{x}$ and $\mathbf{u}$, we get:

$$\dot{\mathbf{x}} = \mathbf{A} \cdot (\mathbf{x} - \mathbf{x_e}) + \mathbf{B} \cdot (\mathbf{u} - \mathbf{u_e}) \tag{4.5}$$

Suppose:

$$\Psi = \mathbf{x} - \mathbf{x_e} \tag{4.6}$$

$$\Upsilon = \mathbf{u} - \mathbf{u_e} \tag{4.7}$$

We have:

$$\dot{\mathbf{x}} = \mathbf{A} \cdot \Psi + \mathbf{B} \cdot \Upsilon \tag{4.8}$$

This is the linearization of the original non-autonomous nonlinear system (4.1) at the equilibrium point $(\mathbf{x_e}, \mathbf{u_e})$. It is obvious that the system (4.8) is a local linear time-invariant system. In the following sections in this chapter, the above linearization method is applied in a computer so as to extract the local linear models. However, before starting the linearization, we need to acquire the equilibrium points of the nonlinear model for different control input signals.

At first, the performance of the nonlinear model is simulated in a computer when the control input voltage $u_e = 0V, 0-1V, \ldots, 84-85V$. At each control voltage, after the step input signal is given to the nonlinear system at time $t = t_0$, the step response of the system is recorded for 20 seconds. In fact, except for small numerical errors, the system can be assumed to be in steady state after 1 or 2 seconds.

In order to check whether the results are correct or not, we substitute the values of the equilibrium point $(\mathbf{x_e}, u_e)$ into the state space function $\mathbf{f}(\mathbf{x_e}, u_e)$. we find that when the input voltage $u_e$ increases, the value of the state space function $\mathbf{f}(\mathbf{x_e}, u_e)$ increases as well. When $u_e$ is $85V$, the norm of $\mathbf{f}(\mathbf{x_e}, u_e)$ becomes 0.53159. However, according to the definition of the equilibrium point, the value of the function $\mathbf{f}(\mathbf{x_e}, u_e)$ should be equal to zero. This means that the above method for calculating the equilibrium points of the nonlinear model is not very accurate. Therefore, a better method needs to be considered.

We use MAPLE instead of MATLAB in our calculation. For the non-autonomous nonlinear system, after the input voltage $u_e$ is given, we solve the following equations:

$$\mathbf{f}(\mathbf{x_e}, u_e) = 0 \tag{4.9}$$

Thus we obtain the values of the steady state $\mathbf{x_e}$, namely the corresponding equilibrium point $(\mathbf{x_e}, u_e)$. The disadvantage of this method is that there exist many groups of numerical solutions for equations (4.9) at each input value $u_e$. But there is only one group of values which is correct from practical point of view among all of the solutions. In order to find out which group of values is the real solution, we need to compare all of them with the approximate solution which is got by the simulation method. Then, we can determine the equilibrium point $(\mathbf{x_e}, u_e)$.

We also substitute the final result $\mathbf{x_e}$ into the equation (4.9), and find that the second method is much more accurate than the first one. For example, when the input voltage $u_e$ is $85V$, the norm of $\mathbf{f}(\mathbf{x_e}, u_e)$ is 0.00187. Therefore, we use the second method with the help of the first one to calculate the equilibrium points $(\mathbf{x_e}, u_e)$ of the nonlinear model at different input voltages $u_e$. The results are shown in tables A.36 and A.37.

## 4.2 First Local Linearized Model

According to the linearization analysis in the above section, it is implemented in a computer by MATLAB functions. The first local linearized model is shown as below:

$$\dot{\mathbf{x}} = \mathbf{A_1} \cdot \mathbf{\Psi} + \mathbf{B_1} \cdot \Upsilon \tag{4.10}$$

$$\dot{\mathbf{x}} = \begin{pmatrix} -87.5851 & -1.6751 \\ 56.7877 & -19.2820 \end{pmatrix} \cdot \Psi + \begin{pmatrix} 8.3333 \\ 0 \end{pmatrix} \cdot \Upsilon \tag{4.11}$$

Its block diagram is built by using SIMULINK toolbox in MATLAB. The diagram is shown in figure 4.1.

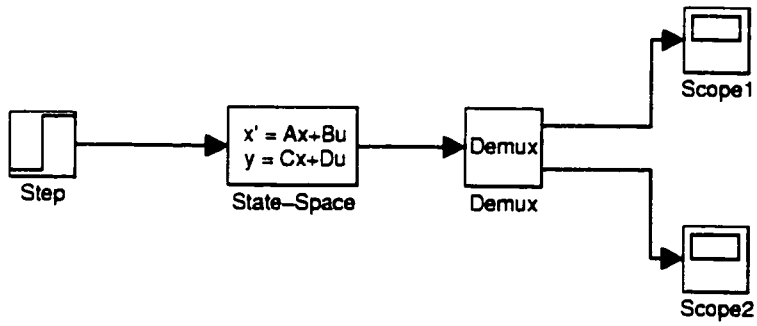


Figure 4.1: Block Diagram of Local Linear Model

Similar to the nonlinear model, the performance of local linear model can be simulated in a computer. When different control input voltages are given to it, the mean values of the steady state are calculated. However, like the nonlinear model, the results obtained in this way are not very accurate. Therefore, MAPLE is used to solve the linear equations:

$$\mathbf{A_1} \cdot \Psi + \mathbf{B_1} \cdot \Upsilon = 0 \tag{4.12}$$

where $\Upsilon = 0V, 1V, 2V, \ldots$ This method gives us unique and more accurate results at various values of $\Upsilon$.

For this local linear model, because we linearized the nonlinear model at the equilibrium point:

$$\mathbf{x_{e1}} = \begin{pmatrix} 0.6655 \\ 0.0450 \end{pmatrix} \tag{4.13}$$

when

$$u_{e1} = 7V \tag{4.14}$$

Substituting the above equations into (4.6) and (4.7), we obtain:

$$\mathbf{x} = \Psi + \mathbf{x_{e1}}$$

$$= \begin{pmatrix} \Psi_1 + 0.6655 \\ \Psi_2 + 0.0450 \end{pmatrix} \quad (4.15)$$

$$u = \Upsilon + u_{e1} = \Upsilon + 7 \quad (4.16)$$

This means that we need to add the values of the equilibrium point of the nonlinear model to the steady states of the local linear model, so as to get the real values of the states. The table A.38 shows the steady values for both $\Psi$ and $\mathbf{x}$.

In order to compare the steady state values of the first local linear model with those of the nonlinear model, when the control input voltage $u = 7V, 8V, \ldots$, we calculate the relative errors of them using the following equations:

$$\sigma_1 = \frac{|x_{1_linear} - x_{1_nonlinear}|}{x_{1_nonlinear}} \quad (4.17)$$

$$\sigma_2 = \frac{|x_{2_linear} - x_{2_nonlinear}|}{x_{2_nonlinear}} \quad (4.18)$$

We find out that when the control input voltage $u = 7V$ and $8V$, both of the relative errors are less than 5%, which satisfy our requirement. However, if the input voltage goes up to $9V$, the $\sigma_1$ is still less than 5%; the $\sigma_2$ will become approximate to 8.5%. Thus, the second local linearized model needs to be found so as to satisfy our requirements.

## 4.3 Second Local Linearized Model

The similar procedure is applied to linearize the nonlinear model at the equilibrium point:

$$\mathbf{x_{e2}} = \begin{pmatrix} 0.7548 \\ 0.3238 \end{pmatrix} \quad (4.19)$$

when

$$u_{e2} = 8V \quad (4.20)$$

Then, we have the second local linearized model:

$$\dot{\mathbf{x}} = \mathbf{A_2} \cdot \Psi + \mathbf{B_2} \cdot \Upsilon \quad (4.21)$$

$$\dot{\mathbf{x}} = \begin{pmatrix} -88.1030 & -1.8427 \\ 62.8708 & -19.0313 \end{pmatrix} \cdot \Psi + \begin{pmatrix} 8.3333 \\ 0 \end{pmatrix} \cdot \Upsilon \quad (4.22)$$

It has the similar block diagram as the first one, which is built in the computer as well. We also used MAPLE to calculate the steady states of the second local linear model, when $\Upsilon = -1V, 0V, 1V, \ldots$ The equilibrium point in equations (4.19) and (4.20) are substituted into (4.6) and (4.7), we have:

$$\begin{aligned} \mathbf{x} &= \Psi + \mathbf{x_{e2}} \\ &= \begin{pmatrix} \Psi_1 + 0.7548 \\ \Psi_2 + 0.3238 \end{pmatrix} \qquad (4.23) \\ u &= \Upsilon + u_{e2} = \Upsilon + 8 \qquad (4.24) \end{aligned}$$

Adding the values of the equilibrium point of the nonlinear model to the steady states of the local linear model, we get the table A.39.

The equations (4.17) and (4.18) are applied to the second local linear model and the nonlinear model, when the control input voltage $u = 7V, 8V, \ldots$ We find that after the input voltage increases to $11V$, the $\sigma_2$ becomes 8.5%. But when the control input voltage $u = 8V, 9V$ and $10V$, all the relative errors are less than 5%. Moreover, the operating range of the second local linear model overlaps with that of the first local linear model, when the control input voltage $u \in [7.9\ 8.1]$. All of these satisfy our requirements for valid local linear models. Therefore, we keep these two local models and find all the other linearized models as well.

## 4.4 Other Local Linearized Models

Applying the same method of linearization and calculation as we used in the first and the second local linear models, we obtain other local linear models at different equilibrium points. They have the same values of matrix **B**:

$$\mathbf{B} = \begin{pmatrix} 8.3333 \\ 0 \end{pmatrix} \qquad (4.25)$$

However, the values of matrix **A** are different from each other. These are shown in the tables A.40 and A.41:

All of these local linear models have the similar block diagram as figure 4.1. And their steady state values can be calculated in MAPLE, when different control

input voltages $u$ are introduced to the linear system separately. With the addition of the corresponding equilibrium point of the nonlinear model to the steady states of the local linear model, the final state values for each linear system are obtained. They are all shown in table A.42 to table A.53.

The equations (4.17) and (4.18) are used to the local linear systems and the nonlinear model to calculate the relative errors between them at various control input voltage $u$. We try to make sure that the errors are within 5%. Furthermore, we also ensure that any two neighbouring local linear models intersect with each other.

There are fourteen local linear models altogether. In order to compare the steady state values of the local linear systems and the nonlinear model, we draw figure 4.2.

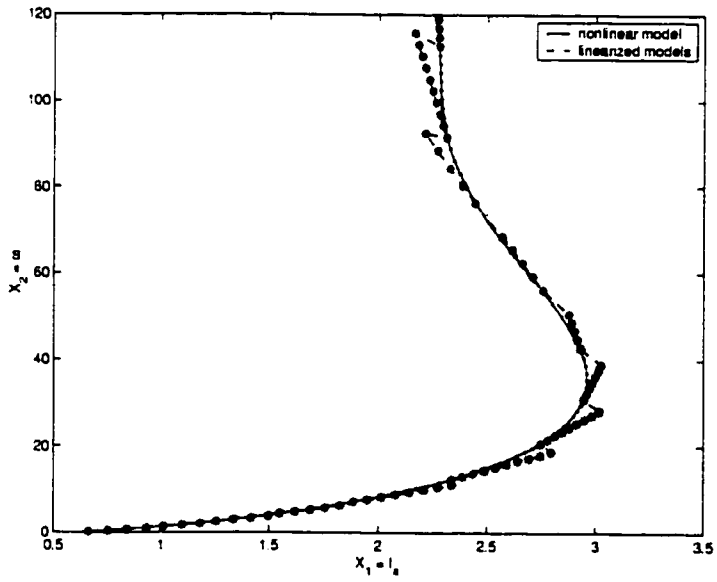


Figure 4.2: Compare the Relationship of $I_a$ and $\omega$ between Nonlinear Model and Linearized Models

The bar graphs of the relative errors between the nonlinear model and the local linear approximations for the armature current $I_a$ and the motor speed $\omega$ are shown separately in figure B.17 and figure B.18.

At this point, all of the local linearized approximations are obtained from the nonlinear plant. A powerful linear control design technique can be used to these linear

models.

# Chapter 5

# Control System Design

## 5.1 $H_\infty$ Optimal Control System

For purpose of analysis and design, we consider the standard continuous-time control system, which has the idealized form shown in figure 5.1 [10].

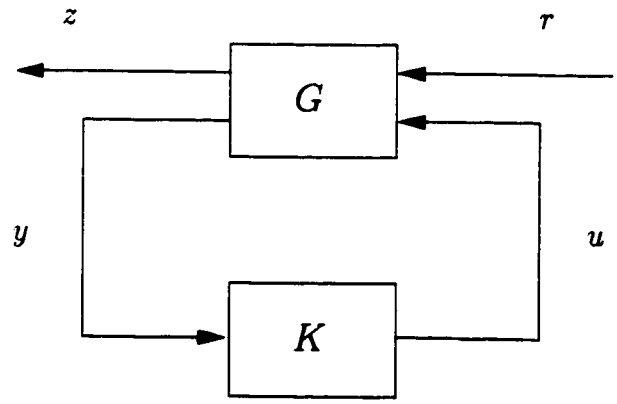


Figure 5.1: Standard Continuous-Time Control System

The $z$, $y$, $r$ and $u$ are continuous-time signals, whose amplitudes can be any real numbers. $z$ represents the signal to be controlled; $y$ is the measured signal, namely the input signal to the controller $K$; $r$ represents the exogenous input to the system, including reference command, disturbance and sensor noise; and $u$ is the control input, namely the input signal to the generalized plant $G$.

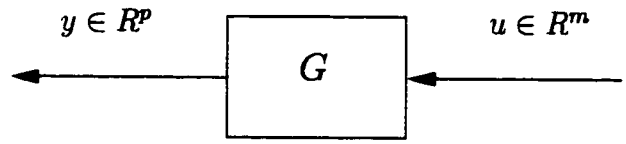


Figure 5.2: Control System

As we know, for the system in figure 5.2, the $H_\infty$ norm of $G$ is defined in equation (5.1).

$$\|\hat{g}\|_\infty = \sup_\omega \sigma_{max}[\hat{g}(j\omega)] \tag{5.1}$$

where $\hat{g}(s)$ is a $p \times m$ complex transfer matrix. $p$ is the dimension of the system output and $m$ is the dimension of the system input. $\sigma_{max}[\hat{g}(j\omega)]$ denotes the maximum singular value of $\hat{g}(j\omega)$. The $H_\infty$ norm of the transfer matrix $\hat{g}(s)$ has the important property:

$$\|\hat{g}\|_\infty = \sup\{\|y\|_2 : \|u\|_2 = 1\} \tag{5.2}$$

this means that the $H_\infty$ norm equals the system's gain, that is, maximum $L_2$ norm of the output over all inputs of unit norm. It is a worst-case system gain for unknown inputs.

Consider the standard control system in figure 5.1. Let $G_{zr}$ denotes the closed-loop system from $r$ to $z$, with transfer matrix $\hat{g}_{zr}(s)$. The $H_\infty$ optimal control problem is to compute an internally stabilizing controller $K$ that minimizes $\|\hat{g}_{zr}\|_\infty$.

For a linear generalized system $G$, it has four types of external variables: $z$, $y$, $r$ and $u$. They are correlated through the linear state space equation:

$$G = \left(\begin{array}{c|c} A & B \\ \hline C & D \end{array}\right) \tag{5.3}$$

Because the input and output of $G$ are partitioned as $\begin{pmatrix} r \\ u \end{pmatrix}$ and $\begin{pmatrix} z \\ y \end{pmatrix}$, we have

$$G = \left(\begin{array}{c|cc} A & B_1 & B_2 \\ \hline C_1 & D_{11} & D_{12} \\ C_2 & D_{21} & D_{22} \end{array}\right) \tag{5.4}$$

In our case, $D_{22} = 0$, that is, the transfer function from $u$ to $y$ is strictly proper. This condition guarantees the existence of closed-loop transfer matrices. The following requirements need to be checked about the open-loop system $G$ as well, so as to guarantee the existence of an optimal controller $K$:

1. $(A, B_2)$ is stabilizable and $(C_2, A)$ is detectable.

2. $D_{12}$ has full column rank and $D_{21}$ has full row rank.

3. $\begin{pmatrix} A - j\omega I & B_2 \\ C_1 & D_{12} \end{pmatrix}$ has full column rank for all $\omega$, and $\begin{pmatrix} A - j\omega I & B_1 \\ C_2 & D_{21} \end{pmatrix}$ has full row rank for all $\omega$.

If all the above requirements are satisfied, in MATLAB, we can use the functions in $\mu$ toolbox to compute the $H_\infty$ optimal controller $K$. Because the controller that actually minimizes $\|\hat{g}_{zr}\|_\infty$ is really hard to obtain, a simpler method is to search for a controller $K$ that gives $\|\hat{g}_{zr}\|_\infty < \gamma$. In MATLAB, the value of $\gamma$ is updated based on a modified bisection algorithm. The iteration procedure continues until the magnitude of the difference between the smallest $\gamma$ value that has passed as the largest $\gamma$ value that has failed less than the pre-specified tolerance.

## 5.2 Continuous-Time $H_\infty$ Optimal Controller Design

We obtained all of the continuous-time local linearized models from the nonlinear plant in the above chapter. Now the closed-loop diagram of the armature voltage controlled series dc motor is shown in figure 5.3.

From figure 5.3 we can see that $P$ is the local linearized model derived from the nonlinear plant. $r = \omega$ represents the reference signal to the closed-loop system. It is the motor speed $\omega$, which is obtained from the nonlinear plant. $y = \Delta\omega$ is the error of the motor speed between the reference signal $\omega$ and the output of the local linear model $\tilde{\omega}$. The $H_\infty$ optimal controller $K$ needs to be designed. $u$ represents the input to the plant, namely the control armature voltage. The weighted error is

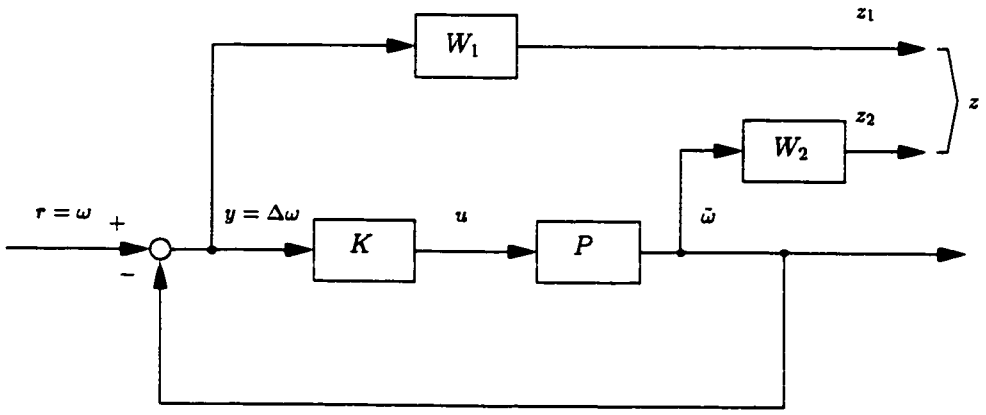


Figure 5.3: Block Diagram of Closed-Loop System

$z = \begin{pmatrix} W_1 y \\ W_2 \tilde{\omega} \end{pmatrix} = \begin{pmatrix} z_1 \\ z_2 \end{pmatrix}$, where the weight $W_1$ is a low pass filter and $W_2$ is a high pass filter.

In this control system design problem, we use mixed-sensitivity $H_\infty$ control, which means to shape the sensitivity function $S = \frac{1}{1+PK}$ along with the closed-loop transfer function $T = \frac{PK}{1+PK}$. We want to reject the disturbance entering at the plant output. In our case, it is typically at the low frequencies. Therefore, it will be successfully rejected if the maximum singular value of $S$ is made small over the same low frequencies. To do this a scalar low pass filter $W_1$ with a bandwidth equal to that of the disturbance can be selected. Hence we have obtained the first cost function $\|W_1 S\|_\infty$. However, this cost function alone is not very practical. The closed-loop transfer function $T$ needs to be shaped as well. It is desirable for tracking problems and noise attenuation. The noise is mainly a high frequency signal, therefore, it can be mostly attenuated if the maximum singular value of $T$ is made small over the high frequencies. A scalar high pass filter $W_2$ with a bandwidth equal to that of the noise is selected. Thus, the second cost function is $\|W_2 T\|_\infty$. The control specification is to find a stabilizing controller $K$ that minimizes $\left\| \begin{pmatrix} W_1 S \\ W_2 T \end{pmatrix} \right\|_\infty$.

At first, we need to convert the closed-loop system in figure 5.3 to the standard

control system in figure 5.1. According to the definitions of $z$, $y$ and $r$, we have:

$$z = \begin{pmatrix} z_1 \\ z_2 \end{pmatrix} = \begin{pmatrix} W_1 y \\ W_2 P u \end{pmatrix} = \begin{pmatrix} W_1(r - Pu) \\ W_2 P u \end{pmatrix} \tag{5.5}$$

$$y = \Delta\omega = r - Pu \tag{5.6}$$

$$r = \omega \tag{5.7}$$

$$\begin{pmatrix} z \\ y \end{pmatrix} = G(s) \begin{pmatrix} r \\ u \end{pmatrix} \tag{5.8}$$

Substituting equations (5.5), (5.6) and (5.7) into (5.8), we get:

$$\left(\begin{array}{c} z_1 \\ z_2 \\ \hline y \end{array}\right) = \left(\begin{array}{c|c} G_{11} & G_{12} \\ \hline G_{21} & G_{22} \end{array}\right) \begin{pmatrix} r \\ u \end{pmatrix} \tag{5.9}$$

$$= \left(\begin{array}{c|c} W_1 & -W_1 P \\ 0 & W_2 P \\ \hline 1 & -P \end{array}\right) \begin{pmatrix} r \\ u \end{pmatrix} \tag{5.10}$$

In MATLAB, we built the block diagram of linear time-invariant model for transfer matrix $G(s)$ and the interconnection matrix. Then we derived the state space model for the generalized plant $G$ in standard control system. Thus the original closed-loop system in figure 5.3 has been converted to the standard form.

Now we need to check whether the generalized plant $G = \left(\begin{array}{c|c} A & B \\ \hline C & D \end{array}\right)$ satisfies all the requirements for the existence of an optimal controller $K$. Before doing the $H_\infty$ optimal controller design, we examine and find that all of the fourteen local generalized plants satisfy the requirements 1, 2 and 3 in the former section. Therefore, by now the $H_\infty$ optimal controller design procedure can be implemented in a computer.

After the $H_\infty$ optimal controller $K$ is obtained, we use the feedback loop to connect the linear model $P$ and the optimal controller $K$ together, so as to get the closed-loop control system. The block diagram is shown in figure 5.4.

When $P$ is the first local linear model, the bode diagram of the corresponding feedback system, namely the closed-loop transfer function $T$ is shown in figure 5.5. Moreover, the closed-loop response of $\omega$ for the first feedback system is shown in figure 5.6 as well.

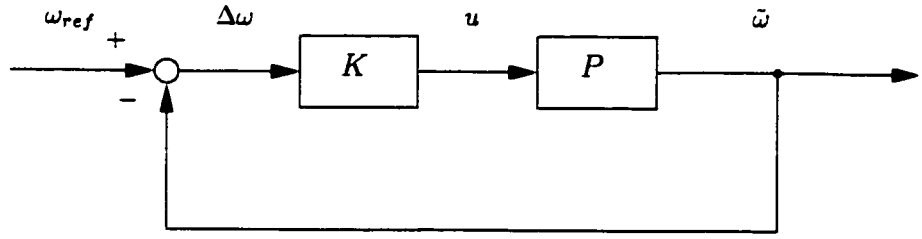


Figure 5.4: Block Diagram of Continuous-Time Feedback System

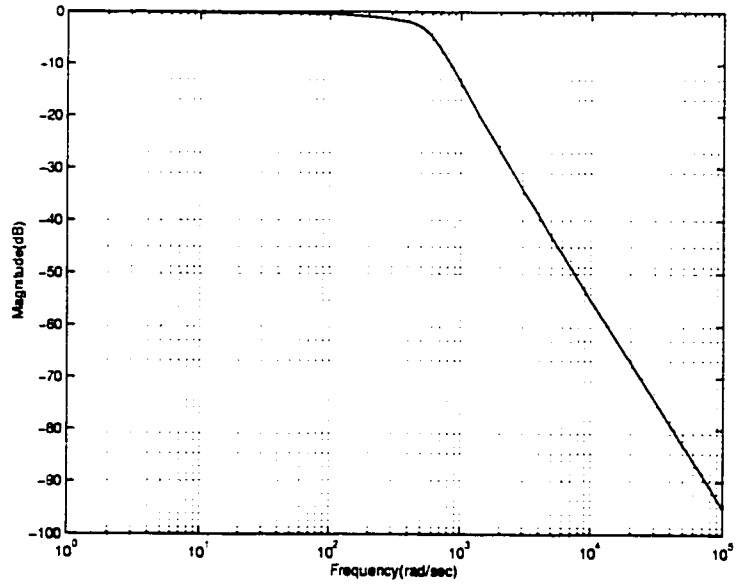


Figure 5.5: The Bode Diagram of Closed-Loop Transfer Function $T$ for First Local Linear System

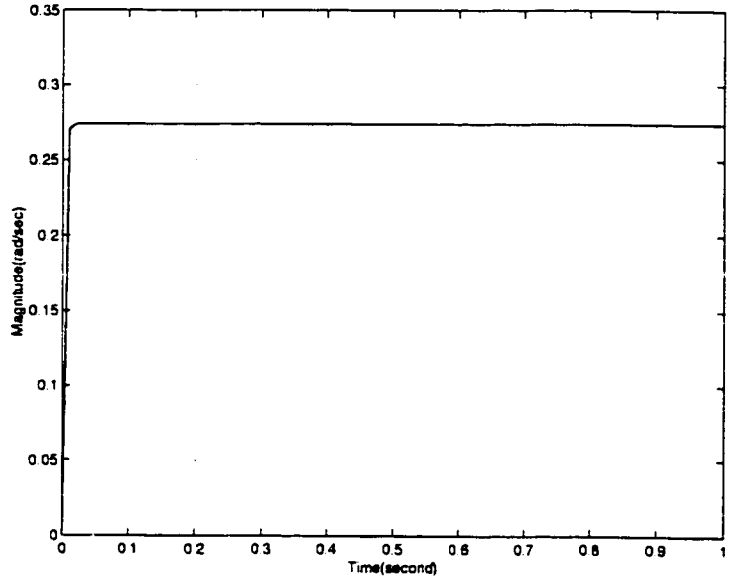


Figure 5.6: The Closed-Loop Response of $\omega$ for First Local Linear System

According to Nyquist criterion, we can say that the closed-loop linear system is stable. And at the low frequencies, the magnitude of the transfer function $T$ is approximate 0 dB, which means that the closed-loop system has good tracking property. On the contrary, at the high frequencies, the magnitude of the transfer function $T$ drops off quickly. This shows the successful noise attenuation for the feedback system. The closed-loop response of $\omega$ indicate the fast transient response and close steady state value to that of nonlinear plant. Therefore, the closed-loop control system has better performance with the help of $H_\infty$ optimal controller $K$.

However, before this $H_\infty$ optimal controller can be applied in the testing experiments, we need to examine the value of the input to the plant $u$ in figure 5.4. Because the first local linearized plant $P$ is only valid when its control input $u$ is less than $1.1V$. We derive the transfer function of $u$ as follows. Since

$$P = \frac{NP}{DP} \tag{5.11}$$

$$K = \frac{NK}{DK} \tag{5.12}$$

$$\frac{u}{\omega} = SK = \frac{K}{1+PK} \tag{5.13}$$

Substituting equations (5.11) and (5.12) into (5.13), we have:

$$\begin{aligned} \frac{u}{\omega} &= \frac{\frac{NK}{DK}}{1+\frac{NP}{DP}\cdot\frac{NK}{DK}} \\ &= \frac{NK\cdot DP}{DP\cdot DK+NP\cdot NK} \end{aligned} \tag{5.14}$$

In MATLAB, by using the transfer function in equation (5.14), the response of the input signal to the plant is obtained. It is shown in figure 5.7.

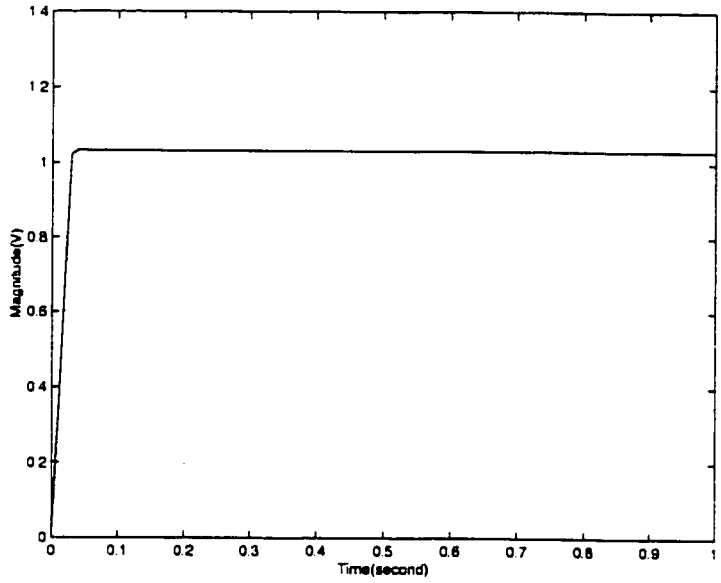


Figure 5.7: The Response of the Input Signal to the Plant for First Local Linear System

From the response diagram, we find that the control input $u$ to the plant is approximately $1.03V$. It is within the allowable control input $1.1V$ , and satisfies our requirement. Therefore, the local linear model $P$ and the $H_\infty$ optimal controller $K$ are both valid for the feedback system.

The bode diagram of the sensitivity function $S$ are plotted as well in figure 5.8. It is clear that at the low frequencies, the magnitude of $S$ is quite small. This property guarantees that the disturbance entering at the plant output will be successfully rejected.

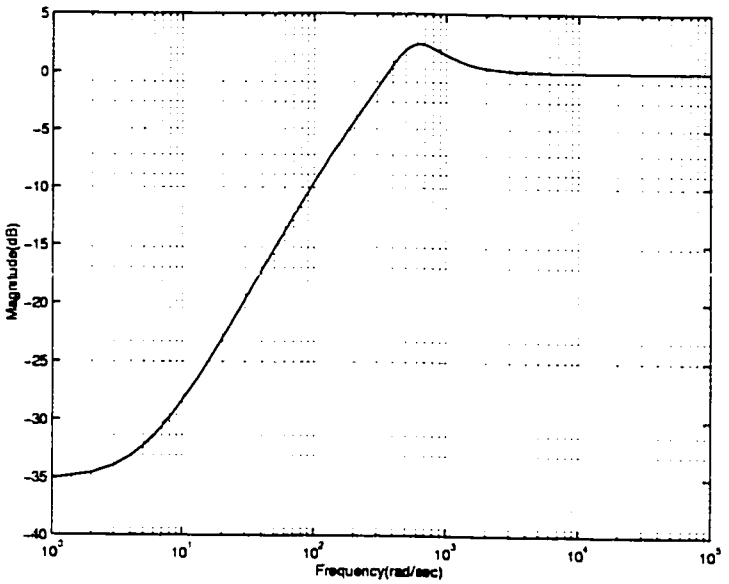


Figure 5.8: The Bode Diagram of the Sensitivity Function $S$ for First Local Linear System

Until now, we finish the $H_\infty$ optimal controller design for the first local linear model. The similar procedure is applied to all the other thirteen local linear models so as to get their corresponding $H_\infty$ optimal controllers.

## 5.3 Characteristics of $H_\infty$ Optimal Controller

During the $H_\infty$ optimal controller design, there are a few points that need to be mentioned. First, by changing the values of the weighting functions $W_1$ and $W_2$, we get different $H_\infty$ optimal controllers $K$ for the same local linear model $P$. The rule to chose which controller satisfies our requirements is to see whether or not the value of the control input to the plant $u$ is within the valid operating range for each local linear model $P$. In our simulation, we find that when different reference motor speeds $\omega$ are applied to the closed-loop system, the relative error between $u$ and the allowable control input is less than 5%. This is true for all of the continuous-time closed-loop systems. This condition guarantees the validation for both the local linear plant $P$ and the $H_\infty$ optimal controller $K$.

Secondly, the $H_\infty$ optimal controller tries to make the output of the feedback system in figure 5.4 as close as possible to the reference signal, which is the desirable speed for the nonlinear plant. Therefore, with the help of the $H_\infty$ optimal controllers, the steady state values of the closed-loop systems are much closer to those of the nonlinear plant than without the $H_\infty$ optimal controllers. This is true for all the fourteen local linear models. Obviously, this demonstrates the improved performance of the feedback system due to the $H_\infty$ optimal controller.

Thirdly, in our control system design, we consider the load torque as flexible. According to the experiments of motor load torque measurements in chapter 3, we know from equation (3.29), that the load torque is a function of the motor speed $\omega$. That means the motor torque will change when the motor runs at different speed. Along this speed and current trajectory, we derive the fourteen local linear models, which have overlap and cover the whole trajectory. The multiple local linear models in the state space is shown in figure 5.9.

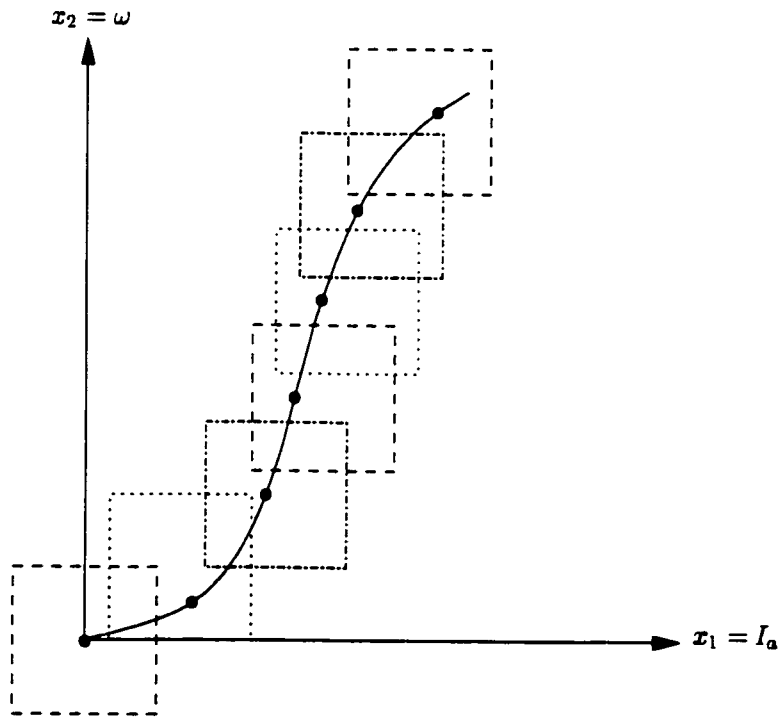


Figure 5.9: Multiple Local Linear Models in the State Space

In practice, if we want to fix the motor load torque at a specific value and we have enough knowledge about how the disturbance will influence the local torque, we may need to cover larger part of the state space. Therefore, more local linear models will be derived at different operating points. And the operating range of all of the local linear models has to be large enough to cover the whole part of the state space that will be used for the possible trajectory. This is shown in figure 5.10.

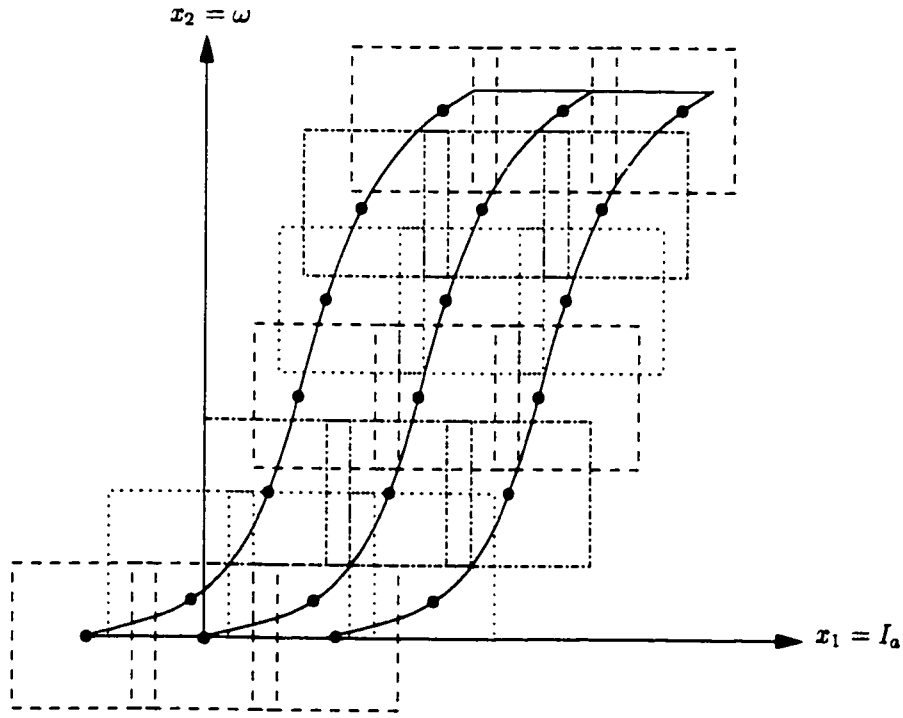


Figure 5.10: Multiple Local Linear Models

Up to now, we have finished the $H_\infty$ optimal controllers design for continuous-time local linear systems. However, whether the $H_\infty$ optimal controllers will work for the nonlinear plant at different operating points is still unknown. I implement the testing experiments in the next chapter so as to find the answer.

# Chapter 6

# Simulation

## 6.1 Introduction of Simulation

For the purpose of verifying the input-output theory, we need to connect all of the $H_\infty$ optimal controllers with the nonlinear plant. Because the controllers work at different speed range, at each operating range, for the nonlinear model, we use the proper controller to link with it and control its speed. Since every two neighbouring controllers have overlap in their operating range, when entering these intersections between them, we switch controllers from the previous one to the follow-up one. In such a way, we can drive the motor starting from zero speed, accelerating, and reaching the desirable speed.

## 6.2 System Configuration

According to the basic idea introduced in the above section, the nonlinear feedback system is built in SIMULINK toolbox. It is shown in figure 6.1.

As we can see, the closed-loop system consists of six major parts:

1. 2-D look-up table and its supplement.
2. Reference signals and switches.

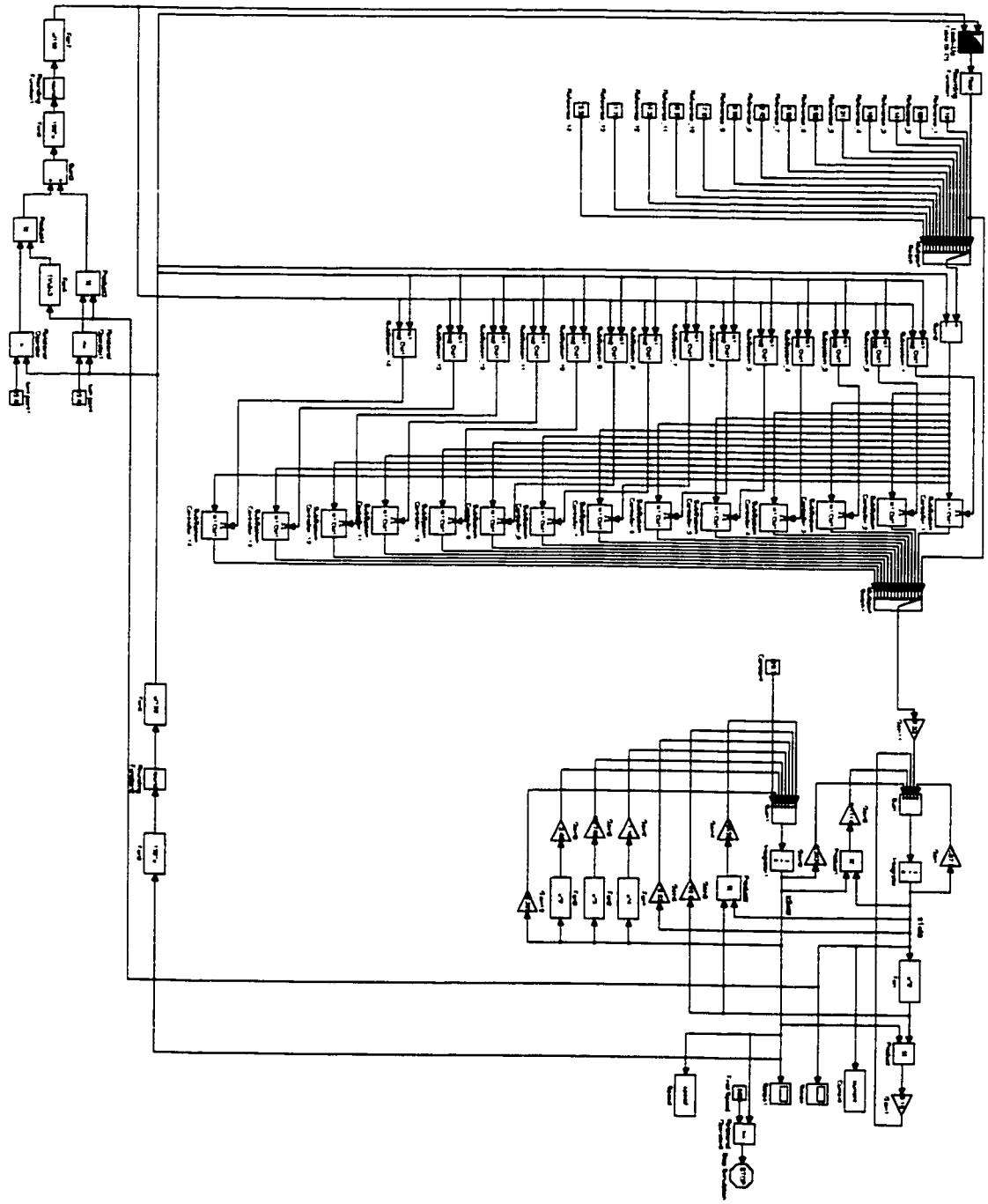

Figure 6.1: Nonlinear Feedback System

3. Logical subsystems.
4. Local linear $H_\infty$ optimal controllers.
5. Nonlinear model.
6. Simulation termination.

We explain their functions separately in the following.

### 6.2.1 2-D Look-Up Table and Its Supplement

In figure 6.1, there is a small square block, which is called 2-D look-up table. Its contents are listed in table 6.1.

| | |
|---|---|
| Row | [-1.04 0.32 0.63 1.69 2.94 4.88 8.94<br>15.41 24.85 35.45 47.42 59.87 79.73 110.67 120.00] |
| Column | [0.00 0.75 0.84 1.10 1.33 1.62 2.07<br>2.52 2.86 2.96 3.20 3.30 3.34 3.40 3.50] |
| Table | [1 1 1 1 1 1 1 1 1 1 1 1 1 1 1;<br>1 2 2 2 2 2 2 2 2 2 2 2 2 2 2;<br>1 2 3 3 3 3 3 3 3 3 3 3 3 3 3;<br>1 2 3 4 4 4 4 4 4 4 4 4 4 4 4;<br>1 2 3 4 5 5 5 5 5 5 5 5 5 5 5;<br>1 2 3 4 5 6 6 6 6 6 6 6 6 6 6;<br>1 2 3 4 5 6 7 7 7 7 7 7 7 7 7;<br>1 2 3 4 5 6 7 8 8 8 8 8 8 8 8;<br>1 2 3 4 5 6 7 8 9 9 9 9 9 9 9;<br>1 2 3 4 5 6 7 8 9 10 10 10 10 10 10;<br>1 2 3 4 5 6 7 8 9 10 11 11 11 11 11;<br>1 2 3 4 5 6 7 8 9 10 11 12 12 12 12;<br>1 2 3 4 5 6 7 8 9 10 11 12 13 13 13;<br>1 2 3 4 5 6 7 8 9 10 11 12 13 14 14;<br>1 2 3 4 5 6 7 8 9 10 11 12 13 14 14] |

Table 6.1: 2-D Look-Up Table

First, we define the value of the row and column parameters. The corresponding possible output values are then defined as the table parameter. This block generates

an output value by comparing the block inputs with the row and column parameters. The first input identifies the row parameter, and the second input identifies the column parameter, as shown by figure 6.2.

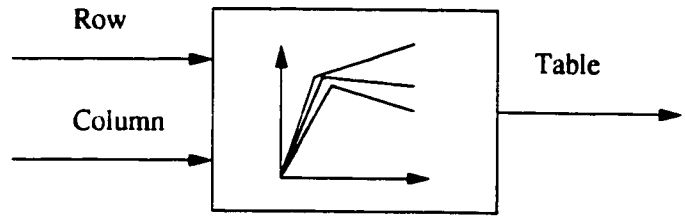


Figure 6.2: 2-D Look-Up Table

If the inputs match row and column parameter values, the output is the table value at the intersection of the row and the column. If the inputs do not match row and column parameter values, the block generates output by linearly interpolating between the appropriate table values. If either or both block inputs are less than the first or greater than the last row or column parameter values, the block extrapolates from the first two or last two points.

In our case, the motor speed and the armature current are introduced from the nonlinear plant to the inputs of the 2-D look-up table block separately. The row parameter represents the switching points of the motor speed, and the column parameter represents the switching points of the armature current for corresponding local linear $H_\infty$ optimal controllers. All of the switching points belong to the intersections of those local models. The table parameter indicates clearly the switching rule: the switching between two neighbouring controllers happens when both the motor speed and the armature current reach the switching points. During the simulation, we find that there is no significant difference between the time for the motor speed to reach its switching value and that for the armature current to reach its switching value. Actually, the latter is a little shorter than the former.

Because the input values given to the 2-D look-up table block are continuously changed, the output of the block is the linear interpolation of the table values. However, in the following part of the control system, the positive integer signals are required. Therefore, the output of the block is introduced to the rounding function

block. This block performs common mathematical rounding functions. According to our requirement, the floor function is selected. It truncates the whole decimal part of the input signal, and generates integer values.

In the 2-D look-up table, both the row values and the column values, which entered as vectors must increase monotonically. This causes another problem in our application. Although the values of the motor speed for the nonlinear plant increase monotonically, the values of the armature current do not follow this rule. After it goes up to the maximum value, it will drop down until the motor reaches its rated speed. Therefore, we cannot simply enter the switching points of the armature current as the column vector. We have to manipulate the values of the armature current after it arrives at its maximum value. The 2-D look-up table supplement accomplishes this task. Before the specific motor speed, which corresponding to the maximum armature current, it generates the same output values as the actual armature current. After that point, it calculates the inverse of the armature current, and adds a constant to it. In this manner, the output of the 2-D look-up table supplement will increase monotonically. Instead of using actual armature current, this output is introduced to the 2-D look-up table as the column input. The column parameter is defined corresponding to the manipulated switching points of the armature current. Now, with the help of the supplementary part, the 2-D look-up table will work properly.

### 6.2.2 Reference Signals and Switches

At the reference signals part, a group of reference signals are provided separately by those constant blocks. These blocks generate specified values independent of time. There are totally fourteen blocks, which correspond to the fourteen local linear $H_\infty$ optimal controllers. We find that when the control input to the nonlinear plant is small, the values of the motor speed are negative, and the values of the armature current are positive. The reason that the nonlinear plant has negative speed values is due to the existence of static friction. When a small control input voltage is given to the motor, although there is current goes through the circuit, which means that the value of the armature current is positive, the motor still cannot overcome the internal static friction. Thus the value of the motor speed in nonlinear plant is negative. The

motor will begin to run only if the control input voltage is large enough to make the motor overcome its internal static friction. Then the value of the motor speed will become positive. This property of the nonlinear plant is reflected in the equation of (3.44), which includes constant value -20.71. However, from practical point of view, we will never control the nonlinear plant to make it work at the operating range where the motor speed is negative. Therefore our linear $H_\infty$ optimal controllers work at the operating ranges where the nonlinear plant generates positive speed values.

We adjust the reference signals so as to make the motor speed reach the desirable values at different operating range. All of the reference signals are connected with the multiport switch block. This block chooses between a number of inputs. Its first (top) input is the control input and the other inputs are the switch inputs. The value of the control input determines which switch input to pass through to the output port. The output of the rounding function block is introduced to the control input in order to determine which reference signal will be given to the nonlinear feedback system at the different operating range. The same multiport switch block is used at the position which links the local linear $H_\infty$ optimal controllers with the nonlinear plant. The output of the rounding function block is introduced to its control input as well. This means that the reference signals and the corresponding $H_\infty$ optimal controllers are switched simultaneously. It is definitely the requirement for the nonlinear feedback system.

### 6.2.3 Logical Subsystems

The first and the second logical subsystems are shown in detail in figure 6.3 and figure 6.4 respectively. All the others have the same structure as the second one, except for the different values in those constant blocks. There are fourteen logical subsystems altogether, which correspond to the fourteen local linear $H_\infty$ optimal controllers. These logical subsystems consist of logical operator blocks and relational operator blocks.

The first logical subsystem generates the enabling signal for the first $H_\infty$ optimal controller. The control strategy is that if either or both of the motor speed and the armature current are less than their first corresponding switching values, the output

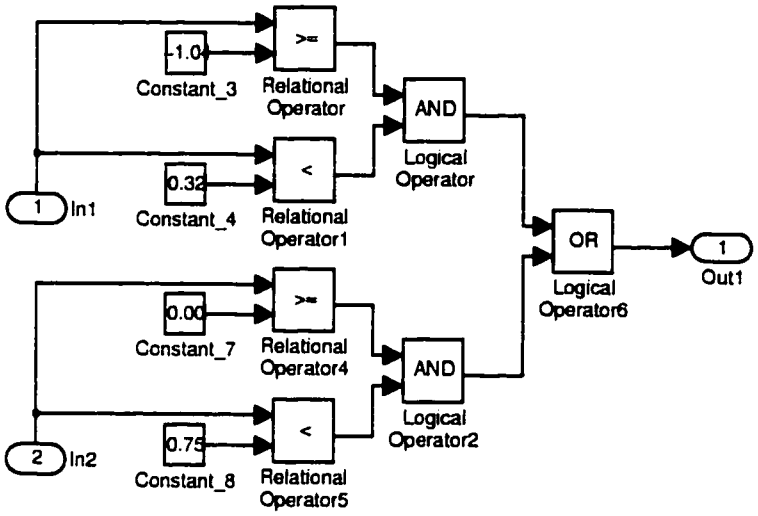


Figure 6.3: First Logical Subsystem

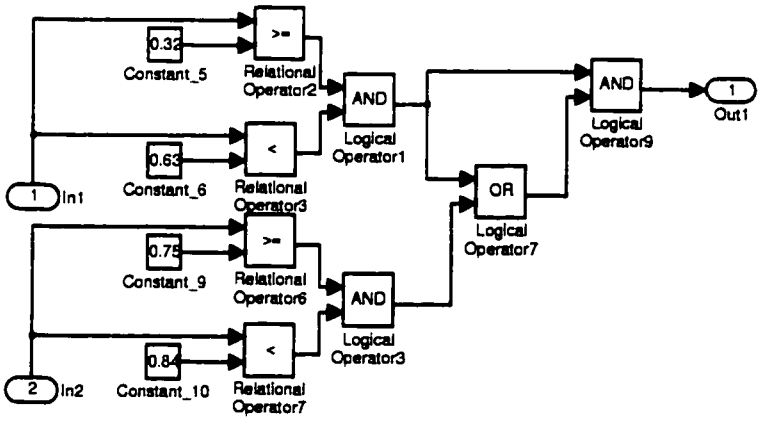


Figure 6.4: Second Logical Subsystem

of the first logical subsystem will be 1, which means that it will keep on enabling the first $H_\infty$ optimal controller until both of the states reach their switching values. The second logical subsystem has similar structure and function as the first one. As mentioned earlier, by simulation we find that the time for the armature current to reach its switching value is shorter than that for the motor speed to reach its switching value. Therefore, another "and" logical operator block is added to the second logical subsystem, so as to ensure that when the armature current reaches its switching value, the second $H_\infty$ optimal controller will not be enabled. The first local linear controller is still used to control the nonlinear plant until the motor speed reaches its switching value as well. The logical subsystems have the same switching points as those in the 2-D look-up table. This condition guarantees that the reference signals, the corresponding $H_\infty$ optimal controllers and the enabling signals are all switched at the same time.

### 6.2.4 Local Linear $H_\infty$ Optimal Controllers

The next important part in the nonlinear feedback system is the local linear $H_\infty$ optimal controllers. There are fourteen optimal controllers. Each of them is a subsystem. They all have similar construction. The first one is shown in figure 6.5.

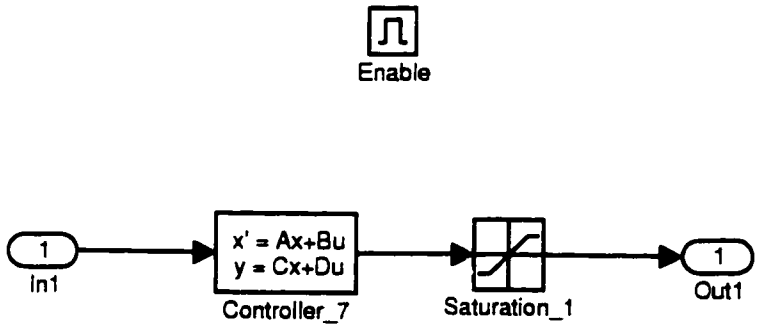


Figure 6.5: First Local Linear $H_\infty$ Optimal Controller

It is easy to see that this subsystem has an enabling port. This makes it an enabled subsystem. It executes while the input received at the enabling port is greater than zero. In the nonlinear feedback system, the outputs of the logical subsystems will enable the different $H_\infty$ optimal controllers when the nonlinear plant reaches

its switching points. The local linear controllers are represented by the state-space blocks. Because the $H_\infty$ optimal controllers are observable, the observable canonical form is used to define their state-space parameters $A$, $B$, $C$ and $D$. In this linear state-space system, we define its behavior not only by matrix coefficients $A$, $B$, $C$ and $D$, but also by the initial state vector, which gives the initial values of the states for the linear controller. For the first local linear controller, its initial states are all set to be zeros, because it is initially relaxed. For the second controller, because after the motor speed and the armature current reach their switching values, the nonlinear feedback system will switch its controller from the first one to the second one automatically. In order to avoid any jump between the outputs of two neighbouring controllers when switching, and furthermore, keep the outputs at the switching point have the same value, we initialize the initial states of the second controller using the final states of the first one. This method is applied to all the other controllers as well. It makes the switching smooth. The saturation block limits the range of the output of the controller, so as to ensure that the control signal to the nonlinear plant is within the allowable range. This guarantees the nonlinear plant works properly.

### 6.2.5 Nonlinear Plant

The nonlinear part of the feedback system is exactly the same as the block diagram of the nonlinear model for series dc motor, which is shown in figure 3.10. It implements the nonlinear behavior of the real series dc motor. Before the simulation, the states of the nonlinear plant needs to be initialized. As mentioned before, due to the internal static friction, when the control input voltage to the nonlinear model is zero, the value of the motor speed is negative. We use this value as the initial condition for the motor speed. As for the armature current, it is approximately zero before starting the simulation. Therefore, both of the initial states are set up. A number of local linear $H_\infty$ optimal controllers are used to control the speed of this nonlinear plant.

### 6.2.6 Simulation Termination

From practical point of view, as the operators, they do not care about the internal construction of the nonlinear feedback system. The only thing they care about is

how to regulate the motor to the desirable speed. Therefore, as designers, we add the simulation termination part to the nonlinear feedback system. In this part, the stop simulation block is used to terminate the simulation when the motor speed reaches the desirable value. Thus the operators only have to change the value of the constant block in the simulation termination part to whatever the desirable speed is. Then after starting the simulation, the motor will stop automatically at that speed. This accomplishes the task for the design purpose.

## 6.3 Simulation Results

In previous section, the construction and the function of the nonlinear feedback system are introduced in detail. Now we perform a computer simulation.

We recall that our objective is to increase the motor speed from 0 rpm to 1200 rpm, "following a stable motion". No attempt, however, will be made to smooth or to speed up the response. The result is shown in figure 6.6.

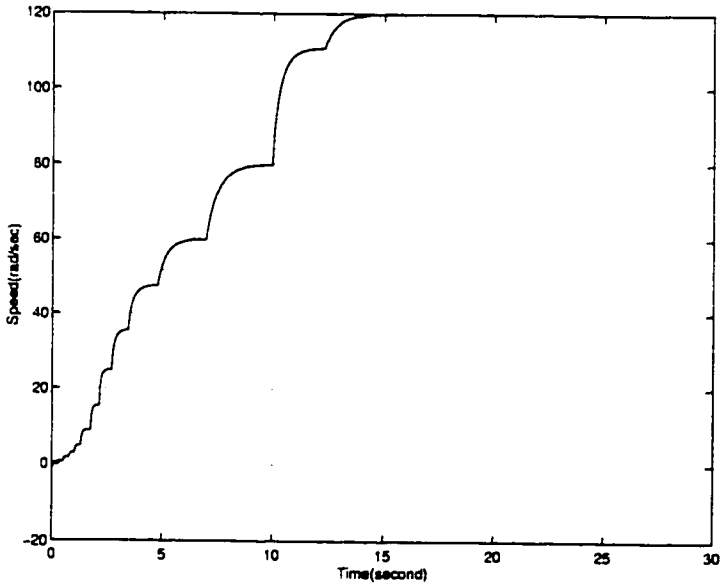


Figure 6.6: Simulation Result of the Motor Speed

This figure should be interpreted as follows: There are fourteen points of discontinuity in this response. Each one of these points corresponds to a switching point

between two neighbouring local controllers. There are two main shortcomings in this response: (i) lack of smoothness, and (ii) speed of response. Both problems are indeed inter-related. The lack of smoothness originated from a very narrow intersection region in the domain of two neighbouring local controllers, which in turn requires waiting virtually until reaching steady states before switching controllers. This limits the speed of response which can be obtained. Suggestions for the improvement of these problems are mentioned in the next chapter.

# Chapter 7

# Discussion and Conclusions

## 7.1 Discussion

In this section, we take a critical look at the results and procedures of the previous chapters.

- The first step of our design consisted of the linearization of the nonlinear plant in order to obtain the local linear time-invariant models at different equilibrium points $(\mathbf{x_e}, u_e)$. For simplicity, we restricted my attention to "steady state error" and required that the percentage steady state error between the nonlinear plant and the linear approximation be less than 5%. This error is regarded as the uncertainty of the linear approximation. In practice, however, robustness constraints dictate that dynamic uncertainty needs to be considered as well. More research is needed to quantify the uncertainty originated by the linear approximation. This problem is important in any situation where a model of a physical system is to be used, and it is critical when feedback system is to be designed based on this model due to the propagation of model uncertainty and consequent the risk of instability. In fact, the study of model uncertainties and their incorporation in feedback design is the subject of the so-called robust control theory which has inspired a lot of interest in recent years. Indeed, our uncertainty research has important connection with robust control theory, and furthermore, may impact the traditional uncertainty description characterized

in the robust control literature.

- When dealing with the series dc motor speed control, our only concern was: starting the motor from zero speed, accelerating, and reaching the desirable final speed. We did not specify any smoothness requirements on the speed response $\omega(t)$. A quick look at the figure 6.6 shows that our approach results in a non-smooth response. The curve of the motor speed looks like piecewise continuous functions. The lack of smoothness is originated by the way in which the switching of the reference signals and the switching points were implemented. In practice, this type of response may be undesirable for certain systems. For example, when dealing with robotic systems, we are typically interested in producing a motion along a predefined trajectory. In order to improve the response curve, two approaches can be considered.

  (i) First, we can enlarge the size of the intersection so as to make sure that the latter part of the fast transient response in each local model falls inside the intersection of two neighbouring local models. Thus, we can select the switching points at the fast transient response part instead of those at the slow part. In such a manner, we not only dramatically shorten the time for speed acceleration, but also remarkably reduce the non-smoothness of the motor speed curve. This idea can be expressed clearly in figure 7.1 and figure 7.2.

  (ii) Secondly, we need to review the space of the input functions. In our case, the exogenous input signals to the nonlinear feedback system are a series of step signals. As a consequence, the output motor speed curve is a group of exponential curves connected successively. The exogenous input signals and the output curve are shown in figure 7.3. In order to improve the response curve, we have to limit the rate of change of the input signals, in other words, limit the derivative of them. Instead of using many "steps", a exponential signal can be applied to the nonlinear feedback system as the exogenous input. In this way, the motor speed curve will become much smoother than before, as long as the rate of change of the motor speed is fast enough to follow that of the exogenous exponential input

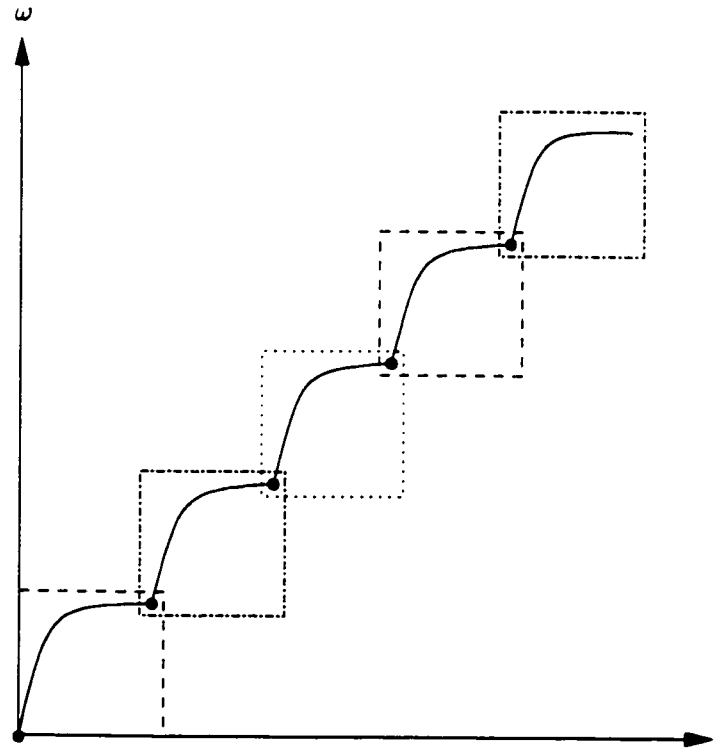


Figure 7.1: Slow and Non-Smooth Speed Acceleration with Small Intersections

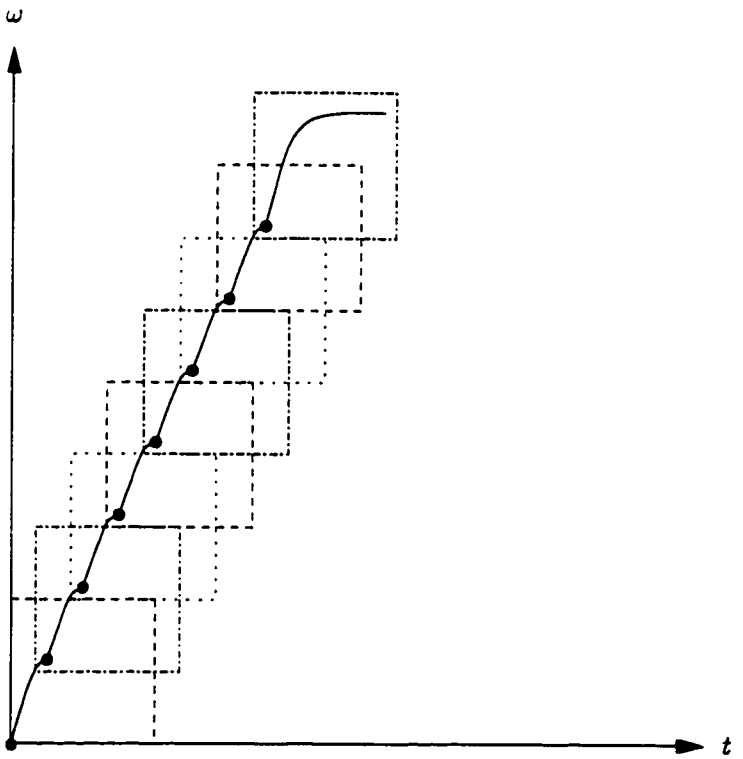


Figure 7.2: Fast and Smooth Speed Acceleration with Large Intersections

signal. Of course, we need to find a specific exponential signal which has the proper rate of change. This approach provides smoother motor speed curve, and at the same time, it dramatically simplifies the reference signals in the nonlinear feedback system with a single exponential input signal. Definitely, the combination of these two approaches can give us satisfactory results.

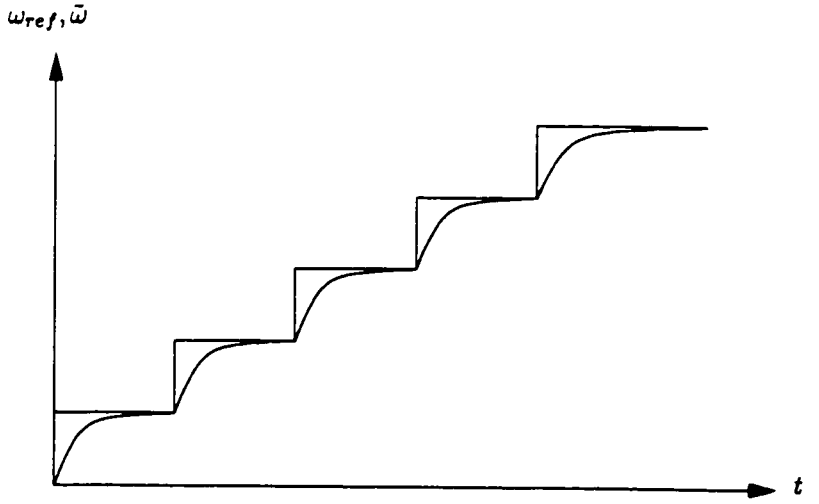


Figure 7.3: Exogenous Input Signals and Output Curve

- Even though our object–the armature voltage controlled series dc motor is successfully operated by the $H_\infty$ optimal controllers using the input-output approach, there are still some problems involved with the control system design. The reason we selected the $H_\infty$ optimal control method is due to its popularity in recent years, and furthermore, it is a well accepted method in robust control system design. However, it may not be the best approach for the nonlinear system.

  First of all, there is an important notion in the input-output approach represented in reference [29], which is so-called the *small signals*. They are defined by the binormed linear subspace $\mathcal{X}_Q$, which means $\| u \|_2 < \infty$ and $\| u \|_\infty < Q$. These signals indeed determine the character of the local linear system, since no model can remain accurate for arbitrarily large signals while maintaining

a predefined degree of accuracy. Therefore, when implementing the controller design procedure, we need to keep track of the input function to the plant, so as to make sure that the "size" of the input function is within the allowable range. Otherwise, the local linear models will become invalid. The $H_\infty$ optimal design method cannot incorporate this important restriction into its design procedure. We have to design the $H_\infty$ optimal controller first, then check the "size" of the input function to the plant only "after" the design is completed. An alternative to this approach would be to use the more recent $L_1$ control theory which is "designed" to limit the "size" of the transient response.

Another feature of $H_\infty$ optimal control method is that, in essence, it is a steady state specification. However, by observing the motor speed curve, we can find that the nonlinear feedback system does not work in steady state conditions during the whole procedure of the speed acceleration except for the final desirable steady speed. We ignore the control of the dynamic state, and on the contrary, excessively emphasize the control of the steady state. As mentioned earlier, the $L_1$ theory can be used to compensate the control of the dynamic state. Alternatively, we may use "windows" in the time domain so as to filter out the actual useful transient state before applying the $H_\infty$ optimal control design procedure. To the best of our knowledge, this approach has not been previously used in the control literature.

- Up until now, we have discussed the problems encountered in this thesis and some potential improvements which can be done in the future. All of these bring up another important question: namely, for what class of systems is the input-output approach suitable. Like any other approach for the analysis and design of nonlinear systems, this approach is not universally recommended.

  The input-output approach appears to be very promising for a variety of systems. The best "candidate" are systems designed to operate for long period of time under similar conditions. This is indeed the case in, for instance, aircraft and process control systems. In the aircraft control systems, the speed and the dynamic pressure are measured by sensors and used as scheduling variables in order to adjust the flight controllers to different operating conditions. Since there is no need for the flight to follow a predefined strict trajectory, and the

aircraft does not need to switch its controllers a lot except for take-off and landing, it is an ideal candidate for the input-output approach. The same thing for the process control systems.

On the other hand, if the system requires a predefined state trajectory, such as the high performance robotic system, this input-output approach may not be recommended, since in order to produce good results, it might be necessary to use too many local models.

## 7.2 Conclusions

In this thesis, we elaborated on the virtues and shortcomings of the theory of an input-output approach to systems described by multiple local linear models [29]. It is a re-formulation of the classical input-output theory. It not only keeps the essence of the classical stability theory, but also overcomes its drawbacks. By defining the local systems as a mapping from *input* to *state*, rather than from *input* to *output*, the theory incorporates initial conditions into the system stability analysis. Unlike most references who search for the *global stability* of the gain scheduling method, the input-output approach concentrates on *local stability*. By introducing the important concept of *stable motion*, it provides a mechanism that ensures "safe" transitions between different operating points. Moreover, the key notion of *small signal* emphasizes that when we define model uncertainties, we should never overlook the class of signals for which this model is assumed to be valid. All of these make the input-output approach a very practical method in dealing with the gain scheduling controlled systems.

This theory was applied to the speed control of a series dc motor. Through this case study, we demonstrate that the theory is well developed and works great for the nonlinear control system. Generally speaking, the input-output approach to gain scheduling method is a rather simple, yet complete characterization of the stability analysis of systems described by multiple models. We believe that it will attract more and more research interests because of its theoretical value, and have more and more extensive applications due to its practical significance.

# Bibliography


[1] D. K. Anand. *Introduction to Control Systems.* Pergamon Press Inc., 1974.

[2] D. P. Atherton. *Nonlinear Control Engineering.* Van Nostrand Reinhold Company Limited, 1975.

[3] R. Bellman and R. Kalaba. *Selected Papers on Mathematical Trends in Control Theory.* Dover, 1964.

[4] S. A. Billings, J. O. Gray, and D. H. Owens. *Nonlinear System Design.* Peter Peregrinus Ltd., London, UK, 1984.

[5] H. S. Black. *Stabilized Feedback Amplifiers.* Bell System Technology Journal, 1934.

[6] H. W. Bode. *Network Analysis and Feedback Amplifier Design.* Van Nostrand, Princeton, N.J., 1945.

[7] Brockett. Feedback invariants for nonlinear systems. In *Proc. VIIth IFAC World Congress, Helsinki*, pages 1115–1120, 1978.

[8] C. T. Chen. *Analysis and Synthesis of Linear Control Systems.* Holt, Rinehart and Winston Inc., 1975.

[9] C. T. Chen. *Linear System Theory and Design.* CBS College Publishing, 1984.

[10] T. W. Chen and B. A. Francis. *Optimal Sampled-Data Control Systems.* Springer-Verlag, London, 1995.

[11] J. J. D'Azzo and C. H. Houpis. *Linear Control System Analysis and Design: Conventional and Modern.* McGraw-Hill, Inc., 1975.

[12] W. R. Evans. Graphical analysis of control systems. In *Trans. AIEE*, volume 67, pages 547–551, 1948.

[13] V. W. Eveleigh. *Introduction to Control Systems Design.* McGraw-Hill Inc., 1972.

[14] A. E. Fitzgerald, Jr. C. Kingsley, and S. D. Umans. *Electric Machinery (Fifth Edition).* McGraw-Hill, Inc., 1990.

[15] T. E. Fortmann and K. L. Hitz. *An Introduction to Linear Control Systems.* Marcel Dekker, Inc., 1977.

[16] T. Gönen. *Electrical Machines.* Power International Press, 1998.

[17] A. L. Greensite. *Control Theory: Elements of Modern Control Theory*, volume I. Spartan Books, New York, 1970.

[18] Y. C. Ho, R. E. Kalman, and K. S. Narendra. Controllability of linear dynamical systems. In *Contributions to Differential Equations*, volume 1. Interscience Publishers, Inc., 1962.

[19] A. Isidori. *Nonlinear Control Systems (Third Edition).* Springer-Verlag London Limited, 1995.

[20] A. Isidori, A. J. Krener, C. Gori-Giorgi, and S. Monaco. Nonlinear decoupling via feedback: A differential geometric approach. In *IEEE Trans. Automat. Control*, volume AC-26, pages 331–335, 1981.

[21] E. I. Jury. *Sampled Data Control Systems.* John Wiley & Sons, Inc. New York, 1958.

[22] R. E. Kalman. On the general theory of control systems. In *Proc. First Intl. Cong. Automatic Cont. Moscow*, volume 1, pages 481–493. Butterworth & Co. (Publishers), Ltd. London, 1961.

[23] R. E. Kalman. Canonical structure of linear dynamical systems. In *Proc. Natl. Acad. Sci. U.S.A.*, volume 48, pages 596–600, 1962.

[24] R. E. Kalman and J. E. Bertram. Control system analysis and design via the second method of lyapunov. In *Transactions ASME*, volume 82, pages 371-400, 1960.

[25] P. V. Kokotović. *Lecture Notes in Control and Information Sciences: foundations of Adaptive Control.* Springer-Verlag, 1991.

[26] P. C. Krause and O. Wasynczuk. *Electromechanical Motion Devices.* McGraw-Hill, Inc., 1989.

[27] J. LaSalle and S. Lefschetz. *Stability by Liapunov's Direct Method.* Academic Press, New York, 1961.

[28] A. M. Lyapunov. *On the General Problem of Stability of Motion.* PhD thesis, Kharkov, 1892.

[29] H. J. Marquez. An input–output approach to systems described using multiple models. In *IEEE Transactions on Circuits and Systems, Part I: Fundamental Theory and Applications*, 1999.

[30] H. Nijmeijer and A. van der Schaft. *Nonlinear Dynamical Control Systems.* Springer-Verlag New York Inc., 1990.

[31] J. R. Ragazzini and G. F. Franklin. *Sampled-Data Control Systems.* McGraw-Hill, New York, 1958.

[32] W. J. Rugh. Analytical framework for gain scheduling. In *IEEE Control Systems Magazine*, volume 11, pages 79–84, 1991.

[33] J. S. Shamma and M. Athans. Analysis of nonlinear gain scheduled control systems. In *IEEE Trans. on Automat. Control*, volume AC-35, pages 898–907, 1990.

[34] J. S. Shamma and M. Athans. Gain scheduling: Potential hazards and possible remedies. In *IEEE Control Systems Magazine*, volume 12, pages 101–107, 1993.

[35] G. R. Slemon and A. Straughen. *Electric Machines.* Addison-Wesley, Reading, 1980.

[36] J. E. Slotine and W. P. Li. *Applied Nonlinear Control.* Prentice-Hall, Inc., 1991.

[37] K. J. Åström and B. Wittenmark. *Adaptive Control (Second Edition).* Addison-Wesley Publishing Co., 1995.

[38] J. T. Tou. *Digital and Sampled Data Control Systems.* McGraw-Hill, New York, 1959.

[39] J. T. Tou. *Modern Control Theory.* McGraw-Hill, New York, 1964.

[40] D. D. Šiljak. *Nonlinear Systems: The Parameter Analysis and Design.* John Wiley & Sons, Inc., 1969.

[41] W. M. Wonham. *Linear Multivariable Control: A Geometric Approach.* Springer-Verlag, New York, 1979.

[42] L. A. Zadeh and C. A. Desoer. *Linear System Theory: the State Space Approach.* McGraw-Hill Book Company, Inc., 1963.

# Appendix A

# Table

| Before Motor Ran | After Motor Ran for 10 Minutes | | |
|---|---|---|---|
| $R_s$ $(\Omega)$ | $V - R_s$ $(V)$ | $I - R_s$ $(A)$ | $R_s$ $(\Omega)$ |
| 1.7 | 2.27 | 1.05 | *2.16* |
| 1.6 | 2.78 | 1.24 | *2.24* |
| 1.8 | 2.15 | 1.03 | *2.09* |
| 1.7 | 2.94 | 1.45 | *2.03* |
| 1.8 | 3.10 | 1.47 | *2.11* |

Table A.1: Measured and Calculated Values of Field Resistance

| Before Motor Ran | After Motor Ran for 10 Minutes | | |
|---|---|---|---|
| $R_a$ $(\Omega)$ | $V - R_a$ $(V)$ | $I - R_a$ $(A)$ | $R_a$ $(\Omega)$ |
| 8.2 | 8.74 | 1.01 | *8.65* |
| 8.4 | 9.20 | 1.03 | *8.93* |
| 8.1 | 9.70 | 1.11 | *8.74* |
| 8.6 | 9.93 | 1.13 | *8.79* |
| 8.7 | 13.90 | 1.60 | *8.69* |

Table A.2: Measured and Calculated Values of Armature Resistance

| $V_{60}$ $(V)$ | $I_{60}$ $(A)$ | $\theta$ $(\circ)$ | $X_s$ $(\Omega)$ | $L_s$ $(mH)$ |
|---|---|---|---|---|
| 24.0 | 1.01 | 58 | *20.15* | *53* |
| 25.7 | 1.01 | 55 | *21.84* | *55* |
| 51.2 | 2.00 | 53 | *20.45* | *54* |
| 63.8 | 2.50 | 54 | *20.65* | *55* |
| 39.8 | 1.50 | 55 | *21.73* | *58* |
| 33.5 | 1.31 | 55 | *20.95* | *56* |
| 51.3 | 1.99 | 56 | *21.37* | *57* |
| 37.1 | 1.53 | 57 | *20.34* | *54* |
| 25.1 | 1.02 | 56 | *20.40* | *54* |
| 39.6 | 1.51 | 55 | *21.48* | *57* |

Table A.3: Measured and Calculated Values of Field Inductance Using $L = \frac{X}{\Omega}$ Method ($\Omega = 377$)

| $V_0$ $(V)$ | $I_0$ $(A)$ | $R_a$ $(\Omega)$ | $V_{120}$ $(V)$ | $I_{120}$ $(A)$ | $Z_{120}$ $(\Omega)$ | $L_a$ $(mH)$ |
|---|---|---|---|---|---|---|
| 1.0 | 0.114 | *8.77* | 6.2 | 0.138 | *44.93* | *58* |
| 1.2 | 0.137 | *8.76* | 8.2 | 0.160 | *51.25* | *67* |
| 1.4 | 0.162 | *8.64* | 10.3 | 0.198 | *52.02* | *68* |
| 1.5 | 0.175 | *8.57* | 11.3 | 0.201 | *56.22* | *74* |
| 1.2 | 0.141 | *8.51* | 8.1 | 0.179 | *45.25* | *59* |
| 1.1 | 0.128 | *8.59* | 7.1 | 0.140 | *50.71* | *66* |
| 1.0 | 0.112 | *8.93* | 6.3 | 0.131 | *48.09* | *63* |
| 1.3 | 0.152 | *8.55* | 9.2 | 0.196 | *46.94* | *61* |
| 1.6 | 0.185 | *8.65* | 12.4 | 0.226 | *54.87* | *72* |
| 1.5 | 0.176 | *8.52* | 11.2 | 0.228 | *49.12* | *64* |

Table A.4: Measured and Calculated Values of Armature Inductance Using $(2 \cdot \Omega \cdot L)^2 + R^2 = Z^2$ Method ($\Omega = 377$)

| $I_s$ $(A)$ | $V_f$ $(V)$ | $I_a$ $(A)$ | $V_a$ $(V)$ | $N_r$ $(rpm)$ |
|---|---|---|---|---|
| 3.49 | 6.76 | 0.12 | 89.1 | 1207 |
| 3.00 | 5.87 | 0.12 | 82.6 | 1213 |
| 2.50 | 4.90 | 0.12 | 73.5 | 1209 |
| 2.00 | 3.90 | 0.14 | 63.2 | 1214 |
| 1.50 | 2.92 | 0.15 | 51.3 | 1214 |
| 1.01 | 1.97 | 0.19 | 39.9 | 1259 |
| 0.51 | 1.00 | 0.29 | 25.3 | 1231 |
| 0.10 | 0.20 | 0.57 | 15.8 | 1168 |

Table A.5: Measured Values of $E_a - I_s$ Curve (first time testing–part I: before switched the connection between the two joints of the field winding)

| $I_s$ $(A)$ | $V_f$ $(V)$ | $I_a$ $(A)$ | $V_a$ $(V)$ | $N_r$ $(rpm)$ |
|---|---|---|---|---|
| 3.50 | 6.72 | 0.12 | 85.0 | 1205 |
| 3.00 | 5.84 | 0.12 | 78.0 | 1208 |
| 2.50 | 4.87 | 0.12 | 69.0 | 1208 |
| 2.01 | 3.90 | 0.14 | 58.0 | 1195 |
| 1.51 | 2.93 | 0.16 | 46.8 | 1202 |
| 1.01 | 1.96 | 0.20 | 33.3 | 1196 |
| 0.51 | 1.00 | 0.34 | 21.9 | 1225 |
| 0.10 | 0.21 | 1.35 | 17.7 | 1224 |

Table A.6: Measured Values of $E_a - I_s$ Curve (first time testing–part II: after switched the connection between the two joints of the field winding)

| $I_s$ $(A)$ | $E_{a1}$ $(V)$ | $E'_{a1}$ $(V)$ | $E_{a2}$ $(V)$ | $E'_{a2}$ $(V)$ | $\bar{E}_a$ $(V)$ |
|---|---|---|---|---|---|
| *3.495* | *88.068* | *87.5572* | *83.968* | *83.6196* | *85.5884* |
| *3.000* | *81.568* | *80.6938* | *76.968* | *76.4583* | *78.5761* |
| *2.500* | *72.468* | *71.9285* | *67.968* | *67.5179* | *69.7232* |
| *2.005* | *61.996* | *61.2811* | *56.796* | *57.0336* | *59.1574* |
| *1.505* | *50.010* | *49.4333* | *45.424* | *45.3484* | *47.3909* |
| *1.010* | *38.266* | *36.4728* | *31.580* | *31.6856* | *34.0792* |
| *0.510* | *22.796* | *22.2219* | *18.936* | *18.5496* | *20.3858* |
| *0.100* | *10.848* | *11.1452* | *6.120* | *6.000* | *8.5726* |

Table A.7: Calculated Values of $E_a - I_s$ Curve (first time testing–part III)

| $I_s$ $(A)$ | $V_f$ $(V)$ | $I_a$ $(A)$ | $V_a$ $(V)$ | $N_r$ $(rpm)$ |
|---|---|---|---|---|
| 3.49 | 6.82 | 0.12 | 89.9 | 1215 |
| 3.01 | 5.91 | 0.12 | 83.3 | 1210 |
| 2.50 | 4.91 | 0.12 | 74.2 | 1224 |
| 2.01 | 3.94 | 0.13 | 64.5 | 1230 |
| 1.50 | 2.93 | 0.15 | 50.0 | 1187 |
| 1.01 | 1.97 | 0.18 | 37.7 | 1200 |
| 0.50 | 0.98 | 0.29 | 25.6 | 1245 |
| 0.10 | 0.20 | 0.55 | 15.9 | 1169 |

Table A.8: Measured Values of $E_a - I_s$ Curve (second time testing–part I: before switched the connection between the two joints of the field winding)

| $I_s$ $(A)$ | $V_f$ $(V)$ | $I_a$ $(A)$ | $V_a$ $(V)$ | $N_r$ $(rpm)$ |
|---|---|---|---|---|
| 3.50 | 6.73 | 0.12 | 84.5 | 1194 |
| 3.00 | 5.79 | 0.12 | 77.3 | 1196 |
| 2.49 | 4.82 | 0.13 | 68.6 | 1200 |
| 2.01 | 3.88 | 0.14 | 57.6 | 1184 |
| 1.52 | 2.93 | 0.16 | 47.3 | 1202 |
| 1.00 | 1.92 | 0.20 | 34.4 | 1211 |
| 0.50 | 0.98 | 0.35 | 21.8 | 1228 |
| 0.10 | 0.21 | 1.20 | 17.2 | 1200 |

Table A.9: Measured Values of $E_a - I_s$ Curve (second time testing–part II: after switched the connection between the two joints of the field winding)

| $I_s$ $(A)$ | $E_{a1}$ $(V)$ | $E'_{a1}$ $(V)$ | $E_{a2}$ $(V)$ | $E'_{a2}$ $(V)$ | $E_a$ $(V)$ |
|---|---|---|---|---|---|
| *3.495* | *88.868* | *87.7709* | *83.468* | *83.8874* | *85.8292* |
| *3.005* | *82.268* | *81.5881* | *76.268* | *76.5231* | *79.0556* |
| *2.495* | *73.168* | *71.7333* | *67.482* | *67.4820* | *69.6077* |
| *2.010* | *63.382* | *61.8361* | *56.396* | *57.1581* | *59.4971* |
| *1.510* | *48.710* | *49.2435* | *45.924* | *45.8476* | *47.5456* |
| *1.005* | *36.152* | *36.1520* | *32.680* | *32.3832* | *34.2676* |
| *0.500* | *23.126* | *22.2901* | *18.830* | *18.4007* | *20.3454* |
| *0.100* | *11.200* | *11.4970* | *6.860* | *6.8600* | *9.1785* |

Table A.10: Calculated Values of $E_a - I_s$ Curve (second time testing–part III)

| $I_s$ (A) | $V_f$ (V) | $I_a$ (A) | $V_a$ (V) | $N_r$ (rpm) |
|---|---|---|---|---|
| 3.50 | 6.63 | 0.12 | 90.0 | 1225 |
| 3.01 | 5.75 | 0.12 | 83.1 | 1225 |
| 2.51 | 4.81 | 0.12 | 73.8 | 1219 |
| 2.02 | 3.86 | 0.13 | 63.7 | 1228 |
| 1.50 | 2.87 | 0.15 | 50.8 | 1215 |
| 1.00 | 1.91 | 0.19 | 37.3 | 1214 |
| 0.51 | 0.98 | 0.28 | 24.8 | 1218 |
| 0.10 | 0.20 | 0.57 | 15.9 | 1205 |

Table A.11: Measured Values of $E_a - I_s$ Curve (third time testing–part I: before switched the connection between the two joints of the field winding)

| $I_s$ (A) | $V_f$ (V) | $I_a$ (A) | $V_a$ (V) | $N_r$ (rpm) |
|---|---|---|---|---|
| 3.50 | 6.75 | 0.12 | 83.7 | 1185 |
| 3.00 | 5.84 | 0.12 | 78.4 | 1214 |
| 2.50 | 4.87 | 0.13 | 68.8 | 1199 |
| 2.01 | 3.91 | 0.14 | 58.8 | 1214 |
| 1.51 | 2.93 | 0.16 | 48.2 | 1230 |
| 1.01 | 1.96 | 0.20 | 35.4 | 1234 |
| 0.51 | 0.99 | 0.35 | 21.9 | 1215 |
| 0.11 | 0.21 | 1.19 | 17.2 | 1210 |

Table A.12: Measured Values of $E_a - I_s$ Curve (third time testing–part II: after switched the connection between the two joints of the field winding)

| $I_s$ $(A)$ | $E_{a1}$ $(V)$ | $E'_{a1}$ $(V)$ | $E_{a2}$ $(V)$ | $E'_{a2}$ $(V)$ | $\bar{E}_a$ $(V)$ |
|---|---|---|---|---|---|
| *3.500* | *88.978* | *87.1612* | *82.668* | *83.7144* | *85.4383* |
| *3.005* | *82.068* | *80.3931* | *77.368* | *76.4758* | *78.4345* |
| *2.505* | *72.768* | *71.6338* | *67.682* | *67.7384* | *69.6861* |
| *2.015* | *62.582* | *61.1550* | *57.596* | *56.9318* | *59.0434* |
| *1.505* | *49.510* | *48.8988* | *46.824* | *45.6820* | *47.2904* |
| *1.005* | *35.666* | *35.2547* | *33.680* | *32.7520* | *34.0034* |
| *0.510* | *22.422* | *22.0906* | *18.890* | *18.6568* | *20.3737* |
| *0.105* | *11.008* | *10.9623* | *6.926* | *6.8688* | *8.9156* |

Table A.13: Calculated Values of $E_a - I_s$ Curve (third time testing–part III)

| $N_r$ $(rpm)$ | $\omega$ $(rad/sec)$ | $T_{load}$ $(N \cdot m)$ | $I_a$ $(A)$ | $V_a$ $(V)$ | $I_f$ $(A)$ |
|---|---|---|---|---|---|
| 0 | *0* | 0 | 0 | 0 | 0.38 |
| 101 | *10.5767* | 0.88 | 1.35 | 19.7 | 0.38 |
| 203 | *21.2581* | 1.50 | 2.26 | 35.3 | 0.37 |
| 309 | *32.3584* | 1.68 | 2.57 | 46.3 | 0.37 |
| 408 | *42.7257* | 1.57 | 2.41 | 53.1 | 0.37 |
| 508 | *53.1976* | 1.40 | 2.16 | 59.4 | 0.37 |
| 606 | *63.4602* | 1.23 | 1.93 | 65.7 | 0.37 |
| 710 | *74.3510* | 1.09 | 1.72 | 72.4 | 0.37 |
| 806 | *84.4041* | 0.98 | 1.56 | 79.1 | 0.37 |
| 909 | *95.1903* | 0.88 | 1.42 | 86.5 | 0.37 |
| 1014 | *106.1858* | 0.81 | 1.32 | 94.4 | 0.37 |
| 1101 | *115.2965* | 0.75 | 1.24 | 101.1 | 0.37 |
| 1200 | *125.6637* | 0.70 | 1.16 | 108.8 | 0.37 |

Table A.14: Measured and Calculated Values of $T_{load} - \omega$ Curve (dynamometer field flux strength 40%: first time testing)

| $N_r$ $(rpm)$ | $\omega$ $(rad/sec)$ | $T_{load}$ $(N \cdot m)$ | $I_a$ $(A)$ | $V_a$ $(V)$ | $I_f$ $(A)$ |
|---|---|---|---|---|---|
| 0 | *0* | 0 | 0 | 0 | 0.38 |
| 102 | *10.6814* | 0.89 | 1.37 | 20.0 | 0.38 |
| 200 | *20.9440* | 1.49 | 2.25 | 34.8 | 0.38 |
| 300 | *31.4159* | 1.69 | 2.59 | 45.7 | 0.37 |
| 400 | *41.8879* | 1.59 | 2.46 | 52.8 | 0.37 |
| 503 | *52.6740* | 1.42 | 2.21 | 59.4 | 0.37 |
| 602 | *63.0413* | 1.25 | 1.97 | 65.7 | 0.37 |
| 708 | *74.1416* | 1.10 | 1.76 | 72.8 | 0.37 |
| 806 | *84.4041* | 0.99 | 1.60 | 79.6 | 0.37 |
| 906 | *94.8761* | 0.89 | 1.47 | 86.9 | 0.37 |
| 1004 | *105.1386* | 0.82 | 1.36 | 94.1 | 0.37 |
| 1108 | *116.0295* | 0.75 | 1.26 | 101.8 | 0.36 |
| 1209 | *126.6062* | 0.70 | 1.18 | 109.4 | 0.37 |

Table A.15: Measured and Calculated Values of $T_{load} - \omega$ Curve (dynamometer field flux strength 40%: second time testing)

| $N_r$ $(rpm)$ | $\omega$ $(rad/sec)$ | $T_{load}$ $(N \cdot m)$ | $I_a$ $(A)$ | $V_a$ $(V)$ | $I_f$ $(A)$ |
|---|---|---|---|---|---|
| 0 | *0* | 0 | 0 | 0 | 0.38 |
| 112 | *11.7286* | 0.71 | 1.09 | 18.3 | 0.38 |
| 209 | *21.8864* | 0.91 | 1.39 | 28.7 | 0.38 |
| 310 | *32.4631* | 0.83 | 1.30 | 36.4 | 0.38 |
| 403 | *42.2021* | 0.73 | 1.15 | 43.0 | 0.38 |
| 511 | *53.5118* | 0.61 | 1.00 | 50.8 | 0.38 |
| 608 | *63.6696* | 0.53 | 0.90 | 58.0 | 0.38 |
| 710 | *74.3510* | 0.46 | 0.82 | 65.9 | 0.37 |
| 810 | *84.8230* | 0.41 | 0.75 | 73.8 | 0.37 |
| 914 | *95.7139* | 0.37 | 0.71 | 82.1 | 0.37 |
| 1006 | *105.3481* | 0.35 | 0.67 | 89.7 | 0.37 |
| 1104 | *115.6106* | 0.32 | 0.64 | 97.8 | 0.37 |
| 1204 | *126.0826* | 0.30 | 0.61 | 106.0 | 0.37 |

Table A.16: Measured and Calculated Values of $T_{load} - \omega$ Curve (dynamometer field flux strength 30%: first time testing)

| $N_r$ (rpm) | $\omega$ (rad/sec) | $T_{load}$ ($N \cdot m$) | $I_a$ ($A$) | $V_a$ ($V$) | $I_f$ ($A$) |
|---|---|---|---|---|---|
| 0 | *0* | 0 | 0 | 0 | 0.37 |
| 125 | *13.0900* | 0.70 | 1.10 | 19.5 | 0.37 |
| 209 | *21.8864* | 0.87 | 1.36 | 28.5 | 0.37 |
| 309 | *32.3584* | 0.83 | 1.32 | 36.3 | 0.36 |
| 403 | *42.2021* | 0.73 | 1.19 | 43.0 | 0.36 |
| 503 | *52.6740* | 0.63 | 1.05 | 50.0 | 0.36 |
| 611 | *63.9838* | 0.53 | 0.92 | 57.9 | 0.36 |
| 702 | *73.5133* | 0.48 | 0.84 | 64.7 | 0.36 |
| 811 | *84.9277* | 0.41 | 0.77 | 73.1 | 0.36 |
| 907 | *94.9808* | 0.38 | 0.72 | 80.6 | 0.36 |
| 1003 | *105.0339* | 0.35 | 0.68 | 88.3 | 0.36 |
| 1108 | *116.0295* | 0.32 | 0.64 | 96.7 | 0.36 |
| 1200 | *125.6637* | 0.30 | 0.62 | 104.3 | 0.36 |

Table A.17: Measured and Calculated Values of $T_{load} - \omega$ Curve (dynamometer field flux strength 30%: second time testing)

| $N_r$ (rpm) | $\omega$ (rad/sec) | $T_{load}$ ($N \cdot m$) | $I_a$ ($A$) | $V_a$ ($V$) | $I_f$ ($A$) |
|---|---|---|---|---|---|
| 0 | *0* | 0 | 0 | 0 | 0.39 |
| 109 | *11.4145* | 0.32 | 0.58 | 13.9 | 0.39 |
| 203 | *21.2581* | 0.33 | 0.60 | 21.9 | 0.38 |
| 303 | *31.7301* | 0.27 | 0.53 | 29.7 | 0.38 |
| 404 | *42.3068* | 0.21 | 0.47 | 37.7 | 0.38 |
| 506 | *52.9882* | 0.19 | 0.43 | 45.9 | 0.38 |
| 610 | *63.8791* | 0.16 | 0.41 | 54.5 | 0.38 |
| 712 | *74.5605* | 0.14 | 0.39 | 62.8 | 0.38 |
| 804 | *84.1947* | 0.13 | 0.38 | 70.4 | 0.38 |
| 906 | *94.8761* | 0.12 | 0.36 | 78.9 | 0.38 |
| 1010 | *105.7670* | 0.11 | 0.35 | 87.6 | 0.38 |
| 1110 | *116.2389* | 0.10 | 0.35 | 96.0 | 0.38 |
| 1204 | *126.0826* | 0.10 | 0.35 | 104.0 | 0.38 |

Table A.18: Measured and Calculated Values of $T_{load} - \omega$ Curve (dynamometer field flux strength 20%: first time testing)

| $N_r$ (rpm) | $\omega$ (rad/sec) | $T_{load}$ ($N \cdot m$) | $I_a$ ($A$) | $V_a$ ($V$) | $I_f$ ($A$) |
|---|---|---|---|---|---|
| 0 | *0* | 0 | 0 | 0 | 0.38 |
| 129 | *13.5088* | 0.31 | 0.57 | 15.6 | 0.38 |
| 208 | *21.7817* | 0.31 | 0.59 | 22.2 | 0.37 |
| 316 | *33.0944* | 0.26 | 0.52 | 30.6 | 0.37 |
| 409 | *42.8304* | 0.21 | 0.47 | 37.9 | 0.37 |
| 503 | *52.6740* | 0.18 | 0.43 | 45.4 | 0.37 |
| 605 | *63.3555* | 0.16 | 0.41 | 53.7 | 0.37 |
| 703 | *73.6180* | 0.14 | 0.39 | 61.7 | 0.37 |
| 809 | *84.7183* | 0.12 | 0.38 | 70.5 | 0.37 |
| 902 | *94.4572* | 0.11 | 0.37 | 78.2 | 0.37 |
| 1009 | *105.6622* | 0.10 | 0.36 | 87.1 | 0.37 |
| 1106 | *115.8200* | 0.10 | 0.35 | 95.2 | 0.37 |
| 1203 | *125.9779* | 0.09 | 0.35 | 103.4 | 0.37 |

Table A.19: Measured and Calculated Values of $T_{load} - \omega$ Curve (dynamometer field flux strength 20%: second time testing)

| $N_r$ (rpm) | $\omega$ (rad/sec) | $T_{load}$ ($N \cdot m$) | $I_a$ ($A$) | $V_a$ ($V$) | $I_f$ ($A$) |
|---|---|---|---|---|---|
| 0 | *0* | 0 | 0 | 0 | 0.39 |
| 100 | *10.4720* | 0.07 | 0.25 | 11.1 | 0.39 |
| 202 | *21.1534* | 0.06 | 0.25 | 19.1 | 0.38 |
| 304 | *31.8348* | 0.05 | 0.25 | 27.7 | 0.38 |
| 405 | *42.4115* | 0.05 | 0.25 | 36.1 | 0.38 |
| 508 | *53.1976* | 0.04 | 0.25 | 44.8 | 0.38 |
| 600 | *62.8319* | 0.04 | 0.26 | 52.6 | 0.38 |
| 705 | *73.8274* | 0.04 | 0.26 | 61.4 | 0.38 |
| 807 | *84.5088* | 0.04 | 0.26 | 70.0 | 0.38 |
| 905 | *94.7714* | 0.03 | 0.26 | 78.3 | 0.38 |
| 1008 | *105.5575* | 0.03 | 0.27 | 87.0 | 0.38 |
| 1107 | *115.9248* | 0.03 | 0.27 | 95.5 | 0.38 |
| 1204 | *126.0826* | 0.03 | 0.27 | 103.8 | 0.38 |

Table A.20: Measured and Calculated Values of $T_{load} - \omega$ Curve (dynamometer field flux strength 10%: first time testing)

| $N_r$ $(rpm)$ | $\omega$ $(rad/sec)$ | $T_{load}$ $(N \cdot m)$ | $I_a$ $(A)$ | $V_a$ $(V)$ | $I_f$ $(A)$ |
|---|---|---|---|---|---|
| 0 | *0* | 0 | 0 | 0 | 0.39 |
| 125 | *13.0900* | 0.07 | 0.26 | 12.6 | 0.39 |
| 207 | *21.6770* | 0.06 | 0.26 | 19.5 | 0.39 |
| 305 | *31.9395* | 0.05 | 0.25 | 27.7 | 0.38 |
| 404 | *42.3068* | 0.05 | 0.25 | 35.9 | 0.38 |
| 504 | *52.7788* | 0.04 | 0.25 | 44.3 | 0.37 |
| 607 | *63.5649* | 0.04 | 0.26 | 52.9 | 0.37 |
| 705 | *73.8274* | 0.04 | 0.26 | 61.2 | 0.37 |
| 805 | *84.2994* | 0.03 | 0.26 | 69.5 | 0.37 |
| 905 | *94.7714* | 0.03 | 0.27 | 78.1 | 0.37 |
| 1008 | *105.5575* | 0.03 | 0.27 | 86.8 | 0.37 |
| 1103 | *115.5059* | 0.03 | 0.28 | 94.9 | 0.37 |
| 1202 | *125.8731* | 0.03 | 0.28 | 103.4 | 0.37 |

Table A.21: Measured and Calculated Values of $T_{load} - \omega$ Curve (dynamometer field flux strength 10%: second time testing)

| $I_a$ $(A)$ | $V_a$ $(V)$ | $N_r$ $(rpm)$ | $\omega$ $(rad/sec)$ | $T_{loss}$ $(N \cdot m)$ |
|---|---|---|---|---|
| 0.31 | 106.4 | 1204 | *126.08* | *0.255* |
| 0.30 | 97.6 | 1105 | *115.72* | *0.246* |
| 0.29 | 88.7 | 1004 | *105.14* | *0.238* |
| 0.28 | 79.8 | 904 | *94.67* | *0.229* |
| 0.27 | 70.8 | 802 | *83.99* | *0.220* |
| 0.27 | 62.1 | 704 | *73.72* | *0.215* |
| 0.26 | 53.5 | 605 | *63.36* | *0.207* |
| 0.24 | 44.8 | 506 | *52.99* | *0.194* |
| 0.23 | 35.9 | 402 | *42.10* | *0.185* |
| 0.22 | 27.8 | 307 | *32.15* | *0.177* |
| 0.21 | 19.0 | 205 | *21.47* | *0.168* |
| 0.20 | 10.6 | 108 | *11.31* | *0.158* |

Table A.22: Measured and Calculated Values of $T_{loss} - \omega$ Curve (first time testing)

| $I_a$ $(A)$ | $V_a$ $(V)$ | $N_r$ $(rpm)$ | $\omega$ $(rad/sec)$ | $T_{loss}$ $(N \cdot m)$ |
|---|---|---|---|---|
| 0.31 | 106.7 | 1208 | *126.50* | *0.255* |
| 0.29 | 97.9 | 1109 | *116.13* | *0.238* |
| 0.28 | 88.9 | 1009 | *105.66* | *0.229* |
| 0.27 | 80.0 | 908 | *95.09* | *0.221* |
| 0.26 | 70.8 | 803 | *84.09* | *0.212* |
| 0.26 | 62.3 | 705 | *73.83* | *0.212* |
| 0.25 | 53.6 | 606 | *63.46* | *0.203* |
| 0.24 | 45.0 | 507 | *53.09* | *0.194* |
| 0.23 | 35.9 | 402 | *42.10* | *0.185* |
| 0.22 | 28.0 | 309 | *32.36* | *0.178* |
| 0.21 | 19.1 | 206 | *21.57* | *0.165* |
| 0.20 | 10.5 | 106 | *11.10* | *0.154* |

Table A.23: Measured and Calculated Values of $T_{loss} - \omega$ Curve (second time testing)

| $V_t$ $(V)$ | $I_a$ $(A)$ | $N_r$ $(rpm)$ | $\omega$ $(rad/sec)$ | $T_{load}$ $(N \cdot m)$ | $E_a$ $(V)$ | $T_e$ $(N \cdot m)$ |
|---|---|---|---|---|---|---|
| 100.0 | 1.33 | 1943 | *203.4705* | 0.36 | *86.035* | *0.5624* |
| 100.0 | 1.51 | 1770 | *185.3540* | 0.48 | *84.145* | *0.6855* |
| 100.0 | 2.01 | 1445 | *151.3200* | 0.82 | *78.895* | *1.0480* |
| 100.1 | 2.51 | 1236 | *129.4336* | 1.75 | *73.745* | *1.4301* |
| 100.0 | 3.01 | 1070 | *112.0501* | 1.56 | *68.395* | *1.8373* |
| 100.0 | 3.51 | 929 | *97.2847* | 1.94 | *63.145* | *2.2783* |

Table A.24: Measured and Calculated Values of Series DC Motor Characteristics (terminal voltage $V_t = 100$V: first time testing)

| $V_t$ $(V)$ | $I_a$ $(A)$ | $N_r$ $(rpm)$ | $\omega$ $(rad/sec)$ | $T_{load}$ $(N \cdot m)$ | $E_a$ $(V)$ | $T_e$ $(N \cdot m)$ |
|---|---|---|---|---|---|---|
| 100.1 | 1.34 | 2040 | *213.6283* | 0.36 | *86.030* | *0.5396* |
| 100.1 | 1.50 | 1870 | *195.8259* | 0.47 | *84.350* | *0.6461* |
| 100.0 | 2.00 | 1498 | *156.8702* | 0.80 | *79.000* | *1.0072* |
| 100.0 | 2.51 | 1259 | *131.8422* | 1.17 | *73.645* | *1.4020* |
| 100.1 | 3.01 | 1091 | *114.2493* | 1.55 | *68.495* | *1.8046* |
| 100.1 | 3.52 | 946 | *99.0649* | 1.93 | *63.140* | *2.2435* |

Table A.25: Measured and Calculated Values of Series DC Motor Characteristics (terminal voltage $V_t$ = 100V: second time testing)

| $V_t$ $(V)$ | $I_a$ $(A)$ | $N_r$ $(rpm)$ | $\omega$ $(rad/sec)$ | $T_{load}$ $(N \cdot m)$ | $E_a$ $(V)$ | $T_e$ $(N \cdot m)$ |
|---|---|---|---|---|---|---|
| 75.0 | 1.00 | 1859 | *194.6740* | 0.13 | *64.500* | *0.3313* |
| 75.1 | 1.49 | 1325 | *135.7537* | 0.44 | *59.455* | *0.6385* |
| 75.0 | 2.01 | 1028 | *107.6519* | 0.80 | *53.895* | *1.0063* |
| 75.0 | 2.51 | 845 | *88.4882* | 1.16 | *48.645* | *1.3798* |
| 75.0 | 3.01 | 703 | *73.6180* | 1.55 | *43.395* | *1.7743* |
| 75.0 | 3.53 | 568 | *59.4808* | 1.94 | *37.935* | *2.2513* |

Table A.26: Measured and Calculated Values of Series DC Motor Characteristics (terminal voltage $V_t$ = 75V: first time testing)

| $V_t$ $(V)$ | $I_a$ $(A)$ | $N_r$ $(rpm)$ | $\omega$ $(rad/sec)$ | $T_{load}$ $(N \cdot m)$ | $E_a$ $(V)$ | $T_e$ $(N \cdot m)$ |
|---|---|---|---|---|---|---|
| 75.1 | 1.00 | 1834 | *192.0560* | 0.15 | *64.600* | *0.3364* |
| 75.1 | 1.49 | 1328 | *139.0678* | 0.45 | *59.455* | *0.6370* |
| 75.1 | 2.02 | 1019 | *106.7094* | 0.81 | *53.890* | *1.0201* |
| 75.1 | 2.50 | 843 | *88.2788* | 1.15 | *48.850* | *1.3834* |
| 75.0 | 3.00 | 700 | *73.3038* | 1.53 | *43.500* | *1.7803* |
| 75.1 | 3.50 | 583 | *61.0516* | 1.91 | *38.350* | *2.1985* |

Table A.27: Measured and Calculated Values of Series DC Motor Characteristics (terminal voltage $V_t$ = 75V: second time testing)

| $V_t$ $(V)$ | $I_a$ $(A)$ | $N_r$ $(rpm)$ | $\omega$ $(rad/sec)$ | $T_{load}$ $(N \cdot m)$ | $E_a$ $(V)$ | $T_e$ $(N \cdot m)$ |
|---|---|---|---|---|---|---|
| 50.1 | 0.76 | 1600 | *167.5516* | 0.02 | *42.120* | *0.1911* |
| 50.1 | 1.01 | 1226 | *128.3864* | 0.14 | *39.495* | *0.3107* |
| 50.1 | 1.31 | 936 | *98.0177* | 0.32 | *36.345* | *0.4857* |
| 50.0 | 1.60 | 766 | *80.2153* | 0.50 | *33.200* | *0.6622* |
| 50.0 | 2.02 | 590 | *61.7847* | 0.79 | *28.790* | *0.9413* |
| 50.0 | 2.33 | 490 | *51.3127* | 1.01 | *25.535* | *1.1595* |
| 50.1 | 2.62 | 412 | *43.1445* | 1.22 | *22.590* | *1.3718* |
| 50.0 | 3.01 | 320 | *33.5103* | 1.51 | *18.395* | *1.6523* |
| 50.1 | 3.48 | 220 | *23.0383* | 1.87 | *13.560* | *2.0483* |

Table A.28: Measured and Calculated Values of Series DC Motor Characteristics (terminal voltage $V_t$ = 50V: first time testing)

| $V_t$ $(V)$ | $I_a$ $(A)$ | $N_r$ $(rpm)$ | $\omega$ $(rad/sec)$ | $T_{load}$ $(N \cdot m)$ | $E_a$ $(V)$ | $T_e$ $(N \cdot m)$ |
|---|---|---|---|---|---|---|
| 50.0 | 0.73 | 1591 | *166.6091* | 0.02 | *42.335* | *0.1855* |
| 50.0 | 1.01 | 1205 | *126.1873* | 0.15 | *39.395* | *0.3153* |
| 50.0 | 1.30 | 932 | *97.5988* | 0.32 | *36.350* | *0.4842* |
| 50.0 | 1.60 | 757 | *79.2729* | 0.50 | *33.200* | *0.6701* |
| 50.0 | 1.99 | 595 | *62.3083* | 0.77 | *29.105* | *0.9296* |
| 50.0 | 2.31 | 489 | *51.2080* | 0.99 | *25.745* | *1.1614* |
| 50.0 | 2.63 | 405 | *42.4115* | 1.22 | *22.385* | *1.3881* |
| 50.0 | 2.96 | 323 | *33.8245* | 1.47 | *18.920* | *1.6557* |
| 50.0 | 3.45 | 212 | *22.2006* | 1.85 | *13.775* | *2.1407* |

Table A.29: Measured and Calculated Values of Series DC Motor Characteristics (terminal voltage $V_t$ = 50V: second time testing)

| $V_t$ $(V)$ | $I_a$ $(A)$ | $N_r$ $(rpm)$ | $\omega$ $(rad/sec)$ | $T_{load}$ $(N \cdot m)$ | $E_a$ $(V)$ | $T_e$ $(N \cdot m)$ |
|---|---|---|---|---|---|---|
| 25.1 | 0.75 | 697 | *72.9897* | 0.02 | *17.175* | *0.1765* |
| 25.0 | 1.00 | 491 | *51.4174* | 0.13 | *14.480* | *0.2816* |
| 25.1 | 1.30 | 332 | *34.7670* | 0.30 | *11.430* | *0.4274* |
| 25.1 | 1.59 | 220 | *23.0383* | 0.49 | *8.385* | *0.5787* |
| 25.1 | 1.95 | 119 | *12.4617* | 0.73 | *4.595* | *0.7190* |

Table A.30: Measured and Calculated Values of Series DC Motor Characteristics (terminal voltage $V_t = 25$V: first time testing)

| $V_t$ $(V)$ | $I_a$ $(A)$ | $N_r$ $(rpm)$ | $\omega$ $(rad/sec)$ | $T_{load}$ $(N \cdot m)$ | $E_a$ $(V)$ | $T_e$ $(N \cdot m)$ |
|---|---|---|---|---|---|---|
| 25.1 | 0.74 | 697 | *72.9897* | 0.02 | *17.330* | *0.1757* |
| 25.1 | 1.00 | 483 | *50.5796* | 0.14 | *14.550* | *0.2877* |
| 25.1 | 1.28 | 330 | *34.5575* | 0.30 | *11.640* | *0.4311* |
| 25.1 | 1.57 | 224 | *23.4572* | 0.48 | *8.565* | *0.5733* |
| 25.1 | 1.94 | 120 | *12.5664* | 0.73 | *4.680* | *0.7225* |

Table A.31: Measured and Calculated Values of Series DC Motor Characteristics (terminal voltage $V_t = 25$V: second time testing)

| $V_t$ $(V)$ | $I_a$ $(A)$ | $N_r$ $(rpm)$ | $\omega$ $(rad/sec)$ |
|---|---|---|---|
| 30.1 | 2.45 | 120 | *12.5664* |
| 35.3 | 2.75 | 151 | *15.8127* |
| 40.1 | 2.98 | 182 | *19.0590* |
| 45.2 | 3.18 | 220 | *23.0383* |
| 49.9 | 3.29 | 267 | *27.9602* |
| 55.0 | 3.25 | 345 | *36.1283* |
| 59.9 | 2.94 | 480 | *50.2655* |
| 64.9 | 2.53 | 653 | *68.3820* |
| 70.2 | 2.24 | 825 | *86.3938* |
| 75.1 | 2.04 | 980 | *102.6254* |
| 80.2 | 1.89 | 1136 | *118.9616* |
| 85.0 | 1.78 | 1280 | *134.0413* |

Table A.32: Measured and Calculated Values of $I_a$, $N_r$ and $\omega$ at Different $V_t$ (dynamometer field flux strength 40%: first time testing)

| $V_t$ $(V)$ | $I_a$ $(A)$ | $N_r$ $(rpm)$ | $\omega$ $(rad/sec)$ |
|---|---|---|---|
| 30.4 | 2.36 | 125 | *13.0900* |
| 34.9 | 2.58 | 151 | *15.8127* |
| 40.8 | 2.86 | 190 | *19.8968* |
| 45.1 | 3.03 | 222 | *23.2478* |
| 50.0 | 3.18 | 267 | *27.9602* |
| 55.3 | 3.20 | 343 | *35.9189* |
| 60.0 | 2.97 | 465 | *48.6947* |
| 65.5 | 2.47 | 689 | *72.1519* |
| 70.0 | 2.21 | 872 | *91.3156* |
| 75.2 | 2.00 | 1065 | *111.5265* |
| 80.2 | 1.85 | 1240 | *129.8525* |
| 85.1 | 1.75 | 1404 | *147.0265* |

Table A.33: Measured and Calculated Values of $I_a$, $N_r$ and $\omega$ at Different $V_t$ (dynamometer field flux strength 40%: second time testing)

| $V_t$ $(V)$ | $I_a$ $(A)$ | $\omega$ $(rad/sec)$ |
|---|---|---|
| 30.1 | *2.2902* | *11.6974* |
| 35.3 | *2.5337* | *15.6665* |
| 40.1 | *2.7166* | *19.8695* |
| 45.2 | *2.8625* | *25.0922* |
| 49.9 | *2.9436* | *30.8920* |
| 55.0 | *2.9539* | *38.9176* |
| 59.9 | *2.8477* | *49.8607* |
| 64.9 | *2.5677* | *67.6446* |
| 70.2 | *2.3421* | *86.7644* |
| 75.1 | *2.2901* | *98.6997* |
| 80.2 | *2.2800* | *109.1042* |
| 85.0 | *2.2528* | *120.0023* |

Table A.34: Simulated Values of $I_a$ and $\omega$ at Different $V_t$ (dynamometer field flux strength 40%: first time testing)

| $V_t$ $(V)$ | $I_a$ $(A)$ | $\omega$ $(rad/sec)$ |
|---|---|---|
| 30.4 | *2.3060* | *13.0900* |
| 34.9 | *2.5165* | *15.8127* |
| 40.8 | *2.7398* | *19.8968* |
| 45.1 | *2.8602* | *23.2478* |
| 50.0 | *2.9446* | *27.9602* |
| 55.3 | *2.9512* | *35.9189* |
| 60.0 | *2.8438* | *48.6947* |
| 65.5 | *2.5296* | *72.1519* |
| 70.0 | *2.3463* | *91.3156* |
| 75.2 | *2.2896* | *111.5265* |
| 80.2 | *2.2800* | *129.8525* |
| 85.1 | *2.2511* | *147.0265* |

Table A.35: Simulated Values of $I_a$ and $\omega$ at Different $V_t$ (dynamometer field flux strength 40%: second time testing)

| $u_e = V_t$ $(V)$ | $x_{1e} = I_a$ $(A)$ | $x_{2e} = \omega$ $(rad/sec)$ | $u_e = V_t$ $(V)$ | $x_{1e} = I_a$ $(A)$ | $x_{2e} = \omega$ $(rad/sec)$ |
|---|---|---|---|---|---|
| 0 | *0.0042* | *-1.0446* | 21 | *1.7579* | *5.9567* |
| 1 | *0.1015* | *-0.9921* | 22 | *1.8229* | *6.5192* |
| 2 | *0.1982* | *-0.9027* | 23 | *1.8863* | *7.0983* |
| 3 | *0.2940* | *-0.7779* | 24 | *1.9480* | *7.6942* |
| 4 | *0.3889* | *-0.6191* | 25 | *2.0081* | *4.3067* |
| 5 | *0.4825* | *-0.4280* | 26 | *2.0665* | *8.9361* |
| 6 | *0.5747* | *-0.2061* | 27 | *2.1233* | *9.5824* |
| 7 | *0.6655* | *0.0450* | 28 | *2.1785* | *10.2461* |
| 8 | *0.7548* | *0.3238* | 29 | *2.2321* | *10.9237* |
| 9 | *0.8424* | *0.6288* | 30 | *2.2840* | *11.6266* |
| 10 | *0.9283* | *0.9588* | 31 | *2.3343* | *12.3444* |
| 11 | *1.0125* | *1.3125* | 32 | *2.3830* | *13.0812* |
| 12 | *1.0950* | *1.6888* | 33 | *2.4301* | *13.8378* |
| 13 | *1.1757* | *2.0867* | 34 | *2.4754* | *14.6148* |
| 14 | *1.2546* | *2.5051* | 35 | *2.5191* | *15.4131* |
| 15 | *1.3317* | *2.9434* | 36 | *2.5611* | *16.2338* |
| 16 | *1.4071* | *3.4009* | 37 | *2.6041* | *17.0777* |
| 17 | *1.4807* | *3.8768* | 38 | *2.6399* | *17.9463* |
| 18 | *1.5526* | *4.3707* | 39 | *2.6767* | *18.8407* |
| 19 | *1.6227* | *4.8822* | 40 | *2.7115* | *19.7625* |
| 20 | *1.6912* | *5.4110* | | | |

Table A.36: Equilibrium Points $(\mathbf{x_e}, u_e)$ of Nonlinear Model (part one)

| $u_e = V_t$ $(V)$ | $x_{1e} = I_a$ $(A)$ | $x_{2e} = \omega$ $(rad/sec)$ | $u_e = V_t$ $(V)$ | $x_{1e} = I_a$ $(A)$ | $x_{2e} = \omega$ $(rad/sec)$ |
|---|---|---|---|---|---|
| 41 | *2.7445* | *20.7135* | 64 | *2.6277* | *63.8099* |
| 42 | *2.7755* | *21.6956* | 65 | *2.5619* | *67.9556* |
| 43 | *2.8046* | *22.7108* | 66 | *2.5003* | *72.1090* |
| 44 | *2.8315* | *23.7618* | 67 | *2.4473* | *76.0710* |
| 45 | *2.8562* | *24.8511* | 68 | *2.4045* | *79.7300* |
| 46 | *2.8787* | *25.9821* | 69 | *2.3712* | *83.0657* |
| 47 | *2.8987* | *27.1583* | 70 | *2.3459* | *86.1078* |
| 48 | *2.9163* | *28.3839* | 71 | *2.3269* | *88.9022* |
| 49 | *2.9311* | *29.6638* | 72 | *2.3128* | *91.4943* |
| 50 | *2.9432* | *31.0034* | 73 | *2.3024* | *93.9235* |
| 51 | *2.9522* | *32.4095* | 74 | *2.2949* | *96.2231* |
| 52 | *2.9579* | *33.8899* | 75 | *2.2897* | *98.4208* |
| 53 | *2.9602* | *35.4537* | 76 | *2.2860* | *100.5404* |
| 54 | *2.9586* | *37.1123* | 77 | *2.2836* | *102.6026* |
| 55 | *2.9528* | *38.8791* | 78 | *2.2819* | *104.6267* |
| 56 | *2.9424* | *40.7707* | 79 | *2.2807* | *106.6315* |
| 57 | *2.9269* | *42.8076* | 80 | *2.2794* | *108.6370* |
| 58 | *2.9058* | *45.0150* | 81 | *2.2778* | *110.6661* |
| 59 | *2.8782* | *47.4242* | 82 | *2.2752* | *112.7479* |
| 60 | *2.8436* | *50.0730* | 83 | *2.2711* | *114.9241* |
| 61 | *2.8012* | *53.0047* | 84 | *2.2642* | *117.2635* |
| 62 | *2.7505* | *56.2628* | 85 | *2.2524* | *119.9047* |
| 63 | *2.6920* | *59.8731* | | | |

Table A.37: Equilibrium Points $(\mathbf{x_e}, u_e)$ of Nonlinear Model (part two)

| $\Upsilon = u - u_{e1}$ $(V)$ | $\Psi_1 = x_1 - x_{1e}$ $(A)$ | $\Psi_2 = x_2 - x_{2e}$ $(rad/sec)$ | $u = V_t$ $(V)$ | $x_1 = I_a$ $(A)$ | $x_2 = \omega$ $(rad/sec)$ |
|---|---|---|---|---|---|
| 0 | *0* | *0* | *7* | *0.6655* | *0.0450* |
| 1 | *0.0901* | *0.2653* | *8* | *0.7556* | *0.3103* |
| 2 | *0.1801* | *0.5305* | *9* | *0.8456* | *0.5755* |

Table A.38: Steady State Values for $\Psi$ and $\mathbf{x}$ (first local linear model: $x_{1e} = 0.6655$, $x_{2e} = 0.0450$ and $u_{e1} = 7$)

| $\Upsilon = u - u_{e2}$ $(V)$ | $\Psi_1 = x_1 - x_{1e}$ $(A)$ | $\Psi_2 = x_2 - x_{2e}$ $(rad/sec)$ | $u = V_t$ $(V)$ | $x_1 = I_a$ $(A)$ | $x_2 = \omega$ $(rad/sec)$ |
|---|---|---|---|---|---|
| -1 | *-0.0885* | *-0.2923* | *7* | *0.6663* | *0.0315* |
| 0 | *0* | *0* | *8* | *0.7548* | *0.3238* |
| 1 | *0.0885* | *0.2923* | *9* | *0.8433* | *0.6161* |
| 2 | *0.1769* | *0.5845* | *10* | *0.9317* | *0.9083* |
| 3 | *0.2654* | *0.8768* | *11* | *1.0202* | *1.2006* |

Table A.39: Steady State Values for $\Psi$ and $\mathbf{x}$ (second local linear model: $x_{1e} = 0.7548$, $x_{2e} = 0.3238$ and $u_{e2} = 8$)

| Local Linear Models | Values for Matrix **A** |
|---|---|
| 1 | $\begin{pmatrix} -87.5851 & -1.6751 \\ 56.7877 & -19.2820 \end{pmatrix}$ |
| 2 | $\begin{pmatrix} -88.1030 & -1.8427 \\ 62.8708 & -19.0313 \end{pmatrix}$ |
| 3 | $\begin{pmatrix} -89.2306 & -2.1608 \\ 74.2528 & -18.4674 \end{pmatrix}$ |
| 4 | $\begin{pmatrix} -91.0960 & -2.5973 \\ 89.4847 & -17.4888 \end{pmatrix}$ |
| 5 | $\begin{pmatrix} -93.7906 & -3.1075 \\ 106.6483 & -15.9957 \end{pmatrix}$ |
| 6 | $\begin{pmatrix} -97.3418 & -3.6435 \\ 123.7828 & -13.9232 \end{pmatrix}$ |
| 7 | $\begin{pmatrix} -103.2826 & -4.3045 \\ 143.3210 & -10.3436 \end{pmatrix}$ |

Table A.40: Values of Matrix **A** for Different Local Linear Models (part one)

| Local Linear Models | Values for Matrix **A** |
|---|---|
| 8 | $\begin{pmatrix} -111.5397 & -4.8546 \\ 157.7950 & -5.7208 \end{pmatrix}$ |
| 9 | $\begin{pmatrix} -121.4309 & -5.1138 \\ 163.8682 & -1.6883 \end{pmatrix}$ |
| 10 | $\begin{pmatrix} -133.9835 & -5.1267 \\ 164.1557 & 1.0754 \end{pmatrix}$ |
| 11 | $\begin{pmatrix} -150.4023 & -4.9624 \\ 160.3874 & 2.4154 \end{pmatrix}$ |
| 12 | $\begin{pmatrix} -180.2363 & -4.5904 \\ 151.0821 & 2.1386 \end{pmatrix}$ |
| 13 | $\begin{pmatrix} -206.9220 & -4.3624 \\ 144.9316 & 0.8834 \end{pmatrix}$ |
| 14 | $\begin{pmatrix} -237.9510 & -4.2961 \\ 143.0854 & 0.1396 \end{pmatrix}$ |

Table A.41: Values of Matrix **A** for Different Local Linear Models (part two)

| $\Upsilon = u - u_{e3}$ $(V)$ | $\Psi_1 = x_1 - x_{1e}$ $(A)$ | $\Psi_2 = x_2 - x_{2e}$ $(rad/sec)$ | $u = V_t$ $(V)$ | $x_1 = I_a$ $(A)$ | $x_2 = \omega$ $(rad/sec)$ |
|---|---|---|---|---|---|
| -1 | *-0.0851* | *-0.3422* | *9* | *0.8432* | *0.6166* |
| 0 | *0* | *0* | *10* | *0.9283* | *0.9588* |
| 1 | *0.0851* | *0.3422* | *11* | *1.0134* | *1.3010* |
| 2 | *0.1702* | *0.6844* | *12* | *1.0985* | *1.6432* |
| 3 | *0.2553* | *1.0265* | *13* | *1.1836* | *1.9853* |
| 4 | *0.3404* | *1.3687* | *14* | *1.2687* | *2.3275* |

Table A.42: Steady State Values for $\Psi$ and $\mathbf{x}$ (third local linear model: $x_{1e} = 0.9283$, $x_{2e} = 0.9588$ and $u_{e3} = 10$)

| $\Upsilon = u - u_{e4}$ $(V)$ | $\Psi_1 = x_1 - x_{1e}$ $(A)$ | $\Psi_2 = x_2 - x_{2e}$ $(rad/sec)$ | $u = V_t$ $(V)$ | $x_1 = I_a$ $(A)$ | $x_2 = \omega$ $(rad/sec)$ |
|---|---|---|---|---|---|
| -2 | *-0.1597* | *-0.8169* | *11* | *1.0161* | *1.2697* |
| -1 | *-0.0798* | *-0.4085* | *12* | *1.0959* | *1.6782* |
| 0 | *0* | *0* | *13* | *1.1757* | *2.0867* |
| 1 | *0.0798* | *0.4085* | *14* | *1.2555* | *2.4952* |
| 2 | *0.1597* | *0.8169* | *15* | *1.3354* | *2.9036* |
| 3 | *0.2395* | *1.2254* | *16* | *1.4152* | *3.3121* |
| 4 | *0.3193* | *1.6339* | *17* | *1.4950* | *3.7206* |
| 5 | *0.3992* | *2.0424* | *18* | *1.5749* | *4.1291* |

Table A.43: Steady State Values for $\Psi$ and $\mathbf{x}$ (fourth local linear model: $x_{1e} = 1.1757$, $x_{2e} = 2.0867$ and $u_{e4} = 13$)

| $\Upsilon = u - u_{e5}$ $(V)$ | $\Psi_1 = x_1 - x_{1e}$ $(A)$ | $\Psi_2 = x_2 - x_{2e}$ $(rad/sec)$ | $u = V_t$ $(V)$ | $x_1 = I_a$ $(A)$ | $x_2 = \omega$ $(rad/sec)$ |
|---|---|---|---|---|---|
| -3 | *-0.2075* | *-1.3831* | *14* | *1.2731* | *2.4938* |
| -2 | *-0.1383* | *-0.9221* | *15* | *1.3423* | *2.9548* |
| -1 | *-0.0692* | *-0.4610* | *16* | *1.4115* | *3.4158* |
| 0 | *0* | *0* | *17* | *1.4807* | *3.8768* |
| 1 | *0.0692* | *0.4610* | *18* | *1.5499* | *4.3378* |
| 2 | *0.1383* | *0.9221* | *19* | *1.6190* | *4.7989* |
| 3 | *0.2075* | *1.3831* | *20* | *1.6882* | *5.2599* |
| 4 | *0.2766* | *1.8442* | *21* | *1.7573* | *5.7210* |
| 5 | *0.3458* | *2.3052* | *22* | *1.8268* | *6.1820* |
| 6 | *0.4149* | *2.7663* | *23* | *1.8956* | *6.6431* |

Table A.44: Steady State Values for $\Psi$ and $\mathbf{x}$ (fifth local linear model: $x_{1e} = 1.4807$, $x_{2e} = 3.8768$ and $u_{e5} = 17$)

| $\Upsilon = u - u_{e6}$ $(V)$ | $\Psi_1 = x_1 - x_{1e}$ $(A)$ | $\Psi_2 = x_2 - x_{2e}$ $(rad/sec)$ | $u = V_t$ $(V)$ | $x_1 = I_a$ $(A)$ | $x_2 = \omega$ $(rad/sec)$ |
|---|---|---|---|---|---|
| -3 | *-0.1927* | *-1.7132* | *19* | *1.6303* | *4.8059* |
| -2 | *-0.1285* | *-1.1421* | *20* | *1.6945* | *5.3770* |
| -1 | *-0.0642* | *-0.5711* | *21* | *1.7587* | *5.9481* |
| 0 | *0* | *0* | *22* | *1.8229* | *6.5192* |
| 1 | *0.0642* | *0.5711* | *23* | *1.8871* | *7.0903* |
| 2 | *0.1285* | *1.1421* | *24* | *1.9514* | *7.6613* |
| 3 | *0.1927* | *1.7132* | *25* | *2.0156* | *8.2324* |
| 4 | *0.2569* | *2.2843* | *26* | *2.0798* | *8.8035* |
| 5 | *0.3212* | *2.8553* | *27* | *2.1441* | *9.3745* |
| 6 | *0.3854* | *3.4264* | *28* | *2.2083* | *9.9456* |
| 7 | *0.4496* | *3.9974* | *29* | *2.2725* | *10.5166* |
| 8 | *0.5139* | *4.5685* | *30* | *2.3368* | *11.0877* |
| 9 | *0.5781* | *5.1396* | *31* | *2.4010* | *11.6588* |

Table A.45: Steady State Values for $\Psi$ and $\mathbf{x}$ (sixth local linear model: $x_{1e} = 1.8229$, $x_{2e} = 6.5192$ and $u_{e6} = 22$)

| $\Upsilon = u - u_{e7}$ $(V)$ | $\Psi_1 = x_1 - x_{1e}$ $(A)$ | $\Psi_2 = x_2 - x_{2e}$ $(rad/sec)$ | $u = V_t$ $(V)$ | $x_1 = I_a$ $(A)$ | $x_2 = \omega$ $(rad/sec)$ |
|---|---|---|---|---|---|
| -5 | *-0.2557* | *-3.5435* | *25* | *2.0285* | *8.0831* |
| -4 | *-0.2046* | *-2.8348* | *26* | *2.0796* | *8.7918* |
| -3 | *-0.1534* | *-2.1261* | *27* | *2.1307* | *9.5005* |
| -2 | *-0.1023* | *-1.4174* | *28* | *2.1818* | *10.2092* |
| -1 | *-0.0511* | *-0.7087* | *29* | *2.2329* | *10.9179* |
| 0 | *0* | *0* | *30* | *2.2840* | *11.6266* |
| 1 | *0.0511* | *0.7087* | *31* | *2.3351* | *12.3353* |
| 2 | *0.1023* | *1.4174* | *32* | *2.3863* | *13.0400* |
| 3 | *0.1534* | *2.1261* | *33* | *2.4374* | *13.7527* |
| 4 | *0.2046* | *2.8348* | *34* | *2.4886* | *14.4614* |
| 5 | *0.2557* | *3.5435* | *35* | *2.5397* | *15.1701* |
| 6 | *0.3069* | *4.2522* | *36* | *2.5909* | *15.8788* |
| 7 | *0.3580* | *4.9606* | *37* | *2.6420* | *16.5875* |
| 8 | *0.4092* | *5.6696* | *38* | *2.6932* | *17.2962* |
| 9 | *0.4603* | *6.3783* | *39* | *2.7443* | *18.0049* |
| 10 | *0.5115* | *7.0870* | *40* | *2.7955* | *18.7136* |

Table A.46: Steady State Values for $\Psi$ and $\mathbf{x}$ (seventh local linear model: $x_{1e} = 2.2840$, $x_{2e} = 11.6266$ and $u_{e7} = 30$)

| $\Upsilon = u - u_{e8}$ $(V)$ | $\Psi_1 = x_1 - x_{1e}$ $(A)$ | $\Psi_2 = x_2 - x_{2e}$ $(rad/sec)$ | $u = V_t$ $(V)$ | $x_1 = I_a$ $(A)$ | $x_2 = \omega$ $(rad/sec)$ |
|---|---|---|---|---|---|
| -6 | *-0.2037* | *-5.6190* | *34* | *2.5075* | *14.1435* |
| -5 | *-0.1698* | *-4.6825* | *35* | *2.5415* | *15.0800* |
| -4 | *-0.1358* | *-3.7460* | *36* | *2.5755* | *16.0165* |
| -3 | *-0.1019* | *-2.8095* | *37* | *2.6095* | *16.9530* |
| -2 | *-0.0679* | *-1.8730* | *38* | *2.6435* | *17.8895* |
| -1 | *-0.0340* | *-0.9365* | *39* | *2.6775* | *18.8260* |
| 0 | *0* | *0* | *40* | *2.7115* | *19.7625* |
| 1 | *0.0340* | *0.9365* | *41* | *2.7445* | *20.6990* |
| 2 | *0.0679* | *1.8730* | *42* | *2.7794* | *21.6355* |
| 3 | *0.1019* | *2.8095* | *43* | *2.8134* | *22.5720* |
| 4 | *0.1358* | *3.7460* | *44* | *2.8473* | *23.5085* |
| 5 | *0.1698* | *4.6825* | *45* | *2.8813* | *24.4450* |
| 6 | *0.2037* | *5.6190* | *46* | *2.9152* | *25.3815* |
| 7 | *0.2377* | *6.5555* | *47* | *2.9492* | *26.3180* |
| 8 | *0.2716* | *7.4920* | *48* | *2.9831* | *27.2545* |
| 9 | *0.3056* | *8.4285* | *49* | *3.0171* | *28.1910* |

Table A.47: Steady State Values for $\Psi$ and $\mathbf{x}$ (eighth local linear model: $x_{1e} = 2.2840$, $x_{2e} = 11.6266$ and $u_{e8} = 40$)

| $\Upsilon = u - u_{e9}$ $(V)$ | $\Psi_1 = x_1 - x_{1e}$ $(A)$ | $\Psi_2 = x_2 - x_{2e}$ $(rad/sec)$ | $u = V_t$ $(V)$ | $x_1 = I_a$ $(A)$ | $x_2 = \omega$ $(rad/sec)$ |
|---|---|---|---|---|---|
| -5 | *-0.0674* | *-6.5463* | *44* | *2.8636* | *23.1173* |
| -4 | *-0.0540* | *-5.2371* | *45* | *2.8771* | *24.4266* |
| -3 | *-0.0405* | *-3.9278* | *46* | *2.8906* | *25.7359* |
| -2 | *-0.0270* | *-2.6185* | *47* | *2.9041* | *27.0452* |
| -1 | *-0.0135* | *-1.3093* | *48* | *2.9176* | *28.3545* |
| 0 | *0* | *0* | *49* | *2.9311* | *29.6638* |
| 1 | *0.0135* | *1.3093* | *50* | *2.9446* | *30.9731* |
| 2 | *0.0270* | *2.6185* | *51* | *2.9581* | *32.2823* |
| 3 | *0.0405* | *3.9278* | *52* | *2.9716* | *33.5916* |
| 4 | *0.0540* | *5.2371* | *53* | *2.9851* | *34.9009* |
| 5 | *0.0674* | *6.5463* | *54* | *2.9985* | *36.2102* |
| 6 | *0.0809* | *7.8556* | *55* | *3.0120* | *37.5194* |
| 7 | *0.0944* | *9.1648* | *56* | *3.0255* | *38.8286* |

Table A.48: Steady State Values for $\Psi$ and $\mathbf{x}$ (ninth local linear model: $x_{1e} = 2.9311$, $x_{2e} = 29.6638$ and $u_{e9} = 49$)

| $\Upsilon = u - u_{e10}$ $(V)$ | $\Psi_1 = x_1 - x_{1e}$ $(A)$ | $\Psi_2 = x_2 - x_{2e}$ $(rad/sec)$ | $u = V_t$ $(V)$ | $x_1 = I_a$ $(A)$ | $x_2 = \omega$ $(rad/sec)$ |
|---|---|---|---|---|---|
| -4 | *0.0514* | *-7.8450* | *52* | *2.9936* | *32.9255* |
| -3 | *0.0385* | *-5.8838* | *53* | *2.9808* | *34.8868* |
| -2 | *0.0257* | *-3.9225* | *54* | *2.9680* | *36.8481* |
| -1 | *0.0128* | *-1.9613* | *55* | *2.9552* | *38.8094* |
| 0 | *0* | *0* | *56* | *2.9424* | *40.7707* |
| 1 | *-0.0128* | *1.9613* | *57* | *2.9296* | *42.7320* |
| 2 | *-0.0257* | *3.9225* | *58* | *2.9167* | *44.6932* |
| 3 | *-0.0385* | *5.8838* | *59* | *2.9039* | *46.6545* |
| 4 | *-0.0514* | *7.8450* | *60* | *2.8910* | *48.6157* |
| 5 | *-0.0642* | *9.8063* | *61* | *2.8782* | *50.5770* |
| 6 | *-0.0771* | *11.7675* | *62* | *2.8653* | *52.5382* |

Table A.49: Steady State Values for $\Psi$ and $\mathbf{x}$ (tenth local linear model: $x_{1e} = 2.9424$, $x_{2e} = 40.7707$ and $u_{e10} = 56$)

| $\Upsilon = u - u_{e11}$ $(V)$ | $\Psi_1 = x_1 - x_{1e}$ $(A)$ | $\Psi_2 = x_2 - x_{2e}$ $(rad/sec)$ | $u = V_t$ $(V)$ | $x_1 = I_a$ $(A)$ | $x_2 = \omega$ $(rad/sec)$ |
|---|---|---|---|---|---|
| -3 | *0.1396* | *-9.2682* | *58* | *2.9407* | *43.7365* |
| -2 | *0.0931* | *-6.1788* | *59* | *2.8942* | *46.8259* |
| -1 | *0.0465* | *-3.0894* | *60* | *2.8477* | *49.9153* |
| 0 | *0* | *0* | *61* | *2.8012* | *53.0047* |
| 1 | *-0.0465* | *3.0894* | *62* | *2.7547* | *56.0941* |
| 2 | *-0.0931* | *6.1788* | *63* | *2.7081* | *59.1835* |
| 3 | *-0.1396* | *9.2682* | *64* | *2.6616* | *62.2729* |
| 4 | *-0.1861* | *12.3577* | *65* | *2.6151* | *65.3624* |
| 5 | *-0.2326* | *15.4471* | *66* | *2.5686* | *68.4518* |

Table A.50: Steady State Values for $\Psi$ and $\mathbf{x}$ (eleventh local linear model: $x_{1e} = 2.8012$, $x_{2e} = 53.0047$ and $u_{e11} = 61$)

| $\Upsilon = u - u_{e12}$ $(V)$ | $\Psi_1 = x_1 - x_{1e}$ $(A)$ | $\Psi_2 = x_2 - x_{2e}$ $(rad/sec)$ | $u = V_t$ $(V)$ | $x_1 = I_a$ $(A)$ | $x_2 = \omega$ $(rad/sec)$ |
|---|---|---|---|---|---|
| -4 | *0.2314* | *-16.3469* | *62* | *2.7315* | *55.7622* |
| -3 | *0.1735* | *-12.2602* | *63* | *2.6737* | *59.8489* |
| -2 | *0.1157* | *-8.1834* | *64* | *2.6159* | *63.9356* |
| -1 | *0.0578* | *-4.0867* | *65* | *2.5581* | *68.0223* |
| 0 | *0* | *0* | *66* | *2.5003* | *72.1090* |
| 1 | *-0.0578* | *4.0867* | *67* | *2.4425* | *76.1957* |
| 2 | *-0.1157* | *8.1734* | *68* | *2.3846* | *80.2824* |
| 3 | *-0.1735* | *12.2602* | *69* | *2.3268* | *84.3692* |
| 4 | *-0.2314* | *16.3469* | *70* | *2.2689* | *88.4559* |
| 5 | *-0.2892* | *20.4336* | *71* | *2.2111* | *92.5426* |

Table A.51: Steady State Values for $\Psi$ and $\mathbf{x}$ (twelfth local linear model: $x_{1e} = 2.5003$, $x_{2e} = 72.1090$ and $u_{e12} = 66$)

| $\Upsilon = u - u_{e13}$ $(V)$ | $\Psi_1 = x_1 - x_{1e}$ $(A)$ | $\Psi_2 = x_2 - x_{2e}$ $(rad/sec)$ | $u = V_t$ $(V)$ | $x_1 = I_a$ $(A)$ | $x_2 = \omega$ $(rad/sec)$ |
|---|---|---|---|---|---|
| -4 | *0.0655* | *-10.7487* | *67* | *2.3925* | *78.1534* |
| -3 | *0.0491* | *-8.0615* | *68* | *2.3761* | *80.8404* |
| -2 | *0.0328* | *-5.3743* | *69* | *2.3597* | *83.5278* |
| -1 | *0.0164* | *-2.6872* | *70* | *2.3433* | *86.2150* |
| 0 | *0* | *0* | *71* | *2.3269* | *88.9022* |
| 1 | *-0.0164* | *2.6872* | *72* | *2.3105* | *91.5894* |
| 2 | *-0.0328* | *5.3743* | *73* | *2.2941* | *94.2765* |
| 3 | *-0.0491* | *8.0615* | *74* | *2.2778* | *96.9637* |
| 4 | *-0.0655* | *10.7487* | *75* | *2.2614* | *99.6509* |
| 5 | *-0.0819* | *13.4358* | *76* | *2.2450* | *102.3380* |
| 6 | *-0.0983* | *16.1230* | *77* | *2.2286* | *105.0252* |
| 7 | *-0.1147* | *18.8101* | *78* | *2.2122* | *107.7123* |
| 8 | *-0.1310* | *21.4973* | *79* | *2.1959* | *110.3995* |
| 9 | *-0.1474* | *24.1845* | *80* | *2.1795* | *113.0867* |
| 10 | *-0.1638* | *26.8716* | *81* | *2.1631* | *115.7738* |

Table A.52: Steady State Values for $\Psi$ and $\mathbf{x}$ (thirteenth local linear model: $x_{1e} = 2.3269$, $x_{2e} = 88.9022$ and $u_{e13} = 71$)

| $\Upsilon = u - u_{e14}$ $(V)$ | $\Psi_1 = x_1 - x_{1e}$ $(A)$ | $\Psi_2 = x_2 - x_{2e}$ $(rad/sec)$ | $u = V_t$ $(V)$ | $x_1 = I_a$ $(A)$ | $x_2 = \omega$ $(rad/sec)$ |
|---|---|---|---|---|---|
| -4 | *0.0080* | *-8.2022* | *77* | *2.2858* | *102.4641* |
| -3 | *0.0060* | *-6.1516* | *78* | *2.2838* | *104.5146* |
| -2 | *0.0040* | *-4.1011* | *79* | *2.2818* | *106.5651* |
| -1 | *0.0020* | *-2.0505* | *80* | *2.2798* | *108.6156* |
| 0 | *0* | *0* | *81* | *2.2778* | *110.6661* |
| 1 | *-0.0020* | *2.0505* | *82* | *2.2758* | *112.7166* |
| 2 | *-0.0040* | *4.1011* | *83* | *2.2738* | *114.7672* |
| 3 | *-0.0060* | *6.1516* | *84* | *2.2718* | *116.8177* |
| 4 | *-0.0080* | *8.2022* | *85* | *2.2698* | *118.8683* |

Table A.53: Steady State Values for $\Psi$ and $\mathbf{x}$ (fourteenth local linear model: $x_{1e} = 2.2778$, $x_{2e} = 110.6661$ and $u_{e14} = 81$)

# Appendix B

# Figure

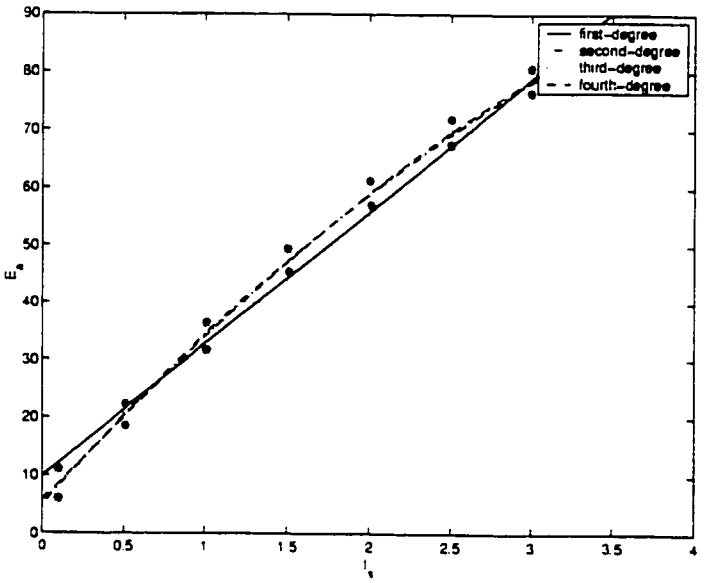


Figure B.1: $E_a$ and $I_s$ Relationship of First Group Testing Data ( No Load, No Belt and Speed = 1200 rpm )

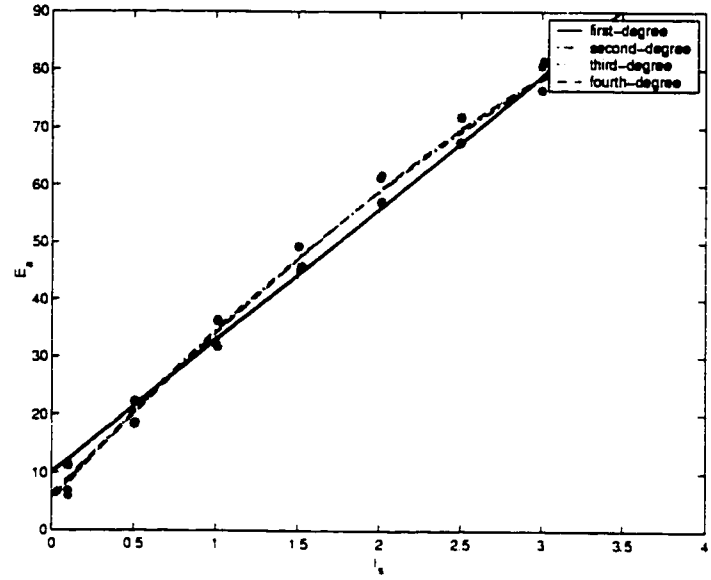


Figure B.2: $E_a$ and $I_s$ Relationship of Second Group Testing Data ( No Load, No Belt and Speed = 1200 rpm )

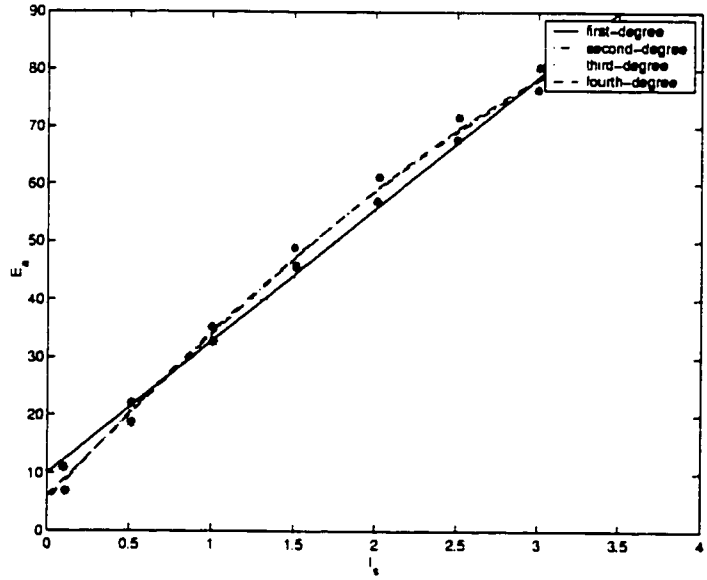


Figure B.3: $E_a$ and $I_s$ Relationship of Third Group Testing Data ( No Load, No Belt and Speed = 1200 rpm )

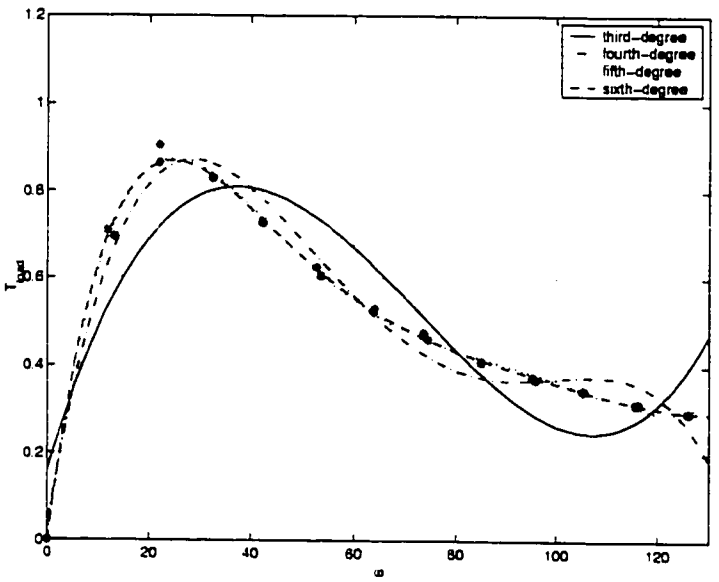


Figure B.4: $T_{load}$ and $\omega$ Relationship ( Dynamometer Field Flux Strength: 30% )

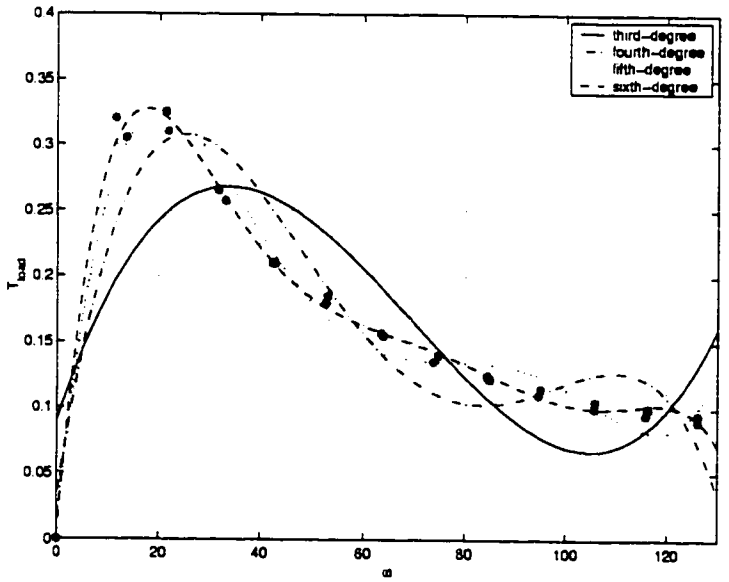


Figure B.5: $T_{load}$ and $\omega$ Relationship ( Dynamometer Field Flux Strength: 20% )

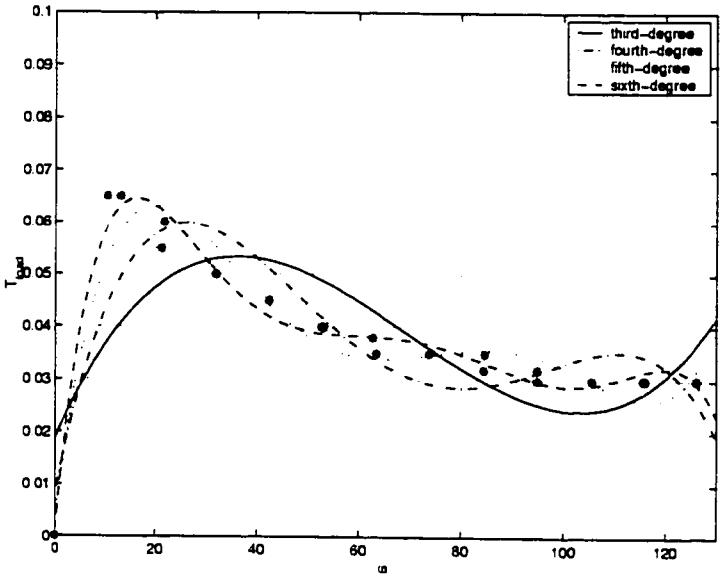


Figure B.6: $T_{load}$ and $\omega$ Relationship ( Dynamometer Field Flux Strength: 10% )

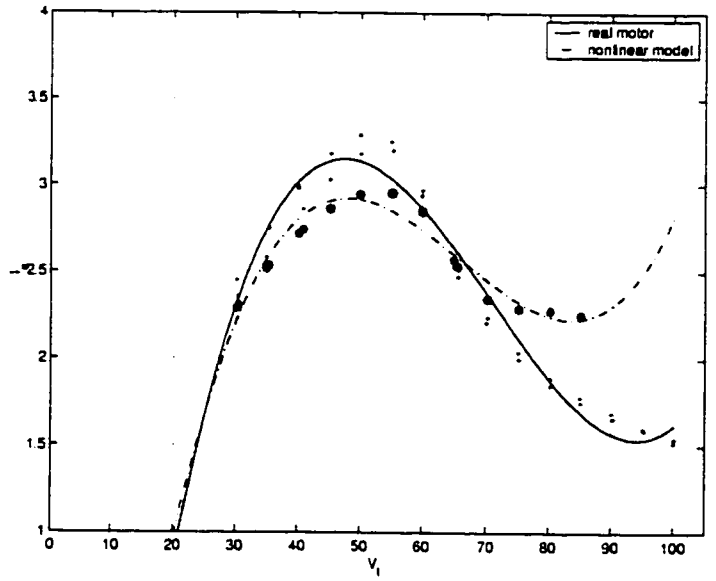


Figure B.7: Compare the Average Relationship of $I_a$ and $V_t$ between Real Motor and Nonlinear Model

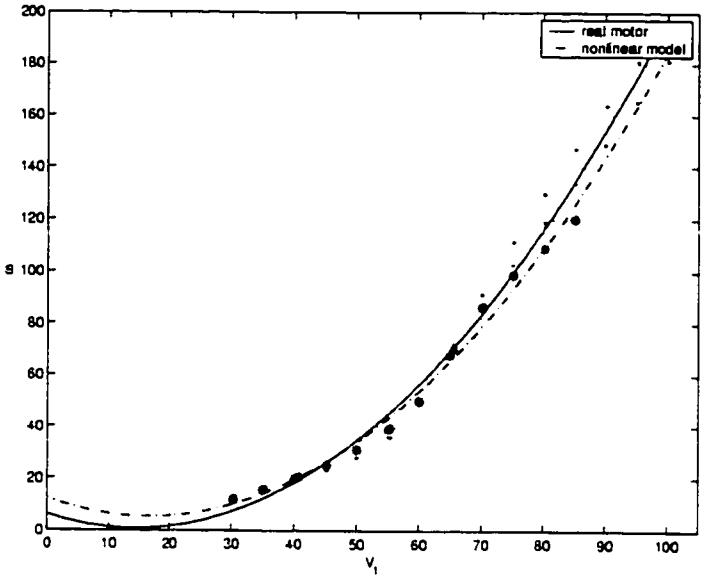


Figure B.8: Compare the Average Relationship of $\omega$ and $V_t$ between Real Motor and Nonlinear Model

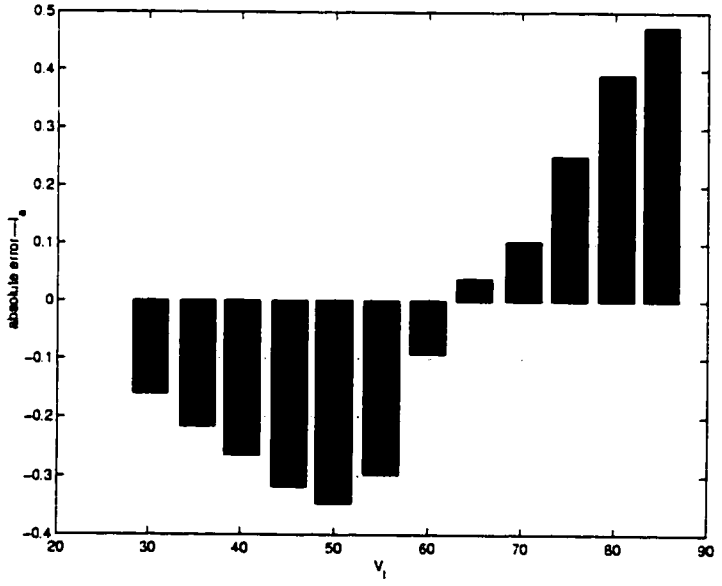


Figure B.9: Absolute Error of $I_a$ between Real Motor and Nonlinear Model ( First Time Testing: Average=-0.0366A, | Average |=0.2454A )

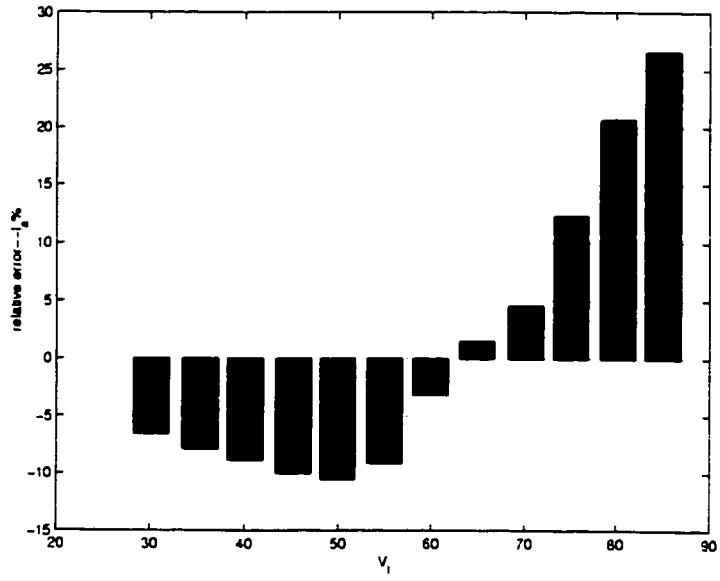


Figure B.10: Relative Error of $I_a$ between Real Motor and Nonlinear Model ( First Time Testing: Average=0.7929%, | Average |=10.1246% )

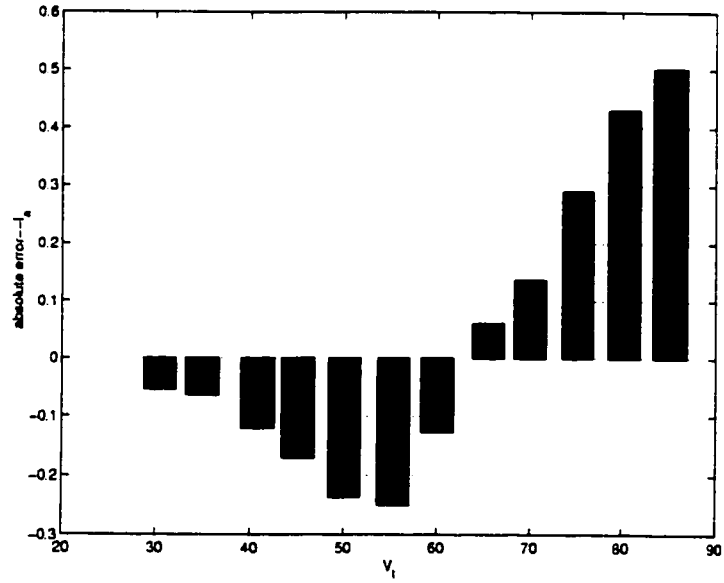


Figure B.11: Absolute Error of $I_a$ between Real Motor and Nonlinear Model ( Second Time Testing: Average=0.0332A, | Average |=0.2029A )

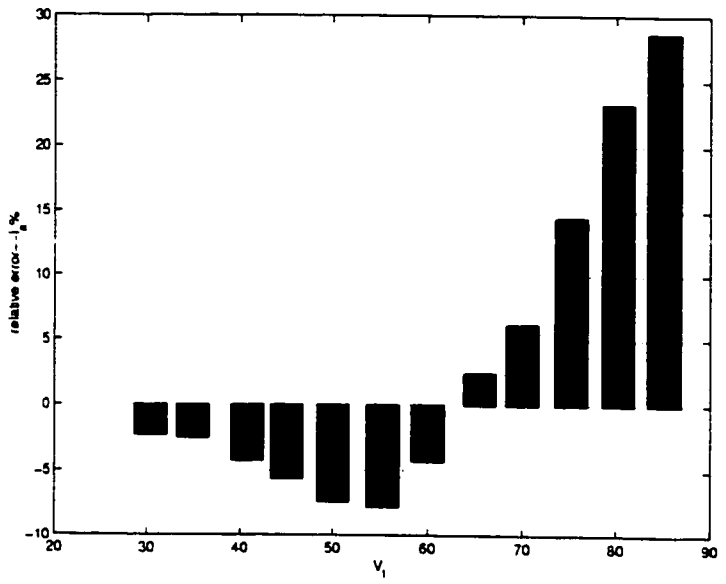


Figure B.12: Relative Error of $I_a$ between Real Motor and Nonlinear Model ( Second Time Testing: Average=3.4129%, | Average |=9.0767% )

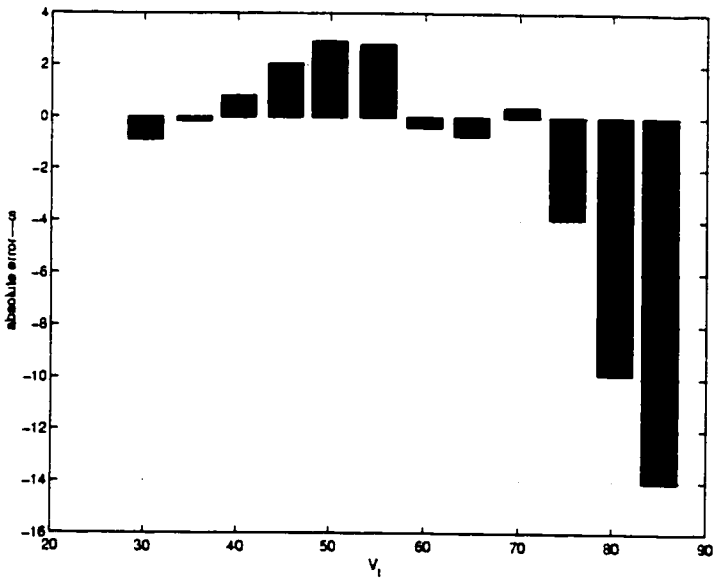


Figure B.13: Absolute Error of $\omega$ between Real Motor and Nonlinear Model ( First Time Testing: Average=-1.7520rad/sec, | Average |=3.2446rad/sec )

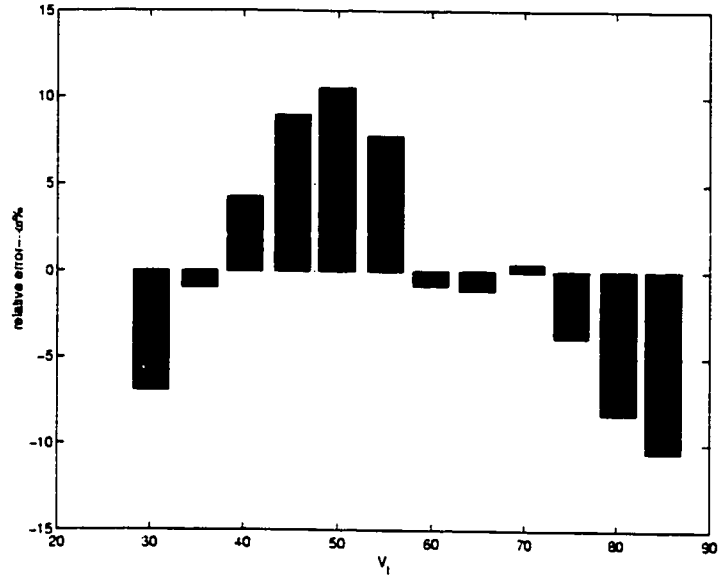


Figure B.14: Relative Error of $\omega$ between Real Motor and Nonlinear Model ( First Time Testing: Average=-0.0421%, | Average |=5.3426% )

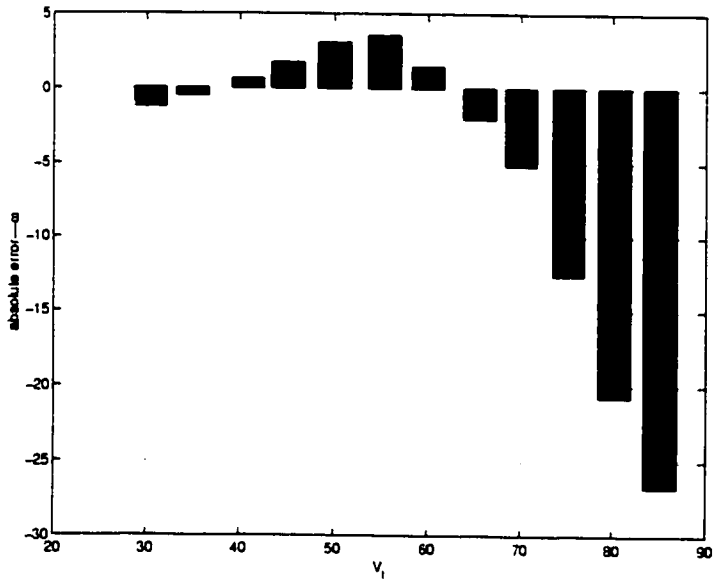


Figure B.15: Absolute Error of $\omega$ between Real Motor and Nonlinear Model ( Second Time Testing: Average=-4.8686rad/sec, | Average |=6.6080rad/sec )

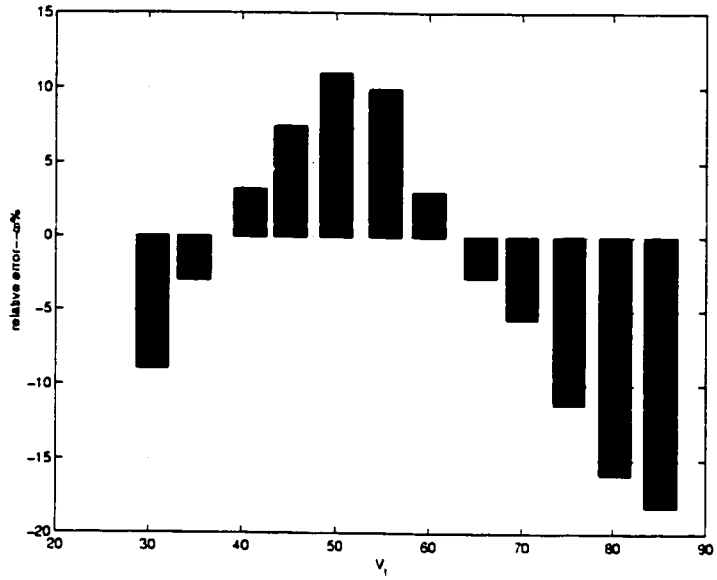


Figure B.16: Relative Error of $\omega$ between Real Motor and Nonlinear Model ( Second Time Testing: Average=-2.6074%, | Average |=8.3561% )

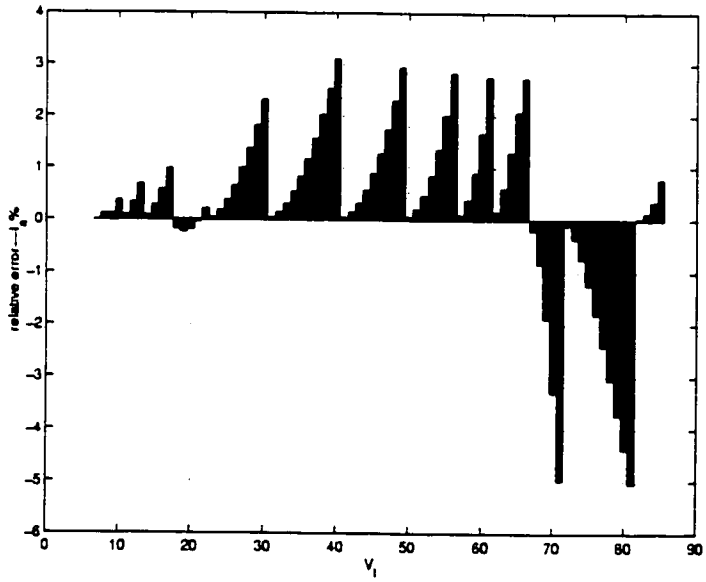


Figure B.17: Relative Error of $I_a$ between Nonlinear Model and Linearized Models

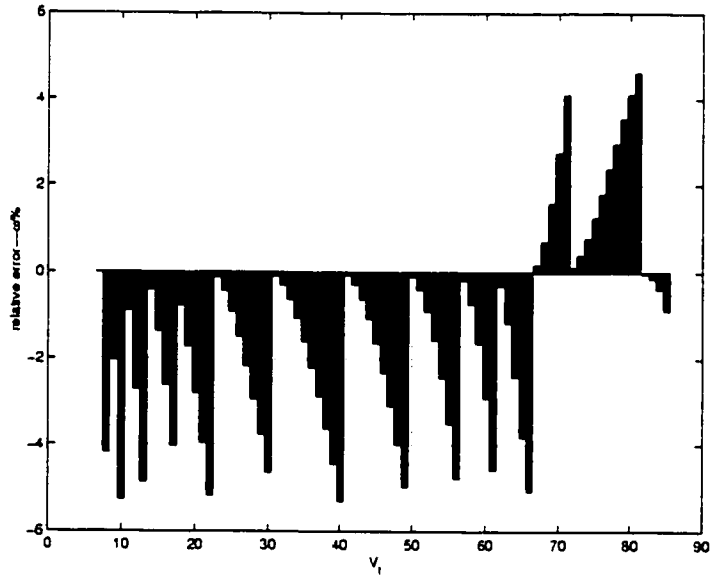


Figure B.18: Relative Error of $\omega$ between Nonlinear Model and Linearized Models